JAN. - APR. 1999
Volume V Number I

ISSN 0859 144X

THE ASEAN JOURNAL OF RADIOLOGY

Published by The Radiological Society and
The Royal College of Radiologists of Thailand,
Bangkok, Thailand

Supported through an educational grant from

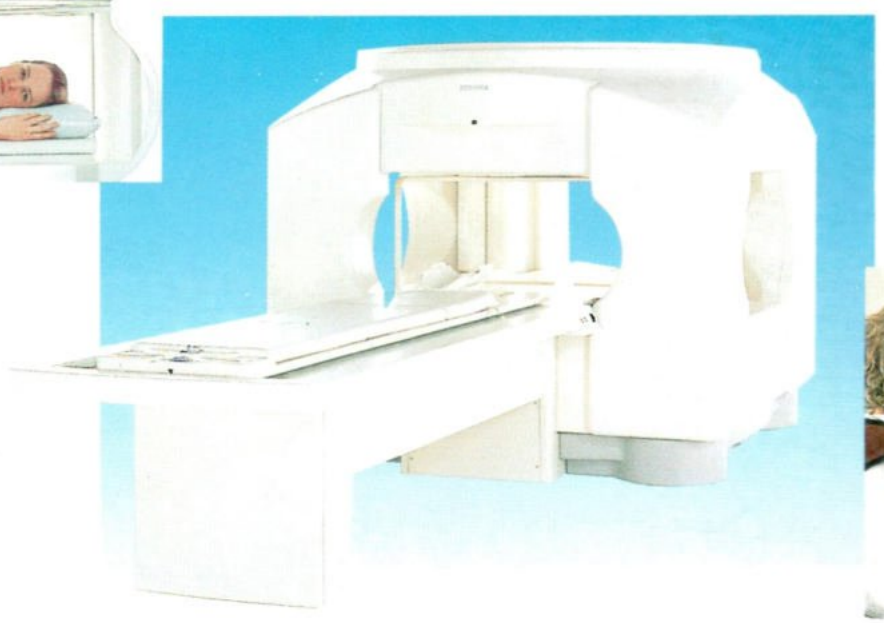

OPART

Superconducting Performance, OPEN MR Advantages.

The pioneer of open MR imaging, Toshiba has now developed a superconducting cryogenless magnet which sets new standards for open MR systems.

OPART takes advantage of the latest technology to provide exceptional image quality through a variety of fast scanning techniques.

A unique open magnet design offers all-round patient access, enabling even large, claustrophobic, and pediatric patients to be scanned with ease.

OPART Advantages

- Fast, flexible throughput for clinical productivity.
- Four sided patient accessibility, enhances patient comfort and throughput.
- A floating tabletop facilitates easy and accurate patient positioning for improved image quality.
- Icon driven computer platform, with user friendly software for true multitasking power.
- Long-term reliability and system upgradeability.
- Scanning is possible while the patient is still connected to ancillary MR compatible monitoring equipment.
- Exceptional performance across a variety of clinical applications.

TOSHIBA

GLOBAL IMAGING▪MEDICAL SYSTEMS

CMC BIOTECH

(SOLE DISTRIBUTOR)

CMC BIOTECH CO., LTD.

364 Muban Town-in-Town, Ladphrao 94 Road, Wangthonglang, Bangkok 10310

Tel. (662) 530-4995-6, 559-3261-2, 559-2179-80, 538-4102, 538-0710 Fax : 530-7231

JAN. - APR. 1999
Volume V Number I

ISSN 0859 144X

THE ASEAN JOURNAL OF RADIOLOGY

Published by The Radiological Society and
The Royal College of Radiologists of Thailand,
Bangkok, Thailand

Supported through an educational grant from

THE ASEAN JOURNAL OF RADIOLOGY

Volume V Number I JAN. - APR. 1999

CONTENTS

THE ASEAN JOURNAL OF RADIOLOGY

Volume V Number I JAN. - APR. 1999

CONTENTS

EUROPEAN SOCIETY OF NEURORADIOLOGY SEMINAR HELD IN VENICE, JUNE 1997 : TRAINING IN NEURORADIOLOGY

Pierre LASJAUNIAS
President of the ESNR

INTRODUCTION

OBJECTIVES

The two-day seminar brought together the chairmen of the different committees of the ESNR. Our aim was to define guidelines on the teaching of Neuroradiology which was felt to be the responsibility of the ESNR, in line with its goals and priorities. The questions concerning our speciality, raised in the first seminar of this group in Bologna (December 1996), and the conclusions of this seminar were partly presented in Oxford 1997. That presentation will be completed in Lisbon in September 1998.

The variety within this group of participants*, both geographically and in its members' practice of neuroradiology, guaranteed a wide range of views. The challenge consisted in considering systems where Neuroradiology remains a technique-oriented speciality, without penalizing others where Neuroradiology is regarded as a clinically-oriented speciality. Our discussions were guided by three concerns : the patient's interest-taking into account the present state of the art -, the flexibility of the training of neuroradiologists over time, and the ESNR tradition and expertise, building on the work already accomplished during the previous presidencies.

BETWEEN OPENMINDEDNESS AND VULNERABILITY

The present trend is to break the various aspects of Neuroradiology into sectors, by defining each section as either neurological, neurosurgical, cardiologic, paediatric, or "purely" radiological. Each sister speciality claims access to neuroradiological practice for itself. The following article published in "Neurology", establishes clearly such intention and the rationale used to support it. J. Brillman, R. Kasdan, L.Wechsler, The neurologist as neuroimager. Neurology 1997; 48:303-311.

Some illustrative parts of this article have been selected :

"Unfortunately, radiologists with no neuroradiology fellowship training often fail to help the clinician. ...In many instances, neurolo -gists use the imaging findings to make clinical decisions without having to consult a neuroradiologist. If there is no need of it, such a consultation delays the work - up and wastes resources.

...Many neurologists are qualified to interprete neuroimages and ultrasounds on their own patients. Indeed,...,neurologists may be best suited and trained for this purpose. ...The clinician is giving meaning to the image. The

* **Invited participants :**
D. Baleriaux, J.F. Bonneville, J.P. Braun, J.V. Byrne, J.C. Casselman, O. Flodmark, A. Goulao, H. Hacker, I. Isherwood, P. Lasjaunias, M. Leonardi, C. Manelfe, I. Moseley, P. Nakstad, L. Picard, C. Raybaud, J. Reul, J. Ruscalleda, U. Salvolini, K. Sartor, E. Schindler, G. Scotti, O. Schubiger, A. Thron, P. Tortori Donati, A. Valavanis, J. Valk, G. Wilms.

neurologist as neuroimager is also often patient friendly. In our patient setting, the convenience offered to patients by having a neurodiagnostic procedure at the time of their evaluation is expedient. ...For hospitalized patients, many practising neurologists are well aware of the need to interprete an image and apply its findings to an emergent setting before the radiologist has reviewed the film. Dictated reports are often placed on the patient's records several days later when therapeutic interventions have already been taken and often after the patient has been discharged. ...If radiologists are the exclusive providers it is likely there will be a demand for higher fees in the absence of a competitve market place. ...Indeed, clinical neurologists may be in the best position to know when a scan is necessary, which type of imaging test to order, and to determine whether contrast enhancement is required. ...Imaging is an integral part of the practice of neurology. ...If properly trained and certified, orthopedists, cardiologists, internists, obstetricians and other specialists should be able to interprete ancillary studies specific to their area of expertise and for the well - being of their patients. Insurers who develop poorly informed exclusionary policies of reimbursing only radiologists for the interpretation of images, must be educated and if necessary, aggressively challenged in the courts."

In such an unfriendly debate the policy and recommendations of the ESNR are exemplary : the historical ties that link the different components of neuroradiology to clinicians, the academic commitment of its members close to other specialities, the quality of its scientific contributions as well as its formal commitment in the initial teaching and continuing education of neuroradiology for 15 years.

The cited article and others in other fields, illustrate the reality of this offensive appetite for Neuroradiology and the attempt to fragment it as a specialty, all of which highlights the value of neuroradiological advances to the practice of medicine. From a positive standpoint, such an aggressive discussion is intended to offer patients the best possible knowledge developed by neuroradiologists over the years. The final purpose of such claims, however, is not to develop what is clearly adequate but only to apply it to the largest possible population. On that former intention we certainly agree, but our ambition takes us further...

RECOMMENDATIONS OF THE XV DIRECTORATE GENERAL OF THE COMMISSION OF THE EUROPEAN COMMUNITIES

These recommendations have been made within the mainframe of the Internal Market and Financial Services, Intellectual and industrial property, Freedom of establishment and freedom to provide services, notably in the regulated professions. The Advisory Committee on Medical Training suggested the EC Member States modify the list of medical specialities, adding some new disciplines. In this proposal the field of radiological activities (generally speaking) could be modified in a larger corpus :
Diagnostic Radiology
Paediatric Radiology
Neuroradiology
Radiotherapy and Oncology
Nuclear Medicine

This proposal acknowledges the specificity of the practice in Neuroradiology and its training, recognises the proposal made by our pioneers and the quality of European Neruoradiology, and takes into due account the position of our Portuguese colleagues who have had a specific training and title for Neuroradiology for fifteen years.

The recommendations will be examined

in the near future by the Governments of the EC Member States and when approved will be voted by the Strasbourg Assembly. Then the EC Member States will be obliged to recognise a specific title awarded by another EC Country. This completely new situation will certainly clarify the need for the specific training we have been proposing for years and foster the development of specific academic courses in Neuroradiology. These recommendations are valid only for the EC Member States, but European Neuroradiology in general, and ESNR in particular, are held in consideration and heard outside Europe and naturally in the non - EC European countries. We can thus foresee major developments for Neuroradiology in Europe.

GENERAL PRINCIPLES OF TRAINING IN NEURORADIOLOGY

Up until such time as a curriculum and certification in Neuroradiology are established, the discussions around practice will be the prevailing component of teaching and specialisation. "There are not enough specialists to interpret neuroradiological examinations, even though all the neuroradiological sectional explorations are not necessarily carried out by neuroradiologists". We therefore need more neuroradiologists as well as a longer or even a more specific training in neuroradiology.

Along with mastering the discipline, consideration should be given to the problem of costs in the development of Neuroradiology. Neuroradiological practice should avoid giving priority to an acquisition of images requested solely by prescribers. The list of the possible diagnostic errors increases when episodic contact with clinicians is a polyvalent radiological practice of neuroradiology. It does not correspond to the quality of care that patients should expect today. The discussions have highlighted in particular, sufficient clinical rotations and training, which best prepare specialists for neuroradiological practice. The group considered that individual imaging competence, technical capabilities and budgets can be taken into account as long as they do not jeopardize the quality and the safety of the diagnostics and care for patients. A line has therefore to be drawn somewhere, and it is suggested it should refer to the medico - legal responsibility of the specialist who agrees to perform and interpret neuroradiological procedures. His/her ability can be questioned simply with the information he gives to the patient. This remark points to the prevalence of decision-making over "blind skill"

Focussing the training organisation in Neuroradiology on X-rays, ultrasonographic imaging, or MRI is to ignore the contents of Neuroradiology, or confuse discipline with practice. One can perceive the various levels between a science (or discipline), a technology, and tools : thermodynamics (a science) permitted the birth of the internal combustion engine (a technology) and finally the construction of cars (tools). Neuroradiology may not be specifically a science, but it is certainly a discipline; it cannot be deemed simply a technology or a tool. An educational programme must teach science, illustrate it with technology, and implement it with the example of tools or applications. For the time being the training programs proposed maintain the confusion between the three levels. They present ephemeral tools pretending they are technologies ignoring where the science or discipline that made them possible stands. Such disorder in scale and priorities can be justified in strict practical training but it is contrary to the principle of constancy and universality that govern education projects. One can understand why ESNR's commitment is to build Neuroradiology teaching as a discipline

and to ensure its excellence through the next generations.

PROPOSALS

- Neuroradiology is performed at its best within an environment of neurological disciplines (neurology, ENT surgery, ophthalmology, maxillofacial surgery, neurosurgery...). The training center should nevertheless have a critical mass of examinations, sufficient both in quality and quantity, as well as tutorship by senior neuroradiologists, to justify its accreditation. The search for a minimum number of explorations per trainee should be made depending on requirements. The accreditation of centres could be under the responsibility of a committee formed by the ESNR in agreement with the competent national and European professional administration body.

NEURORADIOLOGICAL TRAINING OF GENERAL RADIOLOGISTS :

The following conclusions were adopted for the neuroradiological training of general radiologists :

- Neuroradiological training must take place early in the training of general radiology, before the third year, because of the role played in duty shifts by juniors in training.- It must focus on CT and MRI of the skull and spine emphasizing "cross sectional neuroimaging". Myelography and angiography should not be practically taught. The study of radio-isotopes and neurosonography depends very much on the level of each country.

- Six months or seventeen weeks of neuroradiology training are recommended : this would be the minimum time to reach a basic level of knowledge. Harmonization with the ten weeks of head and neck teaching should be well coordinated.

- The training must be continuous during these six months without interruptions, preferably immediately before or after the head and neck part of the training.

- The teaching must be carried out by active neuroradiologists, trained with the recommendations proposed below.- The log-book, its content and its follow-up certifies the training received and guarantee the competence of the individual in reading sectional images.

- For the posts offered to graduated general radiologists in a general radiology department that includes some neuroradiological activities, six months of supplementary training should be required. A network of relations and the use of telediagnostics should be encouraged, in order to avoid the isolation of radiologists in this kind of situation.

- Continuing education should be specifically adapted for all those general radiologists who carry out neuroradiological examinations outside a neuroradiological facility. Someone working without daily contacts with the clinic and fundamental specialists in the neurological and head and neck disciplines will soon alter his competence in neuroradiology.

NEURORADIOLOGICAL SPECIALIZATION IN GENERAL RADIOLOGY

General radiologists who have spent five years in training (and have not shown interest in a particular organ) will have to spend at least two years in training to acquire a neuroradiological specialization. This training is expected in addition to the six months of neuroradiology teaching intervening during the general training. They will receive both academic and practical teaching. The group believes that this training

produces general radiologists with a specific interest in neuroradiology, different from neuroradiologists.

- This training must take place within a neuroscientific center (neurological, neurosurgical, etc...). This training must be carried out full time and continuously.

- The theoretical training must be at least one hour and ideally two hours a week, for forty-eight weeks a year ; the trainee will be exposed to up to a total of about two hundred hours of theoretical training.

- A tutor must be appointed for each future specialist. The ratio between the number of tutors and that of the students must be determined : one to two, one to three. Tutors like teachers, must be actively practising neuroradiologists.

- MRI spectroscopy, functional MRI as well as basic knowledge in neurology, neurosurgery... are necessary. A basic training in paediatrics, head and neck and interventional neuroradiology must be considered.

- A log-book will certify the balance among the different kinds of examinations and procedures (invasive and non invasive) performed during training. No precise recommendation could or should be made concerning the required quantity for each kind of neuroradiological examinations. Such aspect is secured by the procedure for accreditation of the training centres that takes into account the variety and amount of each kind of examinations performed each year.

TRAINING OF NEURORADIOLOGISTS (THE DIRECT LIMB)

The training will last at least 5 years.

- For two years, non neuroradiological rotations should take place, after admission in the speciality training. Each of these rotation years will be evaluated. Among the usual rotations discussed, training in neurology is considered the most useful, while general radiology is not regarded as compulsory. The importance and duration of training rotations in neurosurgery are evaluated differently by members of the group, depending on the future option of the trainee. A compulsory core knowledge of general radiology included in that training will have to be achieved formally at least by a theoretical teaching, if necessary certified with a qualification. Each of these training sections may constitute credits to be used to build bridges (both ways) with the training in general radiology, neurology, neurosurgery... etc.

- There years full time in neuroradiology are necessary (the third year could be the first year of sub-specialised neuroradiology) at least two of them in continuation. Practical and theoretical training will be organised as well as research. A board examination will certify this 5 year curriculum. Adjustments to this frame have been proposed for those who would like to enter sub-specialised neuroradiology.

Paediatric, head and neck and interventional neuroradiology require specific training over 1 or 2 years. For the former, the 5 first years of the curriculum could be as follows :

- in the non neuroradiological rotations, six months in paediatric neurosurgery, six months in paediatrics (or in paediatric neurology), six months in paediatric radiology, six months in adult neuroscience or a research programme

- three years in neuroradiology, including, for example, six months in interventional neuroradiology and six months in head and neck neuroradiology. The sixth year is

considered specifically devoted to paediatric neuroradiology. Paediatric neuroradiology can be certified only at the sixth year of training.

Interventional neuroradiology considers compulsory the practice of diagnostic neuroradiology for two years following the non - neuroradiological rotations ; then two years of interventional neuroradiology are required, the first of which could be the fifth year of the training. For head and neck neuroradiology, it is recommended to enhance rotations in ENT surgery or in cancerology (one year), in interventional neuroradiology (six months) during the clinical rotations ; a year in head and neck neuroradiology should be included in the neuroradiological years. A sixth year of head and neck neuroradiology is equally suggested.

Such recommendations are examples, the detailed programmes and rotations should be flexible and include international programmes and exchanges in specific sectors of neuroradiology, where regional appropriate training facilities are not available.

GENERAL CONCLUSIONS

Some of the most senior professionals and teachers of European neuroradiology have proposed "their" optimal solutions for training in Neuroradiology. The recommendations thus made are independent of political and strategic bias and have in mind both the professional future of the trainees and patients' best interests. The group is aware that these decisions may lead to frank discussions with other related specialities.

1. The present neuroradiological training in general radiology is not sufficient, considering the number of neuroradiological examinations for radiologists working on duty shifts very early in their training.

2. The neuroradiology specialization of radiologists does not train a neuroradiologist but a general radiologist with a particular interest in neuroradiology. Albeit this training is the answer to a current need and to a widespread practice within non - specialized facilities, it would not train optimal teachers and professionals of neuroradiology.

3. All training in neuroradiology must be continuous during the proposed rotations in each curiculum. This training must be organized in neuroradiological departments, offering daily contact with the other neurological specialities.

4. It is mandatory to create a specific educational curriculum for individuals who decide early on to become neuroradiologists. It will prepare trainees for full time neuroradiological practice in neuroradiological facilities (integrated or autonomous) within institutions with neurology and neurosurgery departments. General radiology knowledge must be certified (while the training rotations in general radiology remains optional).

5. This specific training in neuroradiology extends over five of six years. It prepares trainees on all aspects of neuroradiology (adult diagnostic neuroradiology, paediatric neuroradiology, interventional neuroradiology, head and neck neuroradiology, ..).

specialised Radiology
Neuroradiology
1st year
2nd year
3th year
4th year
5th year
6th year
7th year
Ped.N
INR
neurology
neurosurgery
ENT
maxillo-facial
pediatric neurology
pediatrics
pediatric neurosurgery
....
Theoretical courses
Clinical Neuroradiology
Head & Neck, Pediatric,
Interventional, Geriatric, ...
(200 hr. OVER 2 YEARS)
General or pediatric radiology
Optional (clinical, ...)
Clinical sp. > 1,5 y
Clinical Neuroradiology
Head & Neck > 2 y
Sub - specialised Neuroradiology

FOR MORE INFORMATION PLEASE CONTACT

PHILIPS MEDICAL SYSTEMS

- TEL. 745-4090 Ext. 3332
- FAX. 398-0792

Philips Electronics (Thailand) Ltd.
209/2 Sanpavuth Road, Prakanong, Bangkok 10260

PHILIPS

Let's make things better.

PERIPHERAL ANEURYSMS WITH A REVIEW OF THE LITERATURES

Darunee BOONJUNWETWAT, M.D.* Orapin MOOKDADILOK, M.D.*

Peripheral artery aneurysms may be defined as a significant widening of a segment of a peripheral artery. They can be classified in two groups: true and false aneurysms. True aneurysms are the result as atheromatous degeneration in the wall of the artery. False aneurysms arise from rupture in the arterial wall not necessarily associated with atheromatous disease.

The availability of recent imaging modalities enables the correct diagnosis of an aneurysm to be easily made. Objectives of our report are :

1. To raise an awareness that a mass at an unexpected location, though rarity, could be an aneurysm, as in our 4 presenting cases.
2. To demonstrate and compare the acuity and practical use of various imaging modalities in detection of a peripheral aneurysm including arteriography, magnetic resonance imaging and angiography (MRI and MRA), and Doppler imaging.

CASE REPORTS

Case 1 : A 66-year-old chinese woman presented with a slow-growing retromalleolar mass of the left ankle of 3 years duration. There was clinical doubt as to whether this represented a ganglion cyst or an aneurysm. Doppler color imaging (DCI) (Fig.1) clearly showed an eccentric vascular mass with calcified wall connecting with the left posterior tibial artery. After aneurysmectomy with end to end anastomosis, an aneurysm was resected and its three composing layers of the wall proves that this mass is a true aneurysm of the posterior tibial artery.

Case 2 : A 15-year-old Thai man presented with a right lower neck mass, associated with right Horner syndrome of 2 weeks duration. Arteriography (Fig. 2A) revealed a 5 cm saccular aneurysm of the second part of right subclavian artery. Surgery was performed by ligation of the neck of the aneurysm with bypass venous graft from the right common carotid artery to the right subclavian artery distal to the lesion. About 2 weeks after operation, DCI was requested for evalution. Unfortunately, a 3 cm recurrent saccular aneurysm was evident originating at the previous location with patent turbulent flow through the bypassed vein. (Fig. 2B)

Case 3 : A 46-year-old Thai woman, with underlying condition of neurofibromatosis, presented with a painful and pulsatile mass below left angle of mandible for 2 months. MRA, arteriography, and DCI (Fig. 3A, 3B, and 3C), all identified a long tortuous segment of fusiform aneurysm of the left internal carotid artery extending from just distal to the left common carotid bifurcation to its entrance to the petrous bone. Operation, aneurysmectomy with saphenous vein graft, was done.

Case 4 : A 58-year-old Thai woman presented with a firm cervical mass below the left

DCI = Doppler Color Imaging

*Department of Radiology, Faculty of Medicine, Chulalongkorn University, Bangkok Thailand.

angle of mandible for 2 years duration. This mass was first thought to be most likely a carotid body tumor due to its location and chance probability. MRI and MRA of the neck (Fig. 4A, 4B, 4C, and 4D) reveal a hypervascular mass near the bifurcation of left common carotid artery. It is still difficult to distinguish between a hypervascular tumor and an aneurysm; thus, arteriography and DCI (Fig. 4E and 4F) were performed. Both of them accurately showed that this mass was a large well defined aneurysm extending from the left internal carotid artery just distal to the bifurcation. After careful preoperative evaluation, aneurysmectomy and repairment of the anastomosis with the left saphenous vein was executed with favorable result and no complication.

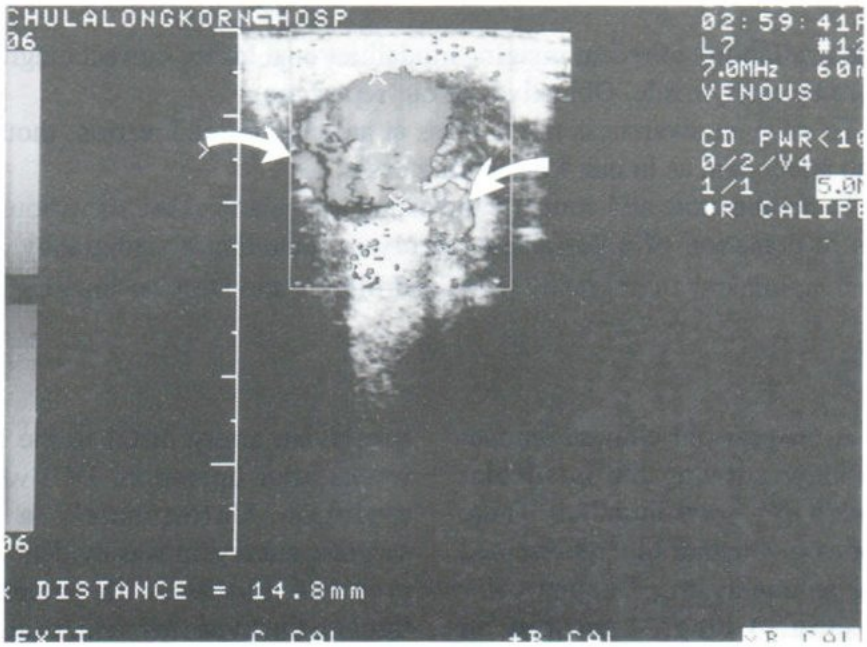

Fig. 1 DCI shows swirling flow pattern within a 2.8 cm mass originating from left posterior tibial artery. Evidence of afferent and efferent vascular dilatation to and fro from this mass is also noted. (arrows)

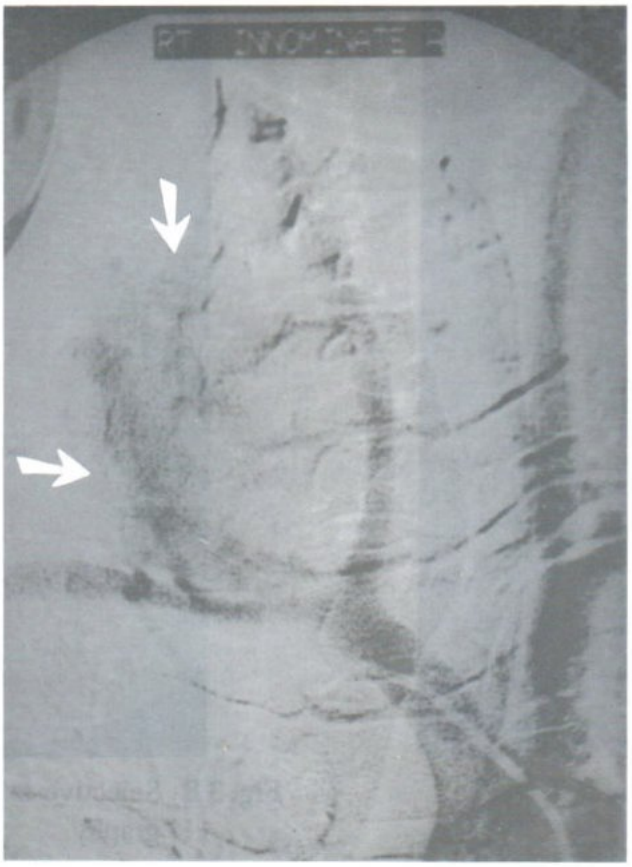

Fig. 2 A Selective right subclavian arteriogram reveals an aneurysm at its second part. (arrows)

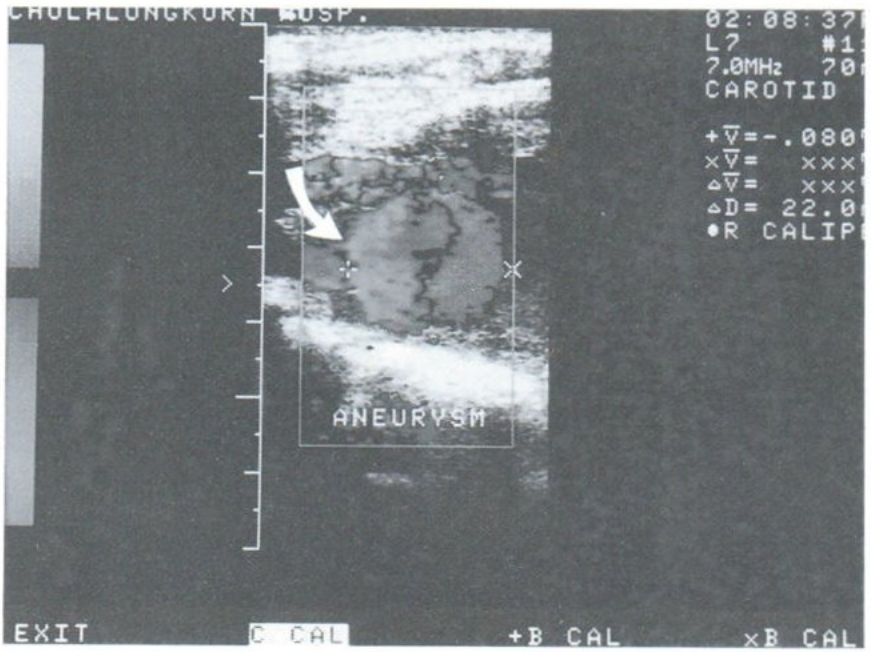

Fig. 2 B DCI performing 2 weeks following ligated neck of the aneurysm of right subclavain artery demonstrates a 3.1 cm aneurysm originating from the right subclavian artery and patent turbulent flow through the bypassed vein, suggestive of a recurrent aneurysm. (arrows)

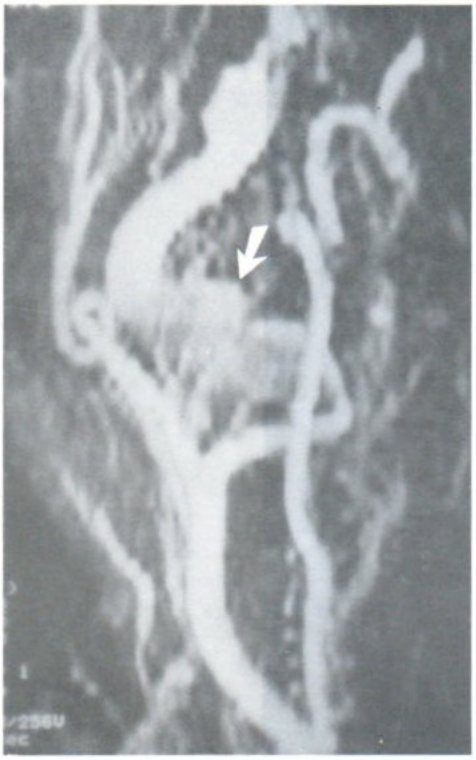

Fig. 3 A MRI lateral view

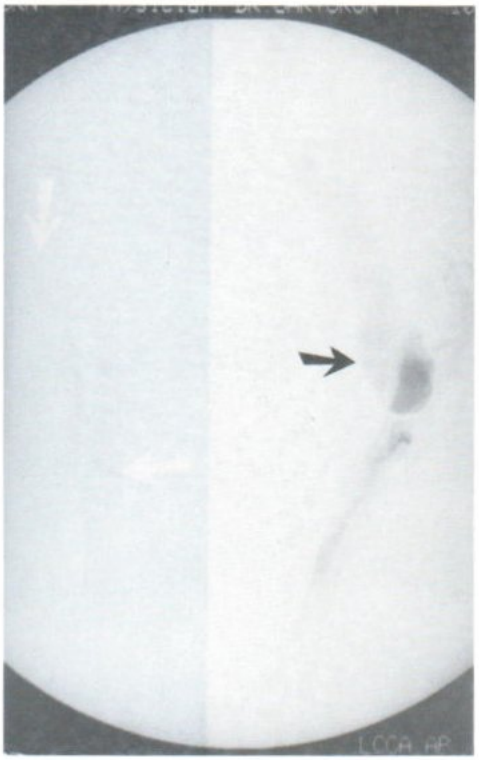

Fig. 3 B Selective left common carotid arteriography

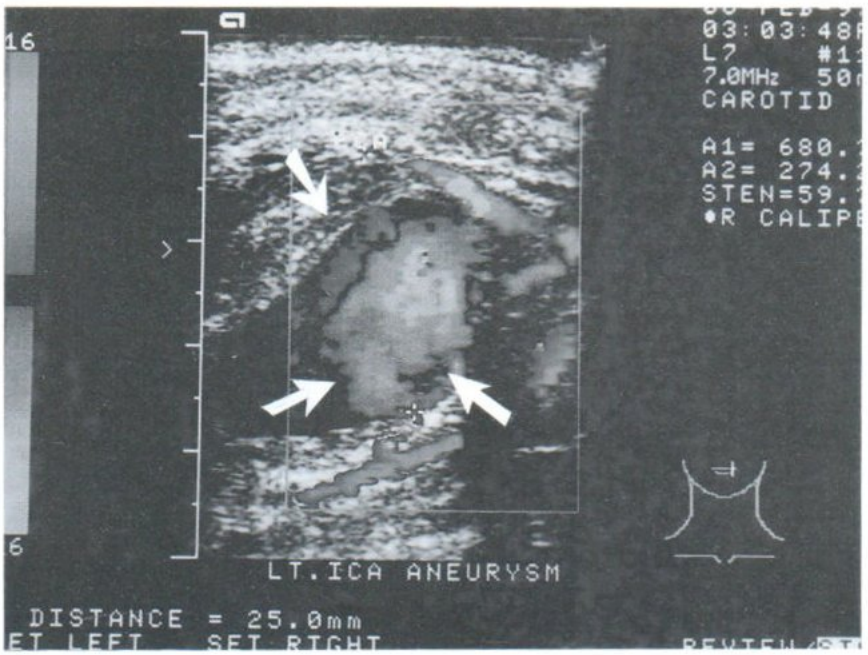

Fig. 3 C DCI, all clearly illustrate that a mass below the left angle of the mandible is a long tortuous segment of a fusiform aneurysm of the left internal carotid artery. Thick wall and internal thrombus are also seen. (arrows)

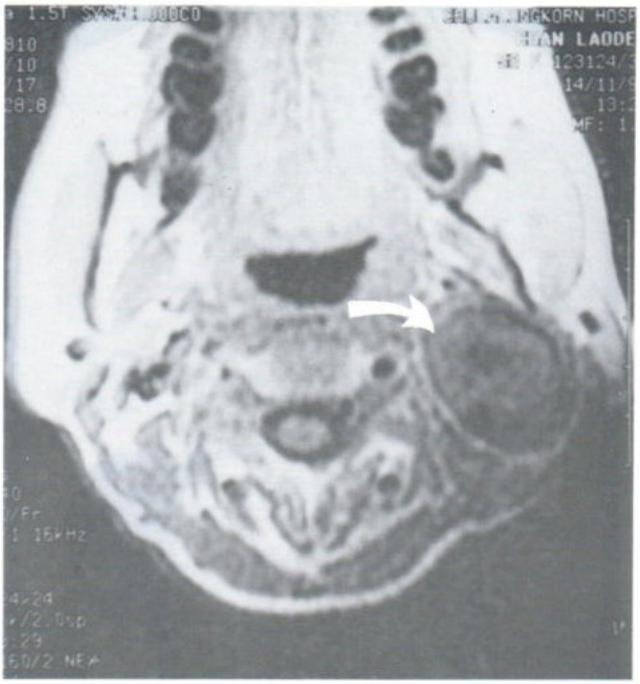

4A

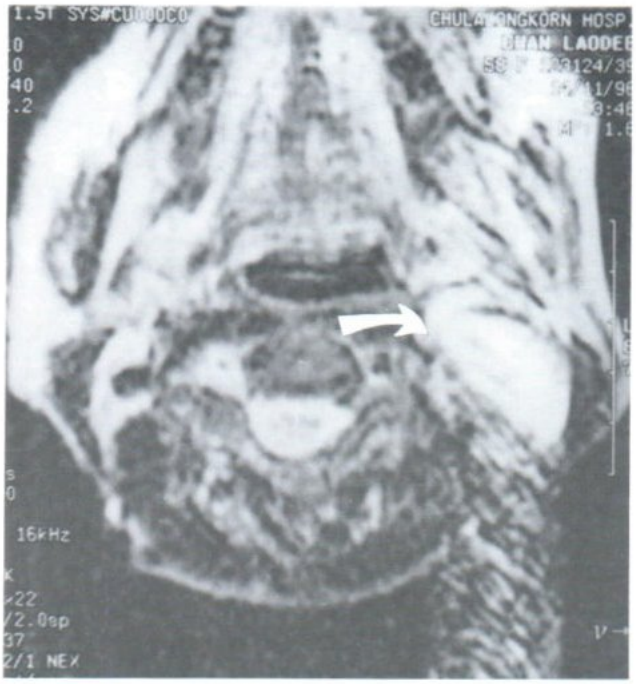

4B

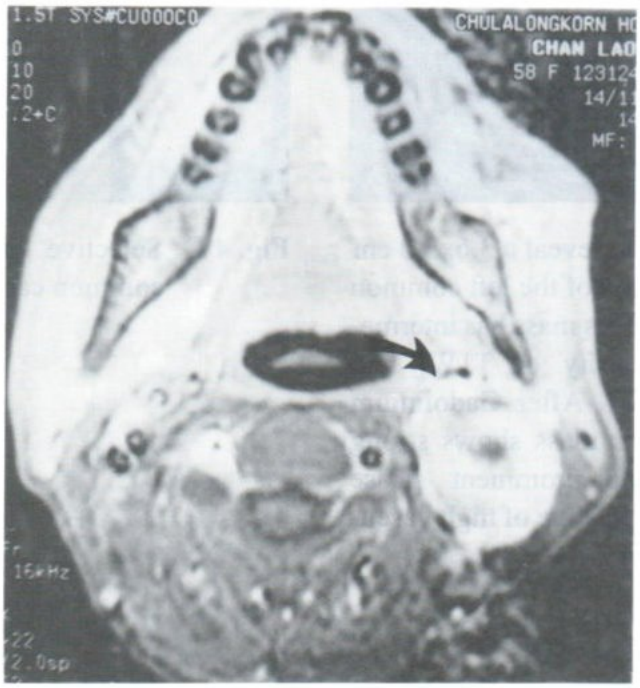

4C

Fig. 4 A, 4 B, 4 C T1WI, T2WI and T1WI with Gadolinium enhancement and fat suppression of MRI

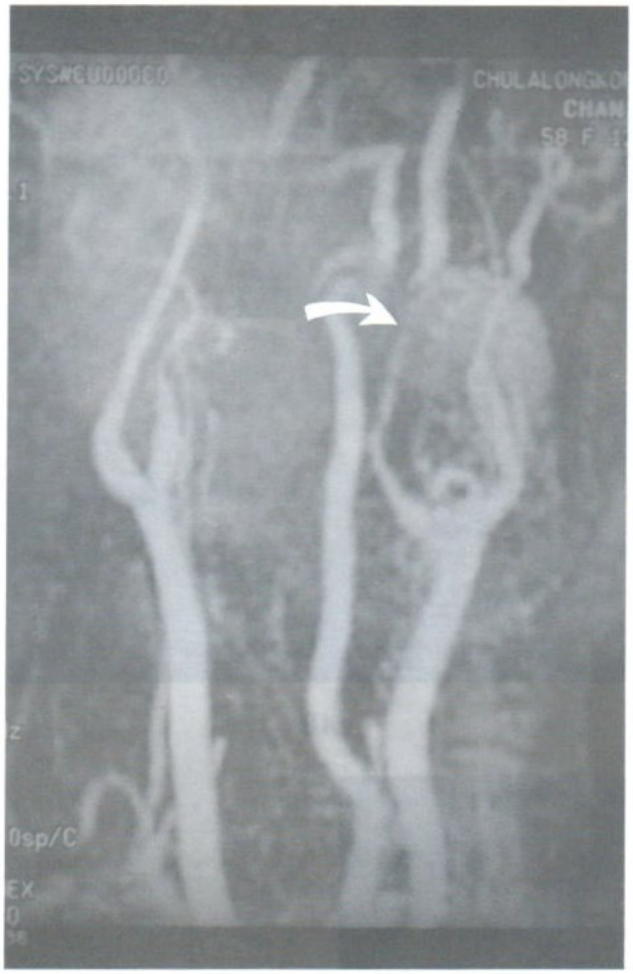

Fig. 4 D MRA of the neck, reveal a 3.6x3.0 cm mass at bifurcation of the left common carotid artery. This mass has intermediate signal intensity on T1WI, and bright SI on T2WI. After Gadolinium enhancement, this mass shows strong enhancement and prominent phase shift artifact, suggestive of high vascular flow of it. (arrows)

Fig. 4 E Selective arteriography of the left common carotid artery.

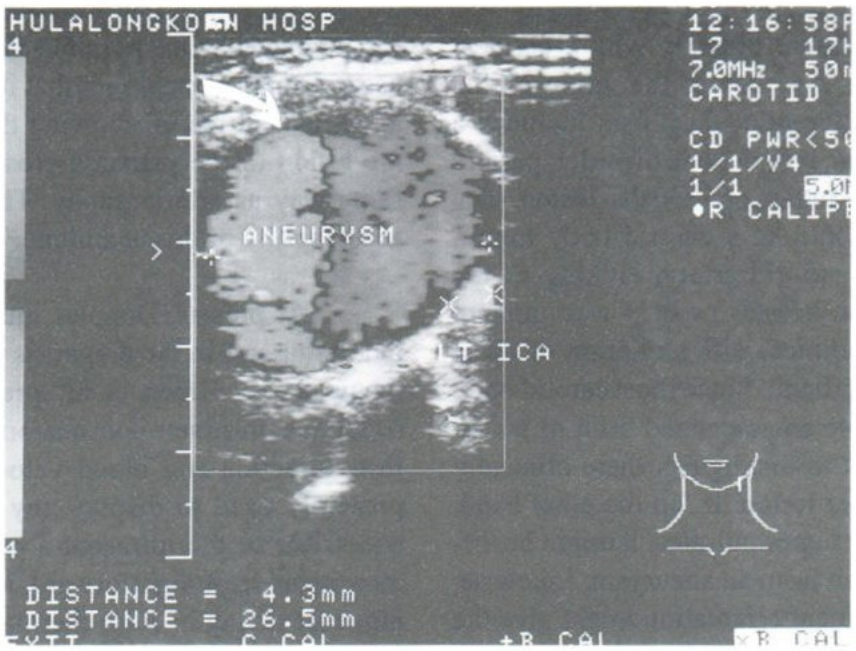

Fig. 4 F DCI, confirm that a large well defined aneurysm has origin from a left internal carotid artery. (arrows)

DISCUSSION

All our 4 presenting cases are rare. Reports of posterior tibial artery aneurysms, as reviewed by Monig et al in 1996, are 6 cases up to that time.[1] Most cases result from trauma. In contrast to traumatic aneurysm, nontraumatic aneurysms are seldom encountered.[1-4] True aneurysms of this artery are very rare and are sporadically reported. To our knowledge, there are 2 reports of true aneurysm of posterior tibial artery. One by Katz et al[2] and the other by Chaillon et al,[3] and both are associated with an underlying systemic disease (one with presence of a lupus-like syndrome and the other with a Behcet's disease). However, a case of us (case 1) showed no obvious evidence of any systemic disease after screening check up. The aneurysms arising in an aberrent subclavian artery are rare; there were 31 cases reported in the literature which had been reviewed by Austin et al in 1985.[5] However, those not arising from a subclavian artery as in a case of us (case 2), also aneurysms of the cervical portion of the internal carotid artery are very uncommon lesions. Beall et al found just 7 aneurysms of the extracranial carotid artery among 2300 procedures for aneurysms performed at Baylor. Raphael et al reported 6 carotid artery aneurysms at the Mayo Clinic from 1936 to 1960.[6] A prospective study of the clinical suspected vascular lesions at the carotid bifurcation by Barry et al,[7] over a 3-year period (1987-1991) of 50 patients revealed just 5 aneurysms. Therefore, our cases illustrate the importance of awareness as well as a high index of suspicion for the diagnosis of peripheral aneurysm, although uncommon.

Peripheral aneurysms may increase in size to cause local symptoms, be a source of distal emboli, thrombose with resulting ischemia of the limb and, occasionally, rupture. The ominous importance of these potential complications justifies emphasis on early recognition and treatment.[8]

When a patient presents with a cervical mass (as in case 2-4) below the angle of the mandible, the differential diagnosis includes a branchial cleft cyst, lymph node disorder, parotid tumor, soft tissue tumor or vascular lesion. The vascular lesion could be a carotid body tumor, aneurysm of the corotid artery, kinking of the carotid bifurcation vessels or only a prominent bifurcation. The clinical differentiation of these lesions could be difficult. Since most carotid body tumors do not have an associated bruit of pulsation, it is difficult to distinguish them clinically from a nonvascular lesion. If, on the other hand, the carotid body tumor pulsates, it might be difficult to distinguish from an aneurysm. Likewise, a kinked or prominent bifurcation might give the clinical impression of an aneurysm.[7] Also, due to the rare incidence of a posterior tibial aneurysm when compares with other possibility such as a more common ganglion cyst, the differentiation of a retromalleolar mass is usually difficult if there is no aid from modern imaging such as noninvasive DCI (as in case 1). Our report shows how various imagings can be used to confirm diagnosis of peripheral aneurysm when clinical doubt exists. Preoperative evaluation is necessary and often involves investigations such as Computer tomography (CT), MRI, MRA, arteriography, fine-needle aspiration biopsy, and Doppler imaging.

Among various helpful modalities, arteriography gives important information about the condition of the proximal arterial branches and the outflow tract, and therefore gives information about possibilities for reconstruction.[1] However, it is considered to be complicated and invasive method. In doubtful cases, CT, MRI, MRA can give further information but they also are expensive investigations. The availability of Doppler imaging provides a noninvasive and relatively inexpensive way of detecting the size and extent of the lesion and, in some institutions, is replacing arteriography[7,9] for those vessels that can be imaged. One possible disadvantage of the use of Doppler imaging is that it does not provide a permanent record showing the relationship of the lesion to the patient's gross anatomy in the same way as arteriography. This may limit the acceptability of this technique.[9]

At present, Doppler imaging is a steadily increasing use in the diagnosis of peripheral soft tissue mass. Green et al[9] presented that this technique illustrates both anatomical detail, blood flow direction and blood velocity spectra. It is presently used to display any arterial segment accessible to the ultrasound probe. DCI makes interpretation straightforward, less time consuming, cost saving in color thermal paper and more reliable, and also is of similar diagnostic value as arteriography.[9] Moreover, the prospective study of Barry et al[7] states that they believe that patients with lesions at the carotid bifurcation of suspected vascular origin should be initially investigated by Doppler imaging and clearly arteriography in these patients can be eliminated. This study found that 11 cases of carotid body tumors have a very high blood flow resulting in a vascular bed with a low resistance. The 'normal' (without a carotid body tumor) external carotid artery supplies a high resistance distal bed. Since a corotid body tumor is primarily supplied by branches of the external carotid artery, its presence would result in reduction of the resistance index in this vessels. Thrombus in an aneurysm might also look like a carotid body tumor but there is no flow in the thrombus. Our experience, as in case 4, advocates this statement. Case 4 of us was underwent almost all vascular imaging modalities. DCI has shown superior data to MRI and MRA which have some problems in discrimination between a high flow of vascular tumor and an aneurysm due to both lesions can cause phase shift artifact and similar signal intensity. Also, DCI is able to give equal information to arteriography but is less invasive and time consuming. Further studies comparing composite Doppler imaging with

arteriography should define the group of patients where invasive diagnosis can be avoided (as in case 1 and 4). Thus, as a trend at present, Doppler imaging might be a favorable first choice for clarifying of a suspected peripheral aneurysm.

REFERENCE

1. S.P. Monig, M. Walter, S. Sorgatz, et al. Ture infrapopliteal artery aneurysms : report of two cases and literature review. J Vasc Surg 1996; 24 : 276-278
2. S.G. Katz, R. D. Kohl, and N. Razack. Bilateral infrapopliteal artery aneurysms. Ann Vasc Surg 1992;6:168-171
3. P. Chaillon, P. Patra, S. Noel, et al. Behcet's disease revealed by double peripheral arterial involvement. Ann Vasc Surg 1992;6:160-163
4. P. Edwards, and L. Kurth. Posterior tibial pseudoaneurysm after calcaneus fracture: A case report. Foot and ankle 1992;13,2: 93-95
5. E.H. Austin, and W.G. Wolfe. Aneurysm of aberrant subclavian artery with a review of the literature. J Vasc Surg 1985;2:571-577
6. D. S. Haynes, M.K. Schwaber, and J.L. Netterville. Internal carotid artery aneurysms presenting as neck masses. Otolaryngology-head and neck surg 1992; 107,6:787-791
7. R. Barry, N.G. Browning, and C.J.C. Nel. Duplex Doppler investigation of suspected vascular lesions at the carotid bifurcation. Ann Vasc Surg 1993;7:140-144
8. J.C. Mayall, R.C. Mayll, A.C.D.G. Mayall, et al. Peripheral aneurysms. Int Angiol 1991;10:141-145
9. I.R. Green, N.J. Dudley, and N. Gravill. Presentation of color flow maps of the peripheral circulation. The British J of Radiology 1994; 67 : 689-694

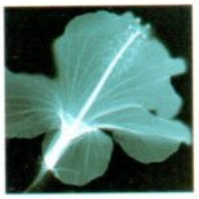

EDUCATION

Asian-Oceanian Seminars on Diagnostic and Interventional Radiology

1 9 9 9

Abdominal Imaging
February 12-13
Dhaka, Bangladesh
Programme Leader:
A.S.Q. Md. Sadeque

Musculo-Skeletal Radiology and Mammography
April 17-18
Singapore
Programme Leader:
J. Hoe

BRACCO
INTERNATIONAL

For further information please contact:
Huntington Communications Pte Ltd
47 Hill Street #07-03
S.C.C.C.I. Building
Singapore 179365
Tel: ++65-339 2883
Fax: ++65-339 2272
E-mail: hcompr@singnet.com.sg

http://www.bracco.com

OCCULT BREAST CARCINOMA PRESENTING WITH AXILLARY METASTASES (A CASE REPORT WITH LITERATURE REVIEWS)

Darunee BOONJUNWETWAT, MD* Kaesorn VAJARAPONGSE, MD*
Wipawan KEERATIKASIKORN ,MD* Pichet SAMPATANUKUL, MD**

The presentation of axillary metastases as the first sign with no breast symptom or lesion is quite rare found less than 1 percent.[1,2] Occult breast carcinoma was first described by Halsted in 1907.[3] The histopathology obtained by axillary node biopsy provides the important guidance for the primary origin. Owing to the lack of breast lesion, the treatment role is controversy for the surgeons to perform the radical mastectomy. Several reports recommended to treat the patient as a stage 2 breast cancer.[4,5] We report a case of histopathological proved metastases from breast carcinoma without breast lesion demonstrated. The purposes of this report are to illustrate the imaging features including mammography, ultrasonography and MRI, and to discuss the differential diagnosis, roles of treatment and literature reviews.

CASE REPORT

A woman aged 54 years old, complained of self palpated mass at left axillary area for 5 months with occasional tenderness. She had no abnormal sign and symptom of both breasts. Physical examination revealed large mass at left axillary area about 5-6 cm. in diameter. There was no definite mass or lesion palpated in both breasts. FNA of left axillary nodes was proceeded and turned out to be malignant cells. Multiple true cut biopsies were performed. The histopathology revealed metastatic carcinoma to lymph node, primary origin likely from mammary ductal carcinoma (Fig. 1A,B). The ER and PR immuno-staining were negative. Mammography showed multiple dense masses at left axillary area with well defined oval shape, contained pleomorphic clustered microcalcifications suggestive of pathologic nodes. The largest mass measured 5x6 cm. The fibroglandular tissues of both breasts revealed normal (Fig. 2A,B). Ultrasonography showed low echoic masses at left axillary area contained spots of bright echoes suggestive of calcifications (Fig. 3A). Supplement color doppler study demonstrated increased vascularity of the masses (Fig. 3B). No mass or cyst was found in both breasts. The MRI showed multiple masses at left axillary area, with low signal intensity on T1WI and high signal intensity on T2WI. There was enhancement of the masses after Gd DTPA contrast injection (Fig. 4A,B). No lesion of both breasts was confirmed. In addition, the sonography of the whole abdomen and bone scan revealed no malignancy. The staging of the carcinoma in this patient was assigned T0N2M0. The patient was treated with systemic chemotherapy, resulting in regression in size of the nodes, followed by axillary nodes dissection and total breast irradiation.

FNA = Fine Needle Aspiration
ER = Estrogen Receptor
PR = Progestrogen Receptor

* Department of Radiology, Faculty of Medicine, Chulalongkorn University, Bangkok, THAILAND.
** Department of Pathology, Faculty of Medicine, Chulalongkorn University, Bangkok, THAILAND.

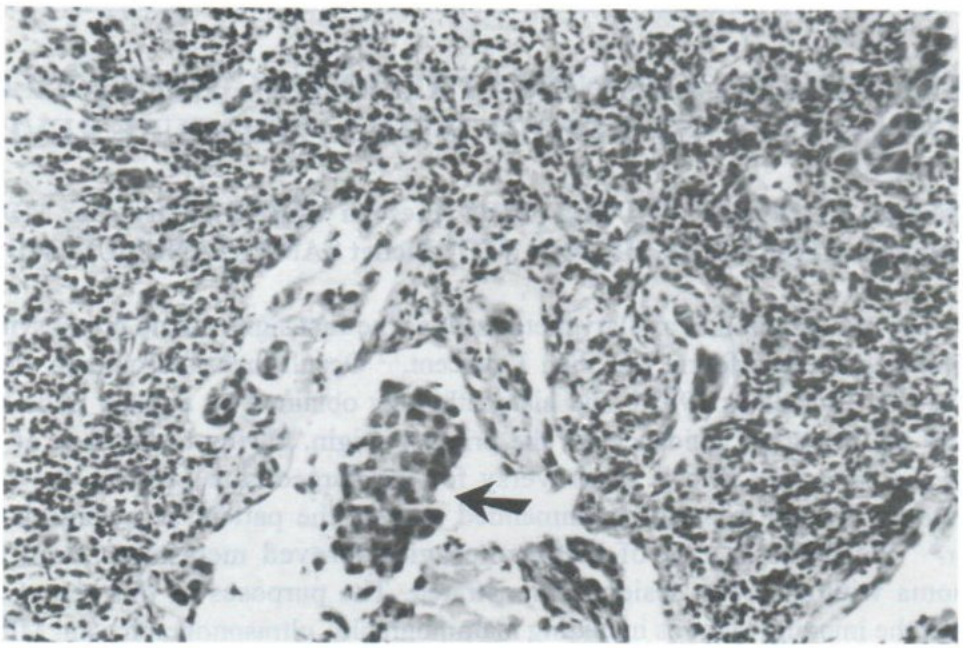

1A

Fig. 1A Demonstration of malignant cells (arrow) occuring in small and large clusters floating in the lymphnode sinuses. (H and E x 200)

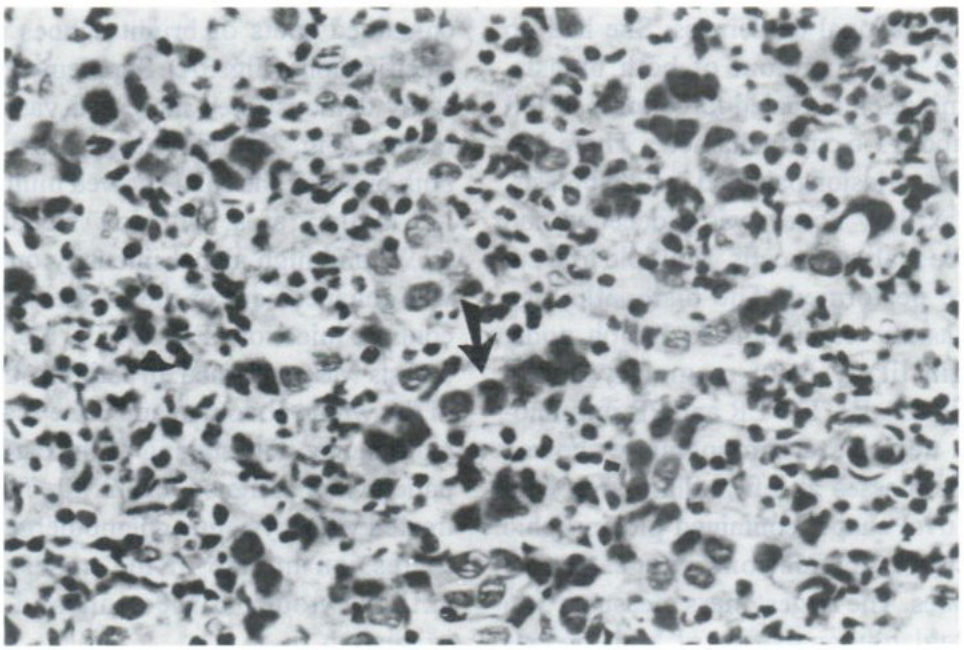

1B

Fig. 1B Illustration of malignant cells with Indian's file arrangement (arrow), the characteristic growth pattern that described in invasive carcinima of breast. (H and E x 400)

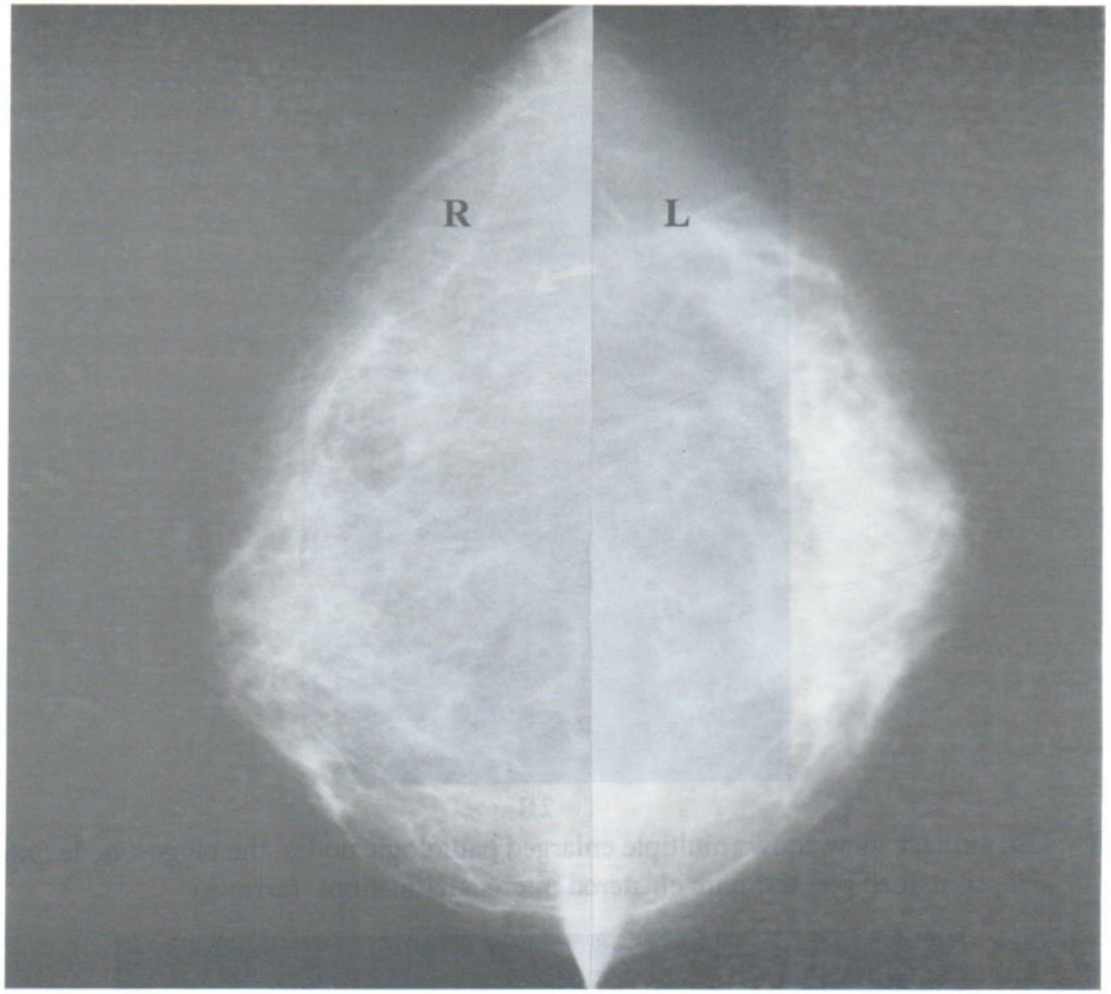

2A

Fig. 2A Mammography, craniocaudal view, showed normal fibroglandular tissue of both breasts.

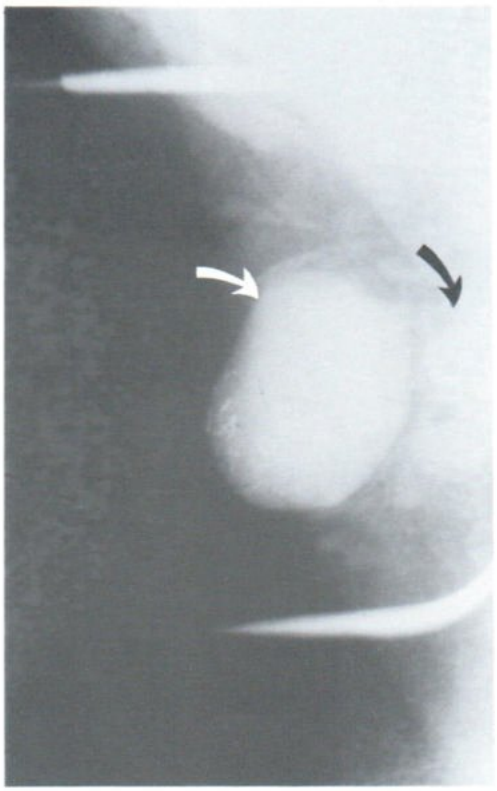

2B

Fig. 2B Left axillary view shows multiple enlarged pathologic nodes, the biggest node 5x6 CM. In size, contained pleomorphic clustered microcalcifications. (arrows)

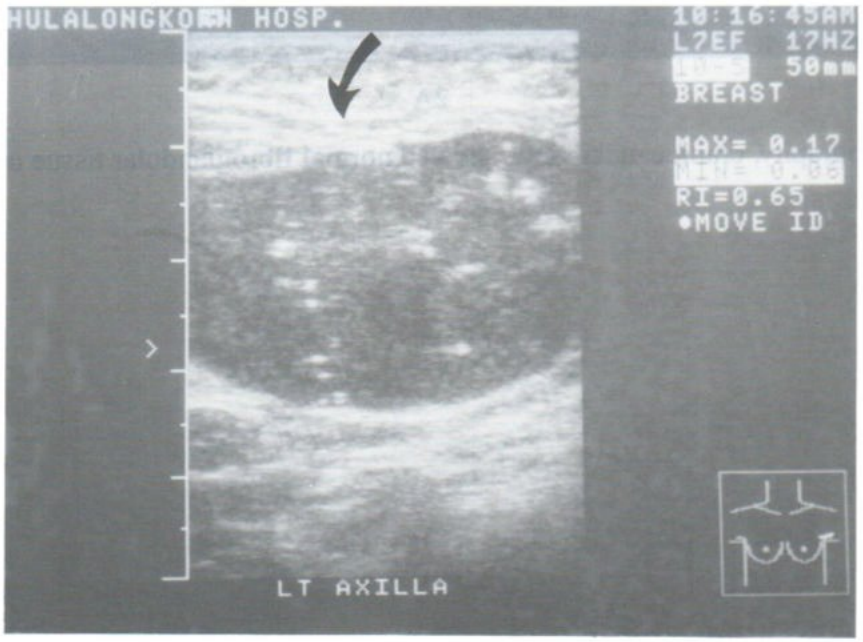

3A

Fig. 3A Ultrasonography of left axilla showed multiple low echoic masses with bright spots in the big mass suggestive of calcifications. (arrow)

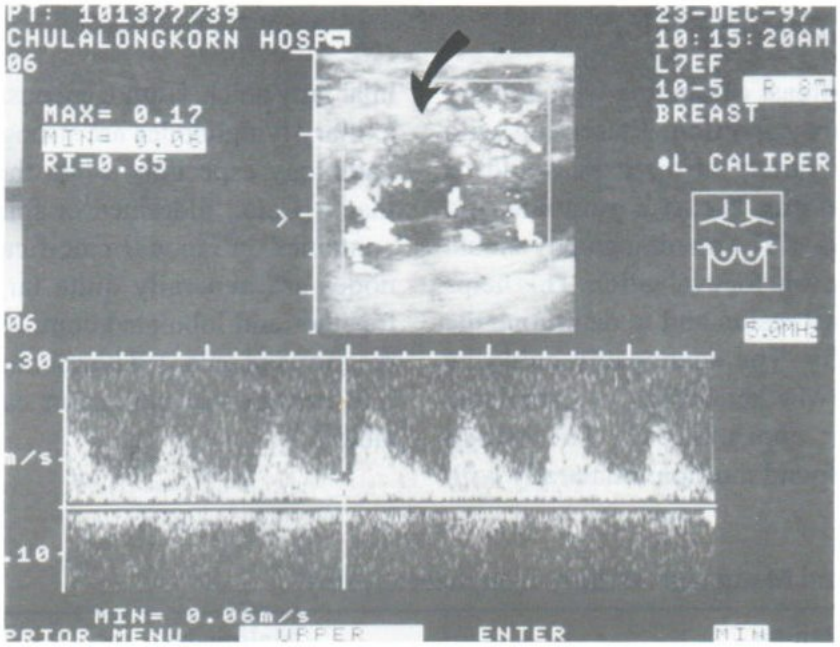

3B

Fig. 3B Color doppler of left axillary masses showed highly vascularity with arterial flow. (arrow)

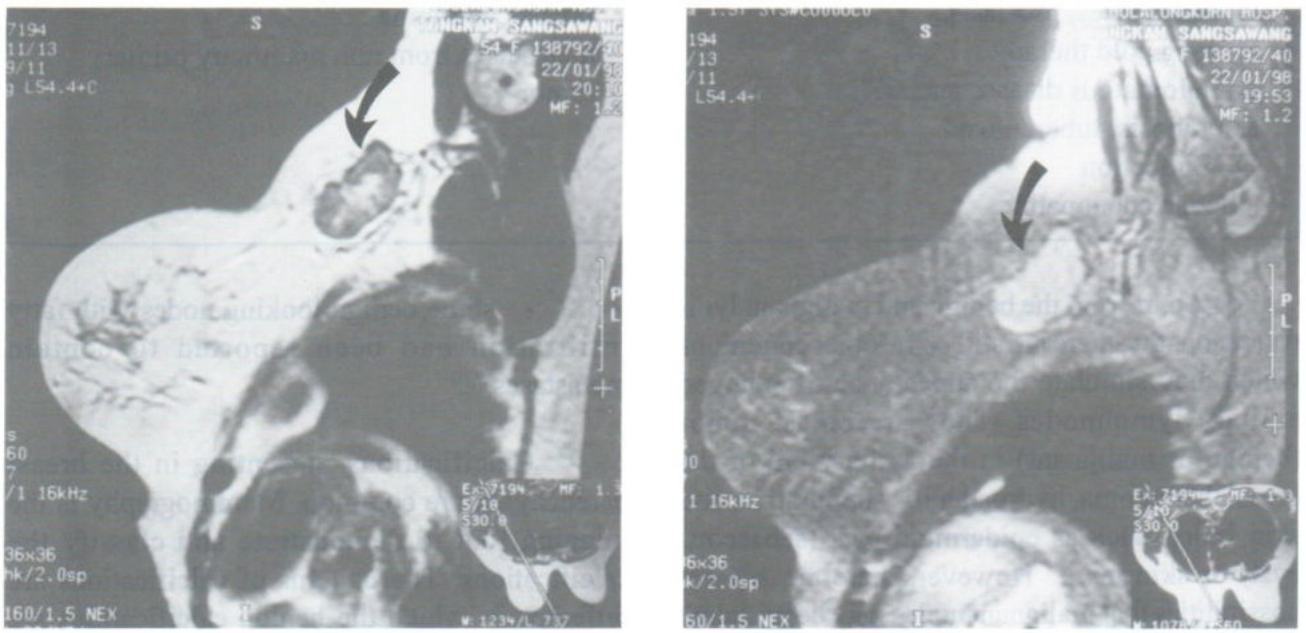

4A 4B

Fig. 4A,B MRI of left breast including axilla (oblique sagittal view) showed multiple masses at left axilla (arrow) with low signal intensity on T1WI (A), high signal intensity on T2WI and getting enhancement after Gd DTPA contrast injection (B). Hemorrhage was seen the biggest node due to recent biopsy performed.

DISCUSSION

An occult breast carcinoma with axillary metastases is a rare condition. Presenting with axillary masses, a variety of diseases would be encountered including breast carcinoma and extramammary causes. The mammography should be the first imaging role for evaluation. This helps to exclude the breast lesion and to determine the axillary adenopathy. The adenopathy could be judged accurately whether benign or pathologic by mammographic appearances.[6,7] The benign nodes are usually found multiple bilaterally with hilar fatty notch. Homogeneously dense (non fatty) axillary lymphnodes are strongly associated with pathology especially when the nodes are larger than 3.3 cm., illdefined or spiculated margin, or contained intranodal calcifications.[8] Malignant nodes are generally quite large, dense, matted together and lobulated contour.[7] The differential diagnosis of enlarged lymphnodes can be grouped into benign and malignant causes as shown in table 1.[6]

Table1. Benign and Malignant Axillary Lymphadenopathy

Benign	Malignant
- acute or chronic inflammation. - arthritic diseases such as : rheumatoid arthritis, systemic lupus erythematoses, psoriasis. - prolong gold therapy - granulomatous disease such as : sarcoidosis, tuberculosis - HIV infection - silicone adenopathy	- lymphoproliferative disease such as : Hodgkin's, non-Hodgkin's lymphoma, leukemia - breast carcinoma - metastases from non mammary primary tumor

Apart from the benign and malignant lymphadenopathy, there are still some other conditions which may simulate the appearance of enlarged axillary lymphnodes. They are breast tumor (benign or malignant) in the axillary tail of the breast, hematoma, hydroadenitis suppurativa, and skin lesion such as epidermoid cyst (sebaceous cyst) or skin nevi. However, there are several possibilities that malignant nodes may be mistaken for benign nodes and vice versa such as :

- the nodes in lymphoma and lymphoid hyperplasia have similar appearance.[6]
- the gold deposition in gold treated rheumatoid arthritis may mimic microcalcifications of malignant nodes.[6]
- some benign looking nodes with fatty infiltration had been reported to contain metastases.[9,10]

Calcifications presenting in the breast parenchyma are common. Mammography is the imaging tool to demonstrate and classify the calcifications. The patterns of calcifications are different, in which the benign calcifications are larger and more likely to be round, monomorphic (uniform in size and shape), and to be scattered as compared to the malignant calcifications which are grouped or clustered, pleomorphic (varying in shape and size), numerous and almost always close together.

A group containing less than five calcifications is unlikely to represent malignancy.[11] On the other hand, the calcification found in axillary lymphnode is extremely rare. Large calcifications in axillary lymphnodes are of no importance. When fine irregular calcifications are present in axillary lymphnodes indicate pathology, commonly caused by metastases and gold deposition in women treated with gold for rheumatoid arthritis.[12,13] As in our case report showed the evidence of pathologic nodes contained pleomorphic clustered microcalcifications.

The microscopic features of the metastatic nodes are devided into three types. The first is large apocrine cell (65%). The second is mammary carcinoma pattern with comedo, cribiform and infiltrating (20%) and the third is mixed pattern.[5] Our case had the histopathology the same as the second type.

In a series of 29 cases of occult breast carcinoma manifested first as the enlarged axillary node, positive or suspicious mammography can lead to the primary tumor in 75% of patient, but when negative does not exclude the breast as the source of carcinoma. A carcinoma of the breast was found by pathologic examination in 44% of patients with negative mammograms. In another series,[14] 48 patients presented with axillary mass which proved to be metastatic carcinoma, the mammography was suspicious or positive for primary breast carcinoma in 24% and negative in 76%[4] All patient received mastectomy and axillary dissection. A primary tumor was histologically found in the breast in 75%. Consequently, the occult breast carcinoma with axillary metastasis is still most likely diagnosis, even though the search for primary tumor was negative, as in our case. The disease is graded as the stage 2 breast carcinoma. Role of treatment from literature reviews recommended combination of mastectomy, radiation and chemotherapy.[4,5] A 5 year survival of disease free was 73%.[5] The prognosis is similar or better than the ordinary stage 2 breast carcinoma. For our case, she was treated with systemic chemotherapy, followed by total node dissection and total breast irradiation. In conclusion, when a patient presenting with axillary adenopathy, the mammography helps to distinguish the benign and pathologic nodes, as well as to exclude the breast lesion. Besides, the histopathology plays the important role in the reading of the etiology and primary origin for further proper management.

REFERENCES

1. William T.Fitts JR, Steiner GC, Enterline HT. Prognosis of occult carcinoma of the breast. American journal of surgery 1963;-106:460-463.
2. Larsen RR,Sawyer KC,Sawyer RB, Torres RC. Occult carcinoma of the breast. American journal of surgery 1964;107: 553-555.
3. Halsted WS. The results of radical operations for the cure of carcinoma of the breast. Annal of surgery 1907;45:1
4. Rosen PP, Kimmel M. Occult breast carcinoma presenting with axillary lymph node metastasis. Human pathology 1990; 21:518-523.
5. Rosen PP, Oberman HA. Unusual clinical presentation of carcinoma. In : Tumors of mammary gland. AFIP, 1993:261-265.
6. Leibman. A.J. and Wong R. Finding on mammography in the axilla. AJR 1997;-169:1385-1390.
7. Kalisher L. Xeroradiography of axillary lymph node disease.Radiology 1975;114:-67-71.
8. Walsh R,Korngunth P J,Soo M S,Bentley R, DeLong D M. Axillary Lymph nodes: Mammographic, pathologic and Clinical Correlation. AJR 1997;168:33-38.

9. Leborgne R, Leborgne F, Leborgne JR. Soft tissue radiolography of axillary nodes with fatty infiltration. AJR 1965;84:513-515.
10. Leborgne R, Leborgne F, Leborgne JR. Soft tissue radiography of the axilla in cancer of the breast. BRIT. J RADIOL, 1963;36:494-496
11. Bassett L W. Mammographic analysis of calcifications. Radiologic clinics of north america 1992;30:93-105.
12. Helvie MA, Rebner M, Sickles EA and Oberman HA. Calcification in metastatic breast carcinoma in axillary lymphnodes. AJR 1988;151:921-922.
13. Bruwer A, Nelson GW, Spark RP. Punctate intranodal gold deposits simulating microcalcifications on mammograms. Radiology 1987;163:87-88
14. Patel J, Nemoto T, Rosner D, Dao T, Pickren JW. Axillary lymph node metastases from an occult breast cancer. Cancer 1981;47:2923-2927.

SONOGRAPHIC PARAMETERS OF QUADRICEPS MUSCLE AND BONE MINERAL DENSITY OF THE HIP: A STUDY IN NORMAL THAI ADOLESCENTS

Suphaneewan JAOVISIDHA MD.[1] Suthiwan KWANBUNBUMPEN Ph.D.[2]
Rojana SIRISRIRO MD.[1] Parichard ROJANAPLAKORN M.Sc. (Bios)[3]
Puangthong KRAIPIBOON MD.[1]

ABSTRACT

Purpose. To study the correlation between sonographically measured parameters of quadriceps muscle and bone mineral density (BMD) of proximal femur in normal Thai adolescents. **Material and Methods.** Fifty-seven school children and normal adolescents were included in this study (30 males, aged 10-17 years old [mean age = 13.2 years old]; and 27 females, aged 9-18 years old [mean age = 13.1 years old]). All subjects were undergone sonographic measurement of thickness, circumference, and cross-sectional area (CSA) of quadriceps muscle as well as thickness of subcutaneous fat of non-dominant thigh. Ipsilateral proximal femoral BMD was measured using Dual-energy X-ray absorptiometry (DEXA). Spearman Rank Correlation and Pearson Product Moment Correlation were used for statistical analysis. **Results and Conclusion.** In females, all quadriceps parameters showed statistically significant correlation ($p<.001 - p<.05$; muscle circumference showed the best correlation) with proximal femoral BMD at all ROIs. In male subjects, the quadriceps parameters showed significant correlation ($p<.01 - p<.05$) with BMD of the femoral neck & the trochanter. No significant correlation was found between quadriceps parameters and BMD of Ward's triangle and thickness of subcutaneous fat.

INTRODUCTION

Real-time sonography has been proved to be a useful imaging technique for the visualization of normal and pathological muscle tissue.[1] The main advantages of the technique are that it is painless, non-invasive, harmless, and can be easily repeated to study the course of disease.[2-5] The quadriceps femoris muscle was frequently chosen to be studied because it is easily accessible and identifiable and not adjacent to femur, which excludes echo reflection of the bone-tissue interface.[6] The thickness of quadriceps muscle measured by ultrasound (US) was reported to change relating to certain diseases i.e., muscular dystrophy[1,7] and multiple organs failure.[8] Significant relationship was found between quadriceps muscle thickness and body weight in adult.[9] Cross-sectional area (CSA) of quadriceps muscle has also been widely studied, particularly in relation to muscle strength.[10-15]

ROI = Region of Interest.

[1] Department of Radiology, Ramathibodi Hospital, Mahidol University, Rama 6 street, Bangkok 10400, Thailand
[2] Department of Graduate Studies, Mahidol University, BKK.
[3] Department of Nursing, Ramathibodi hospital, BKK.

The purposes of this study were to determine the correlation between sonographically measured parameters of quadriceps muscle (the thickness, circumference, and cross-sectional area [CSA]) and bone mineral density (BMD) of the proximal femur and thickness of subcutaneous fat in normal Thai adolescents.

MATERIAL AND METHODS

This study is a part of a larger study on the effect of physical activity on musculoskeletal growth in Thai adolescents. Fifty-eight untrained, normal subjects were included in this study (30 males and 28 females). The age range in male subjects was 10-17 years old (mean age = 13.2 years old); and in females was 9-18 years old (mean age = 13.1 years old). All subjects were undergone sonographic measurement of the thickness, circumference, and cross-sectional area (CSA) of quadriceps muscle as well as the thickness of subcutaneous fat (Figure 1). Because we did measurement only on the non-dominant (left) thigh, one female subject who had non-dominant right side was excluded from the study.

Sonographic measurement. The ultrasound imaging was obtained by gray-scale system of the real-time scanner (Aloka SSD 680, Aloka Co., Ltd., Tokyo, Japan), using a 3.5-MHz linear array transducer. The subjects were examined in supine position with knee extended and the muscle relaxed. The mid thigh was identified as the midway point between the tip of greater trochanter and distal femur center between midpoint of the lateral femoral condyle and the superior fibula head. The electronic light pen was used to measure the parameters. The muscle circumference was calculated using the program of the ultrasound machine, by multiplying the total length of the trace line (cm.) by the scale factor. The cross-sectional area (CSA) was calculated in the same manner, by multiplying the area of one pixel (0.04 mm^2) by the total number of pixels enclosed within the trace line.

Bone mineral measurement. Bone mass measurement was taken, using the dual energy X-ray absorptiometry (DEXA)(LUNAR - DPX model, LUNAR Co., Madison, WI). Bone mineral density (BMD – [gm/cm^2]) of the proximal femur which composed of three regions of interest (ROI): the femoral neck, Ward's triangle, and the greater trochanter were measured. The BMD of proximal femur was performed only on non-dominant (left) side of the remaining 57 subjects in this study, and were analyzed using semi-automatic software of the LUNAR Co. The areas of femoral neck, Ward's triangle, and greater trochanter are shown in Figure 2.

Statistical Analysis. Spearman Rank Correlation and Pearson Product Moment Correlation were performed to determine whether there were correlation between the sonographically measured parameters of quadriceps muscle and the thickness of subcutaneous fat as well as BMD of ipsilateral proximal femur. The statistically significant correlation was considered when the p value was less than 0.05

RESULTS

In female; the thickness, circumference, and CSA of quadriceps muscle showed statistically significant correlation with thickness of subcutaneous fat and BMD of proximal femur in all ROIs (Table 1-3). The circumference of quadriceps muscle showed the most significant correlation (Table 2).

In male subjects; the thickness, circumference, and CSA of quadriceps muscle showed significant correlation with BMD of the femoral neck and the trochanter but not with BMD of Ward's triangle and the thickness of subcutaneous fat (Table 1-3).

Table 1: CORRELATION BETWEEN THICKNESS OF QUADRICEPS MUSCLE AND BMD OF IPSILATERAL PROXIMAL FEMUR, WHEN STRATIFIED SUBJECTS BY GENDER (FEMALE/MALE)

Parameters	Correlation co-efficient	(P value)
	Female (n=27) Age 10-17 (mean 13.2)	**Male (n=30)** Age 9-18 (mean 13.1)
Of non-dominant (left) side		
Femoral neck BMD	0.5158 (<.01)	0.4101 (<.05)
Ward's triangle BMD	0.5021 (<.01)	0.2801 (0.13)
Trochanteric BMD	0.5494 (<.01)	0.4437 (<.05)
Subcu.fat thickness	0.6194 (<.01)	0.0375 (0.84)

Table 2: CORRELATION BETWEEN CIRCUMFERENCE OF QUADRICEPS MUSCLE AND BMD OF IPSILATERAL PROXIMAL FEMUR, WHEN STRATIFIED SUBJECTS BY GENDER (FEMALE/MALE)

Parameters	Correlation co-efficient	(P value)
	Female (n=27) Age 10-17 (mean 13.2)	**Male (n=30)** Age 9-18 (mean 13.1)
Of non-dominant (left) side		
Femoral neck BMD	0.7086 (<.001)	0.4526 (<.05)
Ward's triangle BMD	0.6411 (<.001)	0.2528 (0.18)
Trochanteric BMD	0.6732 (<.001)	0.4873 (<.01)
Subcu.fat thickness	0.4771 (<.05)	0.1417 (0.46)

BMD = Bone Mineral Density.

Table 3: CORRELATION BETWEEN CROSS-SECTIONAL AREA (CSA) OF QUADRICEPS MUSCLE AND BMD OF IPSILATERAL PROXIMAL FEMUR, WHEN STRATIFIED SUBJECTS BY GENDER (FEMALE/MALE)

Parameters	**Correlation co-efficient**	**(P value)**
	Female (n=27) Age 10-17 (mean 13.2)	**Male (n=30)** Age 9-18 (mean 13.1)
Of non-dominant (left) side		
Femoral neck BMD	0.6951 (<.001)	0.4646 (<.05)
Ward's triangle BMD	0.6460 (<.001)	0.2705 (0.15)
Trochanteric BMD	0.6679 (<.001)	0.4965 (<.01)
Subcu.fat thickness	0.4795 (<.05)	0.0438 (0.82)

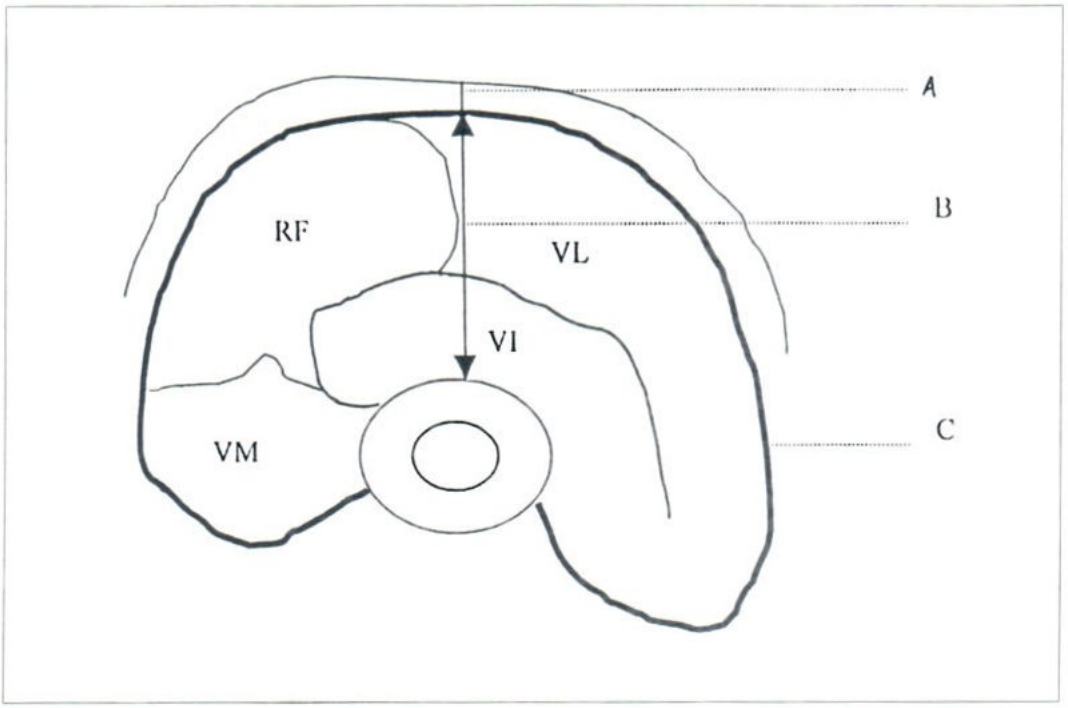

Fig. 1 Cross section of quadriceps femoris muscle, composing of four muscles; rectus femoris (RF), vastus lateralis (VL), vastus intermedius (VI), and vastus madialis (VM). The method of measurement of subcutaneous fat thickness (**A**), the muscle thickness (between arrowhead, **B**), and the circumference of muscle (thick black line, **C**) are demonstrated.

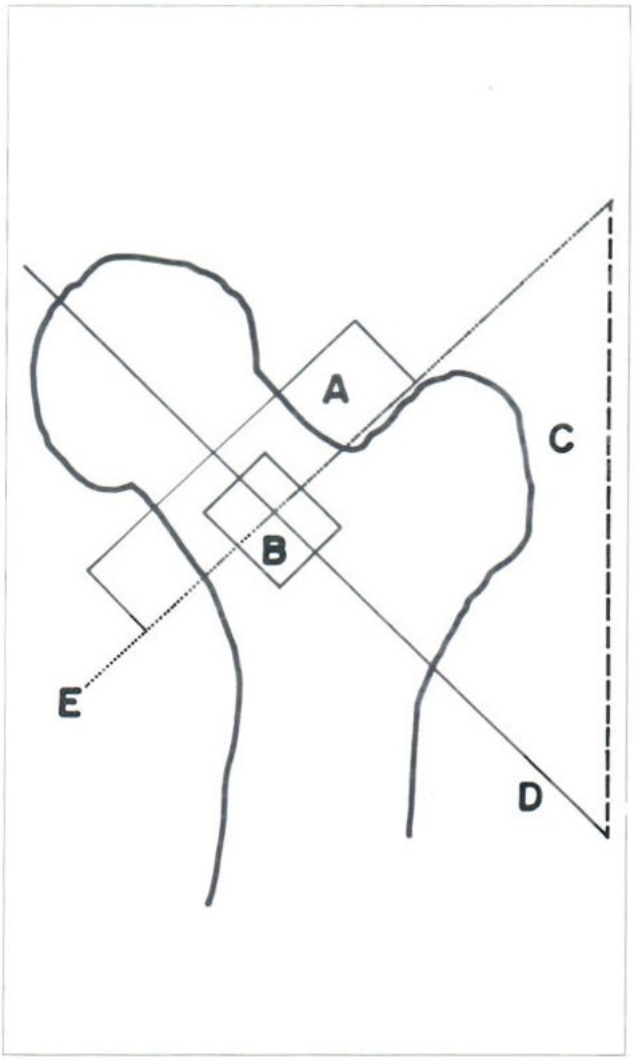

Fig. 2 Diagram of the areas of bone mineral density measurement in proximal femur. **A** (large rectangular) = femoral neck, **B** (small rectangular) = Ward's triangle, **C** (triangle) = trochanter, line **D** = axis, line **E** = the line drawn perpendicular to line **D**.

DISCUSSION

The quadriceps femoris muscle is the great extensor muscle of the leg. It can be divided into four parts; the rectus femoris, the vastus lateralis, the vastus medialis, and the vastus intermedius.[16] The tendons of the four divisions unite in the lower part of thigh to form a single strong tendon attaches to the base of patella. The quadriceps extends the leg upon the thigh. The rectus femoris assists in flexing the thigh on the pelvis, and also can extend the knee and flex the hip simultaneously.

Muscular forces influence bony configuration; in fact, normal skeletal development is dependent upon balanced muscle action.[17] The increase in BMD was reported to be dependent on height, weight, puberty, and other growth variables including skeletal muscle mass.[18] Heckmatt et al.,[19] in a study of 276 children from newborn babies to 12 years of age, noted that the thickness of quadriceps muscle also increased with age. The greatest increase was in the first two years of life, and there was no significant difference in the muscle thickness between sexes at any age. Most of the bone mass at multiple locations will be accumulated by late adolescence,[20] whereas the ability to produce strength proportional to the quadriceps muscle size is greater in young adult than in childhood.[10] These led us to study whether there were correlation between the parameters of quadriceps muscle, which is a strong muscle group supporting movement of lower extremity, and BMD of ipsilateral proximal femur as well as the thickness of subcutaneous fat.

In female subjects, we found statistically significant correlation between CSA of quadriceps muscle and BMD of proximal femur. During childhood, females had similar growth curves in muscle CSA to those of males. An apparent sex separation in muscle CSA took place at 13 years of age and after [21]. BMD was also reported to increase with age during childhood,[18] and bone mass accumulation in healthy female adolescents was pronounced over 3-year period (11-14 years of age).[22] These suggest the simultaneous time frame for bone mass accumulation and muscle growth, and may explain the significant correlation between quadriceps CSA and proxi-

mal femoral BMD in our study. The circumference and thickness of quadriceps muscle have seldom been studied relating to bone mass accumulation. We found significant correlation between the circumference ($p<.001$) and thickness ($p<.01$) of quadriceps muscle and BMD of proximal femur. Among the measured parameters, muscle circumference showed the best correlation with BMD of proximal femur at all ROIs ($r = 0.6411 - 0.7086$).

In male subjects, there was no significant correlation between the measured quadriceps parameters and the thickness of subcutaneous fat. Kanehisa et al.[21] found that in an age span from 13-15 years, fat CSA for males decreased while that for females increased. The decrease amount of fat in male adolescents at the time when muscle mass increased may be the cause of weak correlation in this present study. Bone mass accumulation in male increased significantly until the age of 17.5 years old.[18] The gain in BMD was high in a 4-year period (13-17 years of age), then the increment rate markedly declined. Lu et al.[18] noted that the increase in total-body BMD (TBMD) showed no difference between two sexes until after the age of peak TBMD in females, when the magnitude in the males became greater. The latter was related to higher lean tissue mass and weight. This suggested that TBMD, which is a function of cortical bone, was size dependent. The authors also found that the L2-4 BMD which represented trabecular bone was much less size dependent.[18] In our study, BMD of Ward's triangle which is the area composed almost entirely of trabecular bone also showed no significant correlation with quadriceps parameters, may be explained in a similar manner.

In conclusion, the thickness, circumference, and CSA of quadriceps muscle of non-dominant thigh shows significant correlation with ipsilateral proximal femoral BMD at all ROIs in female adolescents. In male subjects, those quadriceps parameters showed significant correlation only with BMD of the femoral neck and the trochanter, but not with BMD of Ward's triangle.

ACKNOWLEDGMENT

The authors thank Yoshikazu Saito from Aloka Co.Ltd., Tokyo, Japan, and Suchada Sukhochaiyakit from Berli Jucker Co.Ltd. for technical assistance; Choompol Pholpramool Ph.D., Duangporn Benjanarasut M.Sc., and Katekaew Sangchun M.Sc. for their kind co-operation.

REFERENCES

1. Schmidt R, Voit T. Ultrasound measurement of quadriceps muscle in the first year of life: normal values and application to spinal muscular dystrophy. Neuropediatrics 1993; 24:36-42
2. Weiss LW. The use of B-mode ultrasound for measuring the thickness of skeletal muscle at two upper leg sites. J Orthop Sports Phys Ther 1984; 6:163-167
3. Cady EB, Gardener JE, Edwards T. Ultrasonic tissue characterization of skeletal muscle. Eur J Clin Invest 1983; 13:469-473
4. Fisher AQ, Carpenter DW, Hartlage PL, Carroll JE, Stephen S. Muscle imaging in neuromuscular disease using computerized real-time sonography. Muscle Nerve 1988; 11:270-275
5. Kamala D, Suresh D, Githa K. Real-time ultrasonography in neuromuscular problems of children. J Clin Ultrasound 1985;13:465-468
6. Hicks K, Shawker TH, Jones BL, Linzer M, Gerber LH. Diagnostic ultrasound: its use in the evaluation of muscle. Arch Phys Med Rehabil 1984; 65:129-131

7. Heckmatt JZ, Pier N, Dubowitz V. Assessment of quadriceps femoris muscle atrophy and hypertrophy in neuromuscular disease in children. J Clin Ultrasound 1988;16:177-181
8. Campbell IT, Watt T, Withers D, et al. Muscle thickness, measured with ultrasound, may be an indicator of lean tissue wasting in multiple organ failure in the presence of edema. Am J Clin Nutr 1995;62:533-539
9. Freilich RJ, Kirsner RL, Byrne E. Isometric strength and thickness relationships in human quadriceps muscle. Neuromuscul Disord 1995;5:415-422
10. Kanehisa H, Ikegawa S, Tsunoda N, Fukunaga T. Strength and cross-sectional area of knee extensor muscles in children. Eur J Applied Physiol 1994;68:402-405
11. Kanehisa H, Ikegawa S, Fukunaga T. Comparison of muscle cross-sectional area and strength between untrained women and men. Eur J Applied Physiol 1994;68: 148-154
12. Sipila S, Suominen H. Ultrasound imaging of the quadriceps muscle in elderly athletes and untrained men. Muscle Nerve 1991;14:527-533
13. Maughan RJ, Watson JS, Weir J. Muscle strength and cross-sectional area in man: A comparison of strength-trained and untrained subjects. Br J Sports Med 1984; 18:149-157
14. Davies CT. White MJ, Young K. Muscle function in children. Eur J Applied Physiol 1983;52:111-114
15. Maughan RJ, Watson JS, Weir J. Strength and cross-sectional area of human skeletal muscle. J Physiol 1983;338:37-49
16. William PL, Warwick R. Myology. In: William PL, Warwick R, eds. Gray's Anatomy. 36th ed. London, Churchill Livingstone 1980, 595-599
17. Tachdjian MO. Bone. In: Tachdjian MO ed. Pediatric Orthopedics. 3rd ed. Philadelphia, WB Saunders 1990,688-690
18. Lu PW, Briody JN, Ogle GD, et al. Bone mineral density of total body, spine, and femoral neck in children and young adults: A cross-sectional and longitudinal study. J Bone Miner Res 1994;9:1451-1
19. Heckmatt JZ, Pier N, Dubowitz V. Measurement of quadriceps muscle thickness and subcutaneous tissue thickness in normal children by real-time ultrasound imaging. J Clin Ultrasound 1988;16:171-176
20. Matkovic V, Jelic T, Wardlaw GM, et al. Timing of peak bone mass in Caucasian females and its implication for the prevention of osteoporosis: Inference from a cross-sectional model. J Clin Invest 1994;93:799-808
21. Kanehisa H, Ikegawa S, Tsunoda N, Fukunaga T. Cross-sectional areas of fat and muscle in limbs during growth and middle age. Int J Sports Med 1994; 15:420-425
22. Theintz G, Buchs B, Rizzoli R, et al. Longitudinal monitoring of bone mass accumulation in healthy adolescents: evidence for a marked reduction after 16 years of age at the levels of lumbar spine and femoral neck in female subjects. J Clin Endocrinol Metab 1992; 75:1060-1065

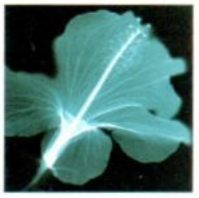

EDUCATION

Asian-Oceanian Society of Neuroradiology and Head & Neck Radiology

As part of the **Bracco International Education Programme**, we are pleased to announce the BRACCO-AOCNHNR '99 Awards and Fellowships at the occasion of the 3rd AOCNHNR in Adelaide, June 18-21 1999.

The purpose of this Award is to promote further research and interest in Neuroradiology and Head & Neck Radiology among the young radiologists in the Asian-Oceanian region.

BRACCO
INTERNATIONAL

For further information please contact:
Bracco International B.V.
47 Hill Street #06-05
S.C.C.C.I. Building
Singapore 179365
Tel: ++65-337 1880
Fax: ++65-337 7576
E-mail: singapore@braccoint.com.sg

http://www.bracco.com

HALLERVORDEN - SPATZ DISEASE DIAGNOSED BY CLINICAL AND MRI FINDINGS : FIRST REPORT IN THAILAND

NITINAVAKARN , Benjaporn MD[1]
TIAMKAO , Somsak MD[2]

ABSTRACT

The diagnosis of Hallervorden-Spatz disease (HSD) has usually been made post mortem. The development of magnetic resonance imaging has increased the number of clinical diagnosis. The characteristic abnormalities in globus pallidus : iron deposition has suggested the possibility of diagnosis. The HSD could be a familial or sporadic disorder.

We present a patient of young male with progressive generalized dystonia and dysarthria ; MRI pallidal abnormalities consisted of decreased signal intensity in T2W, compatible with iron deposit, and a small area of hyper intensity in its internal segment ("Eye of the tiger" sign)

We propose that the combination of these neurological signs with these MRI findings could be considered as highly suggestive diagnosis of HSD in a living patients.

The clinical differential diagnosis is Wilson's disease, by a normal serum copper and ceruloplasmin level.

Key Word, Hallervorden - Spatz disease, Progressive dystonia , dysarthria, Magnetic resonance imaging, "Eye of the tiger". sign.

INTRODUCTION

Hallervorden Spatz (HSD) is a rare condition, most often transmitted as an autosomal recessive trait, which usually become evident during the first two decades of life.[10]

HSD is characterized by extrapyramidal and pyramidal signs ; dystonia, dysarthria, retinal degeneration with a progressive course.[7]

To date, no diagnostic biochemical test is available, although ferrokinetic studies demonstrate iron storage in the basal ganglias of children affected by HSD.

So the diagnosis of HSD is made on the basis of suggestive clinical pictures and confirmed by the characteristic neuropathological findings.

MRI pallidal abnormalitives consisted of decreased signal intensity in T2W image, and a small area of hypersignal intensity in its internal segment, "Eye of the Tiger" sign, described by Sethi et al.[6,7,9]

[1] Department of Diagnostic Radiology
[2] Department of Medicine
Srinakarind Hospital, Faculty of Medicine Khon Kaen University, Thailand 40002

Angelini L et al[1] proposed that the combination of these neurological signs with these MRI findings could be considered as highly suggestive diagnosis of HSD in living patients.

We report a case with clinical features and typical MRI findings.

CASE REPORT

A 28 year-old male presented with dysarthria for 3 years, following by gait difficulties and legs rigidity. Now he had dystonic posturing of arms.

His parents had no neurologic disease nor hepatobiliary disorder.

The neurological examinations showed spastic gait, dysarthria, slow finger movement, generalized hyperreflexia.

No cogwheel regidity was seen

No K-F ring on eye examination was evident.

Normal mood and personality appearance were observed.

Blood chemistry

CBC
Glucose
Renal function
Liver function
} normal finding

- **urine copper**
- **serum copper**
- **serum ceruloplasmin**

} normal study

MAGNETIC RESONANCE IMAGING

MRI scan was performed with a spin echo sequence on a GE 1.5 Tesla Signa Unit T2W (FSR ; TR = 3700 msec, TE = 91 msec EF) was obtained. Five millimeter axial and coronal images revealed striking abnormalities the "EYE OF THE TIGER" Sign. (Fig.1, 2). The low signal normally seen on T2W images in the globus pallidus was markedly exaggerated. This low signal area surrounded a relative circumscribed region of high signal. The low signal was less evident on proton density images. There was no abnormality in the brain stem including substantia nigra, cerebellum, or cerebral hemispheres.

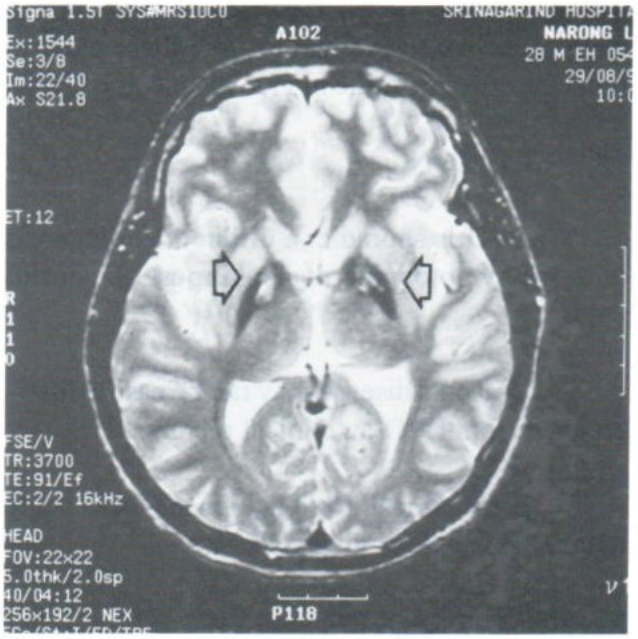

Fig 1. Axial T2W (FSE : TR 3700 ms, TE 91 EF) showing low signal intensity in the regions of globus pallidus (most medial part) and high intensity in the pallidal internal segment give the so-called "Eye of the tiger" sign.

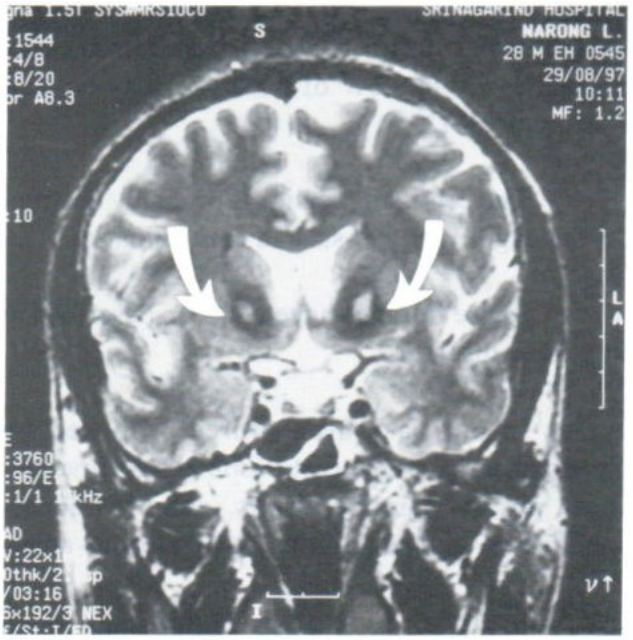

Fig 2. T2W (TR 3760 ms, TE 96/EF) Coronal image showing the characteristic findings of "Eye of the tiger" in pallidal regions (arrows)

DISSCUSSION

The normally comparatively high concentration of iron in the globus pallidus and pars reticulata of substantia nigra are well recognized.[5] Iron is deposited in pathologically high concentration in the brain in several central nervous system degenerative diseases, particularly HSD,[4,10,11] Parkinson disease, Alzheimer's disease.

Hallervorden and Spatz described a progressive disorder (HSD) characterized by dystonia in 1922.[4]

The basic pathology remains unknown; the massive iron deposition in globus pallidus and substantia nigra, the presumably autosomal recessive genetic transmission, and the clinical pictures distinguish the syndrome from other neurodegenerative and extrapyramidal diseases.[10]

Swaiman has proposed the criteria for diagnosis of HSD.[10] Inclusive features are ; onset during first two decades of life, progression of signs and symptoms, evidence of extrapyramidal dysfunction, positive familial history of autosomal recessive trait, and characteristic MRI finding.

Exclusive features include abnormal ceruloplasmin level or/and abnormalities in copper metabolism.

MRI seen to be more specific, it has a capability of detecting magnetic susceptibility effects of iron and orther paramagnetic substances. On

this basis, we could stress that remarkable hypointensity in T2W of ferric ion may be supporting of HSD.

The central hypersignal probably destructive changes with gliosis and demyelination.[2,6,9]

These findings have not been described in any other diseases.

In our case all features proposed by Swaiman are present ; corticospinal tract involvement, positive familial history with MRI abnormalities on globus pallidus as hypodense areas. There is no exclusive features. So these pictures meet the criteria for the in vivo diagnosis of HSD.

CONCLUSION

HSD is sporadic, a differential diagnosis with the symptomatic dystonia must be considered.

Wilson's disease may not be easily differentiated from HSD on clinical pictures.

Biochemical investigation and MRI study may be of value for diagnosis.

Table 1 Differential diagnosis of HSD & Wilson's disease

	HSD	Wilson's disease
age sex family history	no differences	
K-F ring	-	+
surum Cu	normal	↑
serum ceruloplasmin	normal	↑
MRI abnormality	at Pallidal rigions "Eye of the tiger" sign	at Putamen High intensity "Frame" peripherally with high and low intensity spots centrally

REFERENCES

1. Angelini L, Nardocci N, Rumi V, Zorzi C, Strada L, Savoiardo M (1992) Hallervorden-Spatx disease : clinical and MRI study of 11 cases diagnosed in life. J Neurol., 239:417-25
2. Dooling EC, Schoene WC, Richardson EP (1974) Hallervorden-Spatz syndrome. Arch Neurol., 30:70-83
3. Drayer B, Burger P, Darwin R, Riederer S, Herfken R, Johnson GA. MRI of brain iron, AJNR May/June 1986:373-80 and AJR July 1986:103-10
4. Hallervorden J, Spatz H (1922) Eigenartige erkrankung im extrapyramidalen system mit besonderer bet eiligurg des globus pallidus and der substantia nigr. Z Ges Neurol Psychiatr., 79:254-302

5. Halliday W (1995) The nosology of Hallervorden-Spatz disease. J Neurol Sci., 134: 84-91
6. Rutledge JN, Hilal SK, Silver Aj, Dfendini R, Fahn S (1978) Study of movement disorder and brain iron by magnetic resonance. Am J Roentgenol, 149:365-79
7. Savoiardo M, Halliday WC, Nardocci N, Strada L, Angelini L, Rumi V, Tesoro Tess JD (1993) Hallervorden-Spatz disease : MR and pathologic finding. AJNR., 14:-155-62
8. Schaffert DA, Johnsen SD, Johnson PC, Drayer BP (1989) Magnetic resonance imaging inpathologically proven Hallervorden-Spatz disease. Neurology., 39:440-442
9. Sethi KD, Adams RJ. Loring DW, El Gammal T (1988) Hallervorden-Spatz syndrome: clinical and magnetic resonance imaging correlations. Ann Neurol., 24:692-94
10. Swaiman KF (1991) Hallervordenspatz syndrome and brain iron metabolism. Arch Nevol., 48:1285-93
11. Szanto J. Gallyas F (1996) A study of iron metabolism in neuropsychiatric patient ; Hallervorden Spatz disease. Arch Neurol, 14:438-42

VISUAL LOSS FROM INTRACRANIAL PACHYMENINGITIS

NITINAVAKARN , Benjaporn MD.,[1], TIAMKAO , Somsak MD.,[2], THANAPAISARN , Chaivit MD.,[3], CHUANGSHOTI , Shanop MD.,[4].

ABSTRACT

We report a patient with chronic headache and optic neuropathy unrelated to any systemic disease. Widespread dural meningeal thickening shown on enhanced MRI ; biopsy - proven intracranial pachymeningitis from rheumatoid nodule.

She had left-sided optic neuropathy.

She developed cavernous sinus thrombosis, presumably due to compromised dural venous drainage from extensive meningeal inflammation.

Corticosteroid therapy improved visual function and headache.

Gadolinium - enhanced MRI was essential in identifying meningeal inflammation and locating suitable biopsy site.

Key Words. Pachymeningitis, Dura mater , Rheumatoid nodule, Magnetic resonance imaging.

INTRODUCTION

Idiopathic fibrosclerosis of meninges (designated as intracranial pachymeningitis) may occur with or without other systemic involvement. Diffuse thickening of the meninges from tuberculosis, sarcoidosis, rheumatoid arthritis, dural carcinomatosis, meningioma en-plague, and primary intracranial plasmacytoma must be excluded by systemic evaluation, CSF analysis or meningeal biopsy.

We report a case of pachymeningtitis with headache, unilateral ophthalmopathy, histologically proven to be rheumatoid nodule.

CASE REPORT

A 17 year-old girl presented with chronic intermittent headache for 1 year, but intensified in the past 2 months, with blurred vision in the left eye for 2 weeks. No other associated systemic symptoms was evident.

Physical examintion showed normal vital signs

Neuroexaminations revealed fully conscious, no stiffness of neck.

[1] Department of Radiology
[2] Department of Medicine
[3] Department of Surgery Srinakarind Hospital, Khon Kaen University
[4] Department of Pathology Chulalongkorn Hospital Chulalongkorn University Thailand , 40002

EYES EXAMINATION,

Left eye
- mild ptosis, proptosis
- pupil 3 mm. (small relative afferent pupillary defect : 4 mm. of right side)
- normal corneal reflex and eye ground
- limitation of extraoccular muscles movements
- CSF analysis revealed mild pleocytosis, no organism or malignancy cell.

Cranial CT was normal except for slightly increased density along the dura of left frontal region.

During hospital admission, rapid deterioration of vision with nearly blind.

Emergency MRI study and biopsy were performed.

IMAGING STUDY

The patient was imaged with a 1.5T machine (GE signa). All sections were 5 mm. thick. The T1W (TR 600 ms , TE 20 ms) was performed in axial (Fig 1), sagittal (Fig 2) and coronal (Fig 3) plane after administration of contrast medium : Gd-PTPA 0.1 mol/kg

The markedly dense-thick dural enhancement was seen along left side frontal cortex downwardly to cavernous sinus.

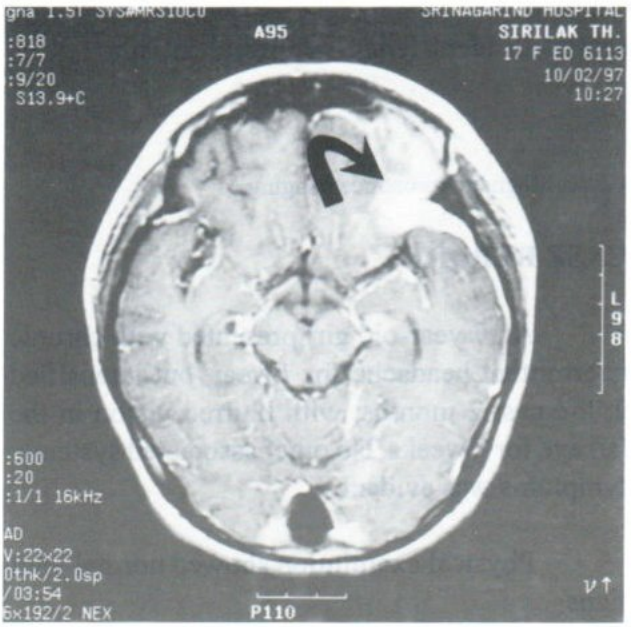

Fig. 1 Gadolinium-enhanced MRI, axial images, (TR 60 ms , TE 20 ms) marked thickening and enhancement of the meninges.

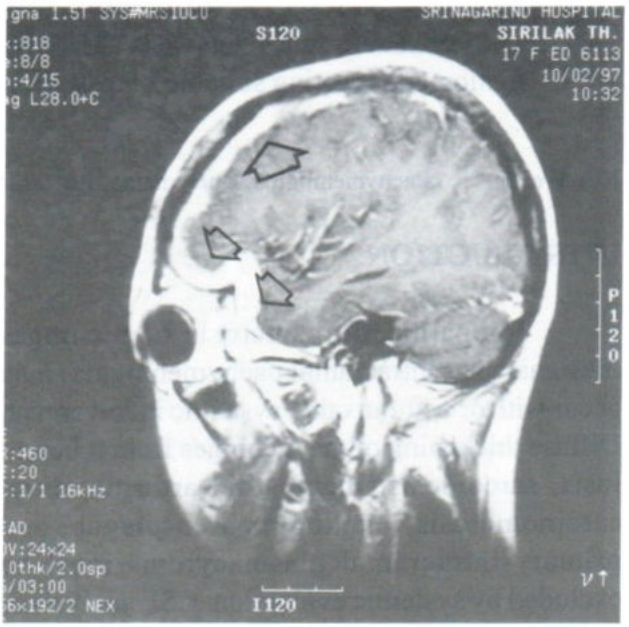

Fig. 2 MR imaging T1W (TR 600 ms, TE 20 ms) after Gd-DTPA, sagittal plane showing diffuse thickening of inferior frontal dura and cavernous sinus (arrows).

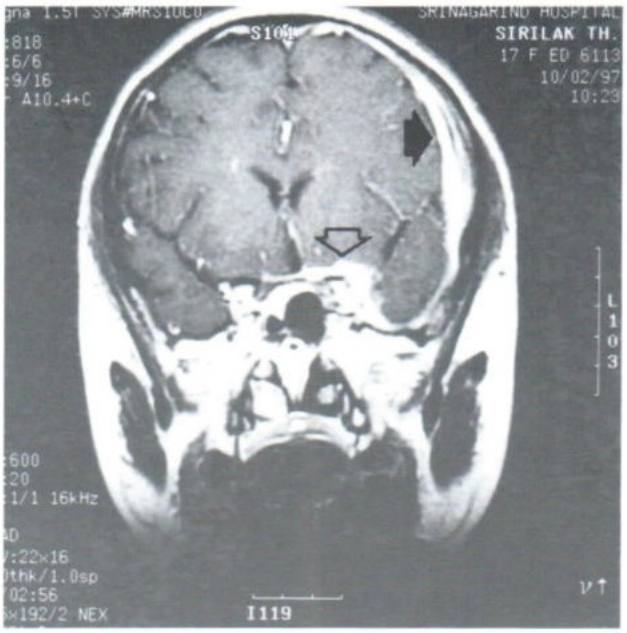

Fig 3. The coronal view showing the correspondance findings in Fig 2 image.

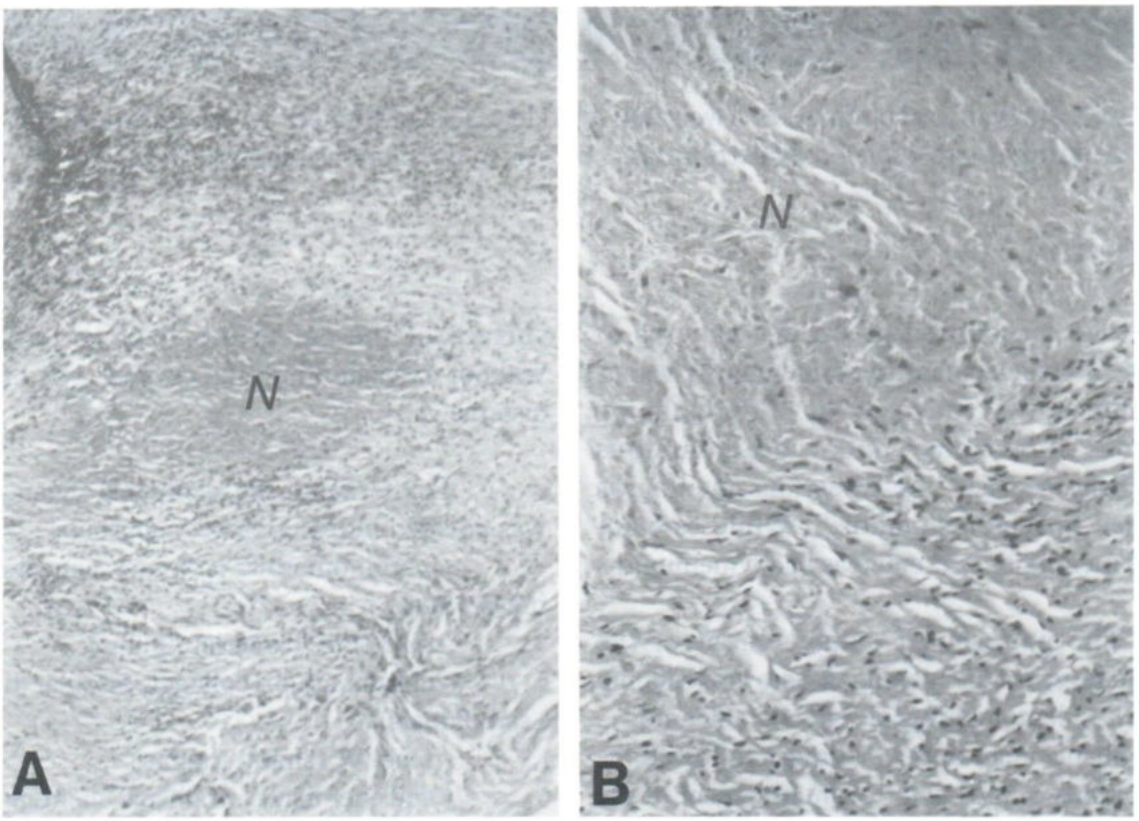

Fig. 4 Pathology of rheumatoid nodule. A. Low-power view shows a focus of (N) surrounded by inflammatory cells. B. High-power view demonstrates a necrotic area (N) rimmed by palisade of spindle-shaped histiocytes.

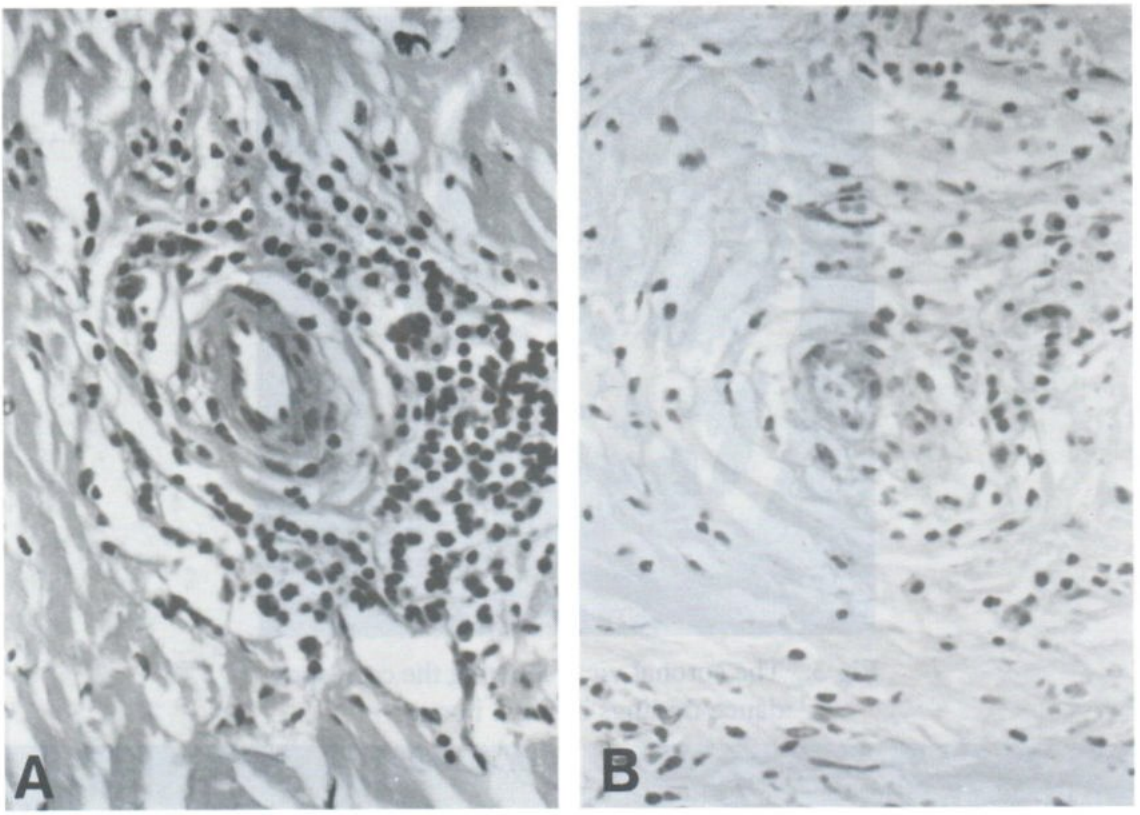

Fig. 5 Pathology of vasculitis. A, B. Two small blood vessels infiltrated by lymphocytes and a few neutrophils are depicted. Note fibrinoid necrosis in the blood vessel wall in B.

DISSUSSION

The recognition of various patterns of meningeal enhancement (leptomeningitis versus pachymeningitis) may help in differentiating between infections and carcinomatous meningitis. Most of the infectious meningitis presented as leptomeningitis.[1-7] While carcinomatous meningitis presented as pachymeningitis.

The patterns of enhancement of the different layers of the meninges were devided into 2 types : 1) leptomeningeal (pia and arachnoid) , when enhancement of the meninges followed the convolutions of gyri and / or involvement of the meninges around the basal cisterns : and 2) pachymeningeal (dura) , when the enhancement was thick and linear or nodular along the inner surface of the calvarium, falx or tentorium without extension into the cortical gyri or basal cisterns.

Further more, the meningeal enhancement was devided into 5 etiologic subgroups ; ie..

- carcinomatous (primary cancers from breast, lung)
- infection (bacteria, fungus)
- inflammation (collagen vascular diseases , sarcoidosis)
- reactive (shunt, trauma)
- and chemical (intrathecal chemotherapy, ruptured dermoid cyst)

The medical history, presentation and CSF

analysis were used to distinguish infections from carcinomatous meningitis.

The meningeal neurological symptoms consistent with meningeal irritation. These included headache, change of mental status, cranial nerve symptoms or seizure. CSF analysis must be done.

The MRI findings of pachymeningitis play role in the differential diagnosis of carcinomatous meningitis and inflammatory meningitis. CSF cytology is negative for malignancy and organism. Dural biopsy may indicate the causes of inflammations eg ; polymyositis, sarcoidosis or idiopathic hypertrophic pachymeningitis.

However, Imaging study especially MRI with Gd-DTPA is the optimal mean of detecting meningeal lesions, even sequele may occur such as brain infarction.

Our case come with chronic headache and left side ophthalmopathy, unrelated to any systemic disease. CSF analysis yielded no malignant cell or organism. After dural biosy, steroid treatment was administered, well response with rapid improvement of vision and heachache.

Dural pathology were shown (in fig 3,4) to be rheumatoid nodule.

Rheumatoid arthritis has also been associated with cranial pachymeningitis; its more common involvement of the cervical spine.[11,12]

CONCLUSION

We report a case of intracranial pachymeningitis from a rhunmatoid nodule without systemic manisfestation.

MRI imaging revealed extension of suitable guideline for biopsy site and help the physicians to recognize this rarely reported disease.

REFERENCES

1. Paakko E. Patronas NJ. Schellinger D. Meningeal Gd-DTPA enhancemtn in patients with malignancies. J Comput Assist Tomogr 1990;14: 542-6
2. Wrobel CJ. Meyer S. Johnson RH. Hesselink JR. MR findings in acute and chronic coccidioidomycosis meningtitis. AJNR 1992;13: 1241-5
3. Sze G. Disease of the intracranial meninges ; MR imaging features. AJR 1993;160: 727-33
4. Sze G. Soletsky S. Bronen R. Krol G. MR imaging of the cranial meninges with emphasis on contrast enhancement and meningeal carcinomatois. AJNR 1989;10:965-75
5. Phillips ME. Ryats TJ. Kambhu SA. Yuk WTC. Neoplastic vs inflammatory meningeal enhancement with Gd-DTPA. J Comput Assist Tomogr 1990;536-41
6. Rodesch G. Van Bogaert P. Mavroudakis N. et al. Neuroradiologic findings in leptomeningeal carcinomatosis : the value interest of gadolinium-enhanced MRI. Neuroradiology 1990;32:26-32
7. Chang KH. Han MH. Roh JK. Kim IO. Han MC. Kim CW. Gd-DTPA-enhanced MR imaging of the brain in patients with meningitis : comparison with CT. AJR 1990;154:809-15
8. Mathews VP. Kuharik MA. Edwards MK. D Amour PG. Azzarelli B. Dreesen RG. Gd-DTPA-enhanced MR imaging of experimental bacterial meningitis: evaluation and comparison with CT. AJNR 1988;9:1045-50

9. Donnet A. Moulin G. Tubiana N. Gras R. Robert JL. Lymphomatous meningitis: neuroradiological appearances. Neuroradiology 1992;34:411-2
10. Tyrell RL II. Bundschuh CV. Modic MT. Dural carcinomatosis: MR demonstration. J Comput Assist Tomogr 1987;11:329-32
11. Bathon JM, Moreland LW, DiBartolomeo AG. Inflammatory central nervous system involvement in rheumatoid arthritis. Semin arthritis Rheum 1989;18:258-66
12. Weinstein GW, Powell SR, Thrush WP. Chiasmal neuropathy secondary to rheumatoid pachymeningitis. Am J Ophthalmol 1987;104:339-40
13. Steven R. Hamilton, MD. Craig H. Smith, MD and Simmons Lessell, MD. Idiopathic Hypertrophic Cranial Pachymeningitis. J. clin neuro-ophthal 1993;13(2):127-34
14. Farhad Kioumehr, M. Reza Dadsetan, Nancy Feldman, Glenn Mathison, Homayoon Moosavi, Seyed A. Roohollamini, and Ramesh C. Verma. Post contrast MRI of cranial Meninges; Leptomeningitis Versus Pachymeningitis J. of Comp. Ass. Tomo. 1995;19(5):713-20

MYCOTIC ANEURYSM OF THE ABDOMINAL AORTA : CT FINDINGS

NITINAVAKARN , Benjaporn MD.[1]
THANTISIRIND , Chirdchai MD.[2]

ABSTRACT

We present a case of mycotic aneurysm of abdominal aorta that was diagnosed by CT (computed tomography)

The accuracy of CT as the first imaging technique of this condition is reviewed in the light of our results and those reported in the literatures.

Key words Aneurysm , aortic Aneurysm , mycotic , infected , CT.

INTRODUCTION

Mycotic aneurysms of the aorta are life threatening conditions because of the natural course toward generalized sepsis and rupture. Therefore, early and appropriate therapy is essential to the final outcome. Mycotic aneurysms of the aorta usually present with vague or nonspecific symptoms, which often hinder the correct diagnosis until a CT, ultrasound or aortography is obtained.

We present a patient with mycotic aneurysm of the abdominal aorta in whom an initial ultrasound and CT were diagnostic. A final diagnosis was made by surgical resection.

CASE REPORT

A 45 year-old man of underlying diabetic mellitus presented with a 3 months history of low back pain. Ten years before admission, he had undergone right hip prosthesis for fracture femoral neck.

During these period of 3 months, he was investigated by IVP, and lumbar CT , but no definite diagnosis and treatment.

One month before admission, he had the 4th Lumber vertebral body osteolytic lesion, and got treatment as Tuberculous spondylitis.

On admission, he had pneumonia and pulsatile abdominal mass.

Chest film showed a right upper lobe pulmonary infiltration.

IMAGING STUDY

Abdominal sonography disclosed an aortic aneurysm with ill-defined aortic wall.

Contrast-enhanced CT showed an infrarenal aortic aneurysm, surrounded by a rim-enhancing hypodense collection that extended into the psoas muscles, and eroded the anterior aspect of adjacent lumbar vertebral body. (Fig. 1, 2).

[1] Department of Radiology
[2] Department of Surgery
Srinakarind Hospital, Faculty of Medicine, Khon Kaen University, Thailand. 40002

OUTCOME

Emergency surgery, an infrarenal aneurysm with necrotic aortic wall and abscess collection at the psoas muscle left side with erosion to the adjacent anterior surface of lumbar spine was disclosed. Aortic resection and graft was done.

Blood culture yielded Salmonella group B.

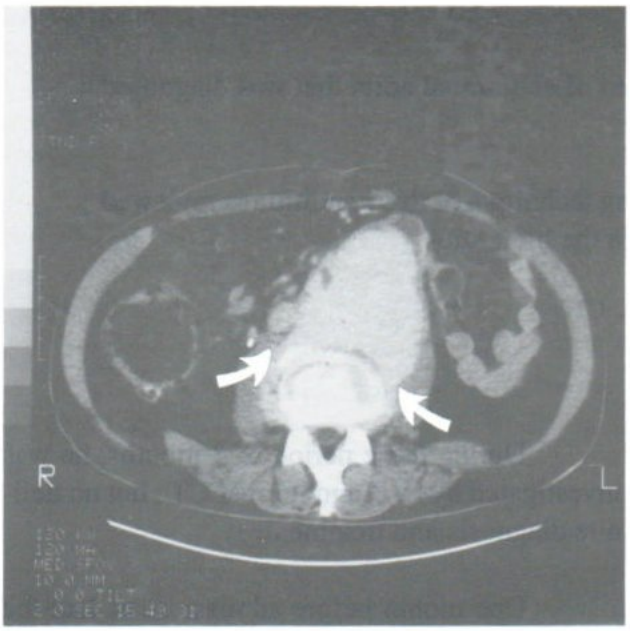

Fig. 1 Axial CECT of the abdominal aorta showing an infrarenal aneurysm with an enhancing rim collection (Large arrow) and psoas muscles involvement (curve arrows).

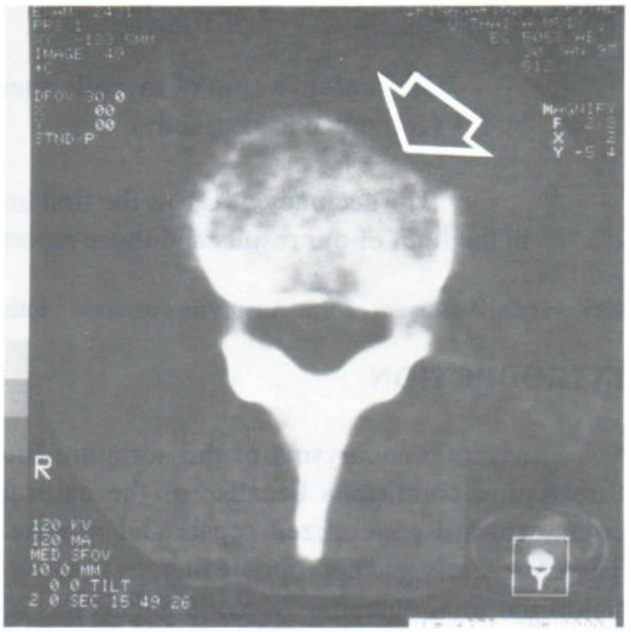

Fig. 2 Axial CT., bone algorithm showing osteolytic bone destruction of the adjacent lumbar vertebra (arrow).

DISCUSSION

The term "mycotic aneurysm" was first used by Osler in 1885[11] to describe aneurysm arising from septic emboli.

Although previously infected aneurysms developed secondary to an endocarditis,[1] the term "mycotic aneurysm" now encompasses any infected aneurysm regardless of the source of infection.

Two main routes have been described that can result in a mycotic aneurysm. The first route refers to all those cases in which there is a source of septic emboli or bacteremia. Microorganisms lodge in the intimal layer of the involved vessel. Bacteria may also colonize the vessel wall through the vasa vasorum.[3,4] Endocarditis, in the preantibiotic area, was the most common source of septic emboli; predilection for the ascending aorta.[4] IV drug abuse and vascular catheters may be the prime causes. Joint prostheses can serve both as a surface for bacterial seeding and as a septic source.

The second route consists of extravascular infection foci, such as spondylodiscitis, with secondary invasion of adjacent arteries. Our case seem to be caused from this mechanism.

Other predisposing factors to the development of a mycotic aneurysm include malignancies, alcoholism, steroid treatments, diabetes mellitus and autoimmune diseases.

A primary source of infection can be defficult to find, definite conclusion is about 50% of cases.[7]

Salmonella is the microorganism most frequently implicated in abdominal aortic aneurysm.

Mycotic aneurysms can be especially treacherous because they often prsent with nonspecific clinical mainisfestations.

Fever, back pain, and a pulsatile abdominal mass rank among the most frequently reported clinical findings. Therefore the correct diagnosis is in imaging study to clarify the clinical findings.

CT findings in mycotic aneurysms publications have a remarkable degree of diagnostic accuracy[4,6,8,9] suggestive features are :

1. The sudden appearance of an aneurysm on a previously normal aorta in a febrile patient is a definite clue to the infective nature of the aneurysm. (The limitation is no previous CT study)

2. A soft tissue mass surrounding the aneurysm is also a very specific sign. Our case showed perianeurysmal low attenuation collections with rim enhancement and psoas involvement, suggesting abscess formation.

3. An adjacent vertebral osteomylitis is not only a sign of mycotic aneurysm, but also a potential infective source.

4. Gas within the aortic wall or in paraaortic location as a result of an aortoenteric fistula has been described.[8]

5. An saccular contour, eccentric type or unusual location of an aneurysm.

Aortogram serves to show signs of suggestive diagnosis : atypical location, a saccular shape, an eccentric location on the wall of aorta.

Ultrasound is hepful to demonstrate the retroperitoneal collections.

MRI is an excellent technique to study mycotic aneurysm due to the depiction of vascular structures, retroperitoneal extension and discovertebral abnormalities. MRI has additional advantage in case of limitation for IV contrast in CT and arteriogram.

CONCLUSION

Mycotic aneurysms of the abdominal aorta are rare and convey a very poor prognosis. Thus early detection and surgical treatment become the mainstay of effective intervention.

Mycotic aneurysm can be difficult to be suspected clinically, and a definite diagnosis may not be reached until an imaging study has been obtained. Both CT and MR imaging are very reliable because they are capable of disclosing nearly as much relevant information and direct visualization of perivascular abnormalities.

REFERENCES

1. Patel S, Johnston KW. Classification and management of mycotic aneurysms. Surg Gynecol Obstet 1977;144:691-94
2. Zak FG, Strauss L, Saphea I. Rupture of diseased large arteries in the course of enterobacterial (Salmonella) infections, N Engl J Med 1958;258-824

3. Mendelowitz DS, Ramstedt R, Yao JS, et al. Abdominal aortic salmonellosis. Surgery 1979;85:514-19
4. Gonda RL, Gutierrez OH, Azodo MV. Mycotic aneurysms of the aorta : radiologic features. Radiology 1988;168:343-46
5. Shetty PC, Krasicky GA, Sharma RP, et al. Ycotic aneurysms in intravenous drug abusers : the utility of digitial substraction angiography. Radiology 1985;155:319-21
6. Atlas SW, Vogelzang RL, Bressler EL, et al. CT diagnosis of a mycotic aneurysm of the thoracoabdominal aorta. J Comput Assist Tomogr 1984;8:1211-12
7. Davies OG, Thombum JD, Powell P. Cryptic mycotic abdominal aortic aneurysms. Am J Surg 1978;136:96-101
8. Moriarty JA, Edelman RR, Tumeh SS. CT and MRI of mycotic aneurysms of the abdominal aorta. J Comput Assist Tomogr 1992;16:941-43
9. Wide CC, Tan L Cheong FW. Case report: computed tomography and ultrasound diagnosis of mycotic aneurysm of the abdominal aorta due to salmonella. Clin Radiol 1987;38:325-26
10. Johansen KJ, Davin J. Mycotic aortic aneurysms : a reappraisal. Arch Surg 1983; 118:583-88
11. Osler W. The Gulstonian lectures on malignant endocarditis. Br. Med J 1885;1: 467-69
12. Gomes MN, Choyke PL. Infected aortic aneurysms : CT diagnosis. J Cardiovasc Surg 1992;33:684-89
13. Brown SL, Busutill RW, Baker JD, et al. Bacteriologic and surgical determinants of survival in patients with myotic aneurysms. J Vasc Surg 1984;1:541-47
14. Chan FY, Crawford ES, Coselli JS, Sati HJ, Williams TW. In situprosthetic graft replacement for mycotic aneurysm of the aorta. Ann Thorac Sur 1989;47:193-203
15. Vogelzang RL, Sohaey R. Infected aortic aneurysms : CT appearance. J Comput Assist Tomogr 1988;12:109-112
16. Blair RH, Resnik MD, Polga JP. CT appearance of mycotic abdominal aortic aneurysms. J Assist Tomogr 1989;13:101-104

MRI OF BRACHIAL PLEXUS INJURY COMPARED WITH INTRAOPERATIVE FINDINGS

Sukhonta SANMAHACHAI[1], Eimorn MAIRAING[1], Jiraporn SRINAKARIN[1], Kittiwan VIPULAKORN[2], Kitti JIRARATTANAPOCHAI[2], Wuttisak BOONPONGSATHIAN[1]

ABSTRACT

Brachial plexus MRI of 11 patients who had both clinical and intraoperative findings of traumatic brachial plexus injury (BPI) in Srinagarind Hospital KKU during June 1997 – January 1998 were reviewed. The sensitivity of MRI for BPI compared with intraoperative findings was 88.88%, 9.09% false positive and 9.09% as false negative or doubtful result. Particularly on T2W images, we could document the lesions as a high signal intensity of CSF around the affected nerve roots. The increased signal intensity of the nerve tissue and muscles are due to oedema, distortion of the nerves, hematoma and posttraumatic neuroma. 8/11 (72.7%) had preganglionic rootlet avulsion, with 61.29% associated pseudomeningocoele, predominantly C7,8 root involvement. One from this group was considered as false positive result. One case had only neural contusion and other two cases were documented as perineural fibrosis intraoperation.

Abbreviation: BPI = Brachial Plexus Injury.

INTRODUCTION

Brachial plexus injury (BPI) may be a result of trauma of the neck, shoulder or upper extremity. Potential mechanism is a direct traction on the plexus by shoulder compression or dislocation with fixation of the plexus between the clavicle and first rib. The injury occurs in association with fracture of the lower cervical transverse process, first rib and clavicle and frequently accompanied by vascular injury and hematoma (Fig. 1.1 - 1.4).[9,15,16] The majority of patients need times for follow-up and only a few of them can recover. The reasons usually include: extensive scaring, retrograde neuronal reaction & degeneration, associated root avulsion, considerable gap to be bridged, and block of the regenerating axons in the mass of scar.[10,9] MRI essentially provides precise type and level of injury, for early operative plan to avoid muscle degeneration and achieving improvement of the outcomes.[3,9,10,2]

MATERIALS AND METHODS

Brachial plexus MRI of 11 patients who had both clinical and intraoperative findings of traumatic brachial plexus injury in Srinagarind Hospital, K.K.U. during June 1997-January 1998 were studied.

In addition to this study, the previous MRI

[1] Department of Radiology,
[2] Department of Orthopaedics, Faculty of Medicine, Khon Kaen University, Thailand.

of 18 BPI patients in Srinagarind Hospital for a period of 2 years since March 1996 until May 1997 were also reviewed. The causes of injury were 15 motorcycle accidents, 2 birth trauma and 1 unknown. There are 14 male and 4 female, age ranges from 2mo to 57 yr and Rt:Lt side = 8:10. The associated injuries were found to be fractures of 2 scapulae, 2 upper ribs and 1 C7 transverse process. Associated injuries, such as two diaphragmatic paralysis, 1 localized cord infarction and 1 axillary atery injury were found.

In addition to the previous data, we performed MRI of BPI in 11 from 19 new patients since June 1997 until January 1998. All of them have been documented in the operative note findings. They were 18 male and 1 female, age ranges from 3 to 34 yrs (M=22.31), injured side; Rt:Lt = 6:13 and MRI of Rt:Lt = 5:6. The causes of injury were 18 motorcycle accidents and 1 crushing injury. The MRI protocol was described in table 2.

8/11 patients clinically had suspected lesions in all the 3 trunks of brachial plexus and the other 3 patients, clinically the lesions confined to the upper trunk. The time interval between the injury and MRI studies ranging from 20-106 days and the time interval between the MRI and the operation ranging from 8-47 days.

The operations performed by different techniques, depending upon the MRI findings. Operative procedures were Free functioning Gracillis transfer, Nerve graft, Neurotization, Neurolysis, ORIF of clavicle and Shoulder fusion. The operation times were range from 1.5-7 hrs., depending on the techniques used.

RESULTS

Of all the MRI of BPI patients reviewed, the most common findings was preganglionic avulsion with/without pseudomeningocoele. Other findings as extrinsic compression, post ganglionic disruption, neuroma, and contusion were also clearly documented from MRI. For the previous MRI findings of the 18 BPI in Srinagarind Hospital, before this study was undertaken since March 1996 until May 1997 as shown in Table 1., it was found that preganglionic rootlet avulsion with/without pseudomeningocoele was the most common lesion (n=12), predominantly involving at the level of C8(n=9), followed by C7(n=8), C6(n=6), C5(n=3) and T1(n=1) respectively. The other causes of BPI from MRI findings were extrinsic compression from other causes (hematoma, scar, granulations) (n=8), contusion without disruption (n=4) and post-ganglionic disruption (n=2).

For the present study , since June 1997 until January 1998 , of the 11 new cases,the MRI findings in comparison with the intraoperative findings, were classified into main 3 groups: 1) Preganglionic avulsion with/without pseudomeningocoele (8/11), 2) Neural contusion (1/11) and 3) Perineural fibrosis (2/11). The accessory MRI findings including : scar of the distal avulsed stump (7/11), hematoma (1/11) and fracture clavicle (4/11) were also seen.

1) PREGANGLIONIC AVULSION WITH/ WITHOUT PSEUDOMENINGOCOELE: (TABLE 3)

These patients had injury between spinal ganglion and cord, frequently produced pseudomeningocoele (61.29% of the affected roots). The mechanism of injury caused by direct traction on the plexus during shoulder compression and fixation of the plexus between the clavicle and the first rib. (Fig 2) On the coronal MRI, it may be recognized by hammocking or coiling of the proximal nerve portions. From table 3, four patients had total rootlet avulsion. The most common nerve roots which were injured, were at the level of C7(n=8), following by the level

of C8(n=7), C5(n=6), C6(n=6) and T1 (n=4) respectively.

Seven cases from this group were confirmed intraoperatively as true positive results, except in case no. 3 which was considered as false positive. (Fig 3) Because having only visualised pseudomeningocoele, interpretation could be missed, if the traction force was only pulling out the nerve off the rootsleeves without overcoming the elastic tolerance of nerves.[3]

All of these patients required secondary operation, such as Free Functioning Gracillis Transfer, Nerve graft and Neurotization. There is no chance for the damaged nerves to recover by themselves, the operation should be performed early to avoid the muscle degeneration. MRI excellently documented the correct diagnosis of this type of injury, so it played an important role to improve the operative outcome by early detection of type and level of injury.

2) NEURAL CONTUSION WITHOUT DISRUPTION:

Demonstration of upstream hyperintensity in the nerve on FSE T2WI, reflected an increasing axonoplasmic fluid and the disorder flow of the endoneurial fluid,[1] caused by direct contusional force acting on the plexus. No neural disruption was seen intraoperatively. This patient was gradually recovered without neurodeficit after 2 weeks follow-up (Fig 4). This type of injury showed a good prognosis, because no effect from neural disruption, neural gap or scar and less retrograde neuronal reaction and degeneration occurred than other groups. Only conservative treatment without surgical intervention was required in this type of injury.

3) PERINEURAL ADHESION: (FIG 5)

Two cases were classified in this group. MRI findings revealed thickening, slight derangement and perineural hypointensity in both T1W and T2W images from fibrosis around the nerve without demonstrable nerve disruption. The case who was considered to be true negative for nerve disruption (9.09%), was confirmed intraoperatively and only neurolysis was performed.

The other case was considered as false negative (9.09%), because the operation revealed the nerve inseparable from the scar, causing by partial neural disruption but MRI could not detect this abnormality. This group of patients recovered slower than the second group. The prognosis was possibly modified if the detection and the treatment was delayed after the injury.

MRI of BPI patients can give the precise type and the level of injury in the majority of patients for correct therapeutic planning and early operation to improve the operative outcomes.

Table 1 Previous data : MRI findings of the18 BPI patients, Srinagarind Hosp.(March1996-May1997)

I. Preganglionic avulsion with/without pseudomeningocoele: 12cases (66.66%): C8 (9*), C7 (8*), C6 (6*), C5 (3*), T1 (1*)
II. Postganglionic: 4 cases (22.22%): neuroma 3 from 4
III. Contusion without disruption: 2 cases (11.11%)
IV. Extrinsic compression: 8 cases (44.44%): hematoma (3), scar (3), granulations (2)

(*) number of affected roots.
N.B. : Some of the patients had combined , more than one findings of the BPI from MRI.

Table 2 MR Imaging protocol for BPI in Srinagarind Hospital (June 1997-January 1998)

Equipment: GE Signa 1.5 Tesla Horizon Echospeed
Gradiant 22 milli Tesla/meter, system software 5.6
Imaging analysis software: GE RFM (multiplanar reformatting)
Anterior neck coils or CTL phase array coils
SE data acquisition: (Cor., sag., axial)
T1W (600-800/20: TR/TE) Thickness 3mm, gap 0.5-1 mm
Respiratory motion compensation
3-4 NEX, 256x192 matrix, FOV 20-24
FSE data acquisition:
T2W (4-5000/80-100: TR/TE) Thickness 3 mm, gap 0.5-1 mm
Echo train 4 or 8, fat and vessel suppression
4 NEX, 512x512-256x256 matrix

Table 3 8/11 patients of preganglionic avulsion

NO. \ Root	C5	C6	C7	C8	T1
1	+	+	+*	+	+*
2	+*	+*	+*	-	-
3 (FP)	+	+*	+*	+*	+*
4	-	-	+*	+*	-
5	+	+*	+*	+	+
6	-	-	+	+	-
7	+	+	+*	+*	+
8	+*	+*	+*	+*	-
	6(2)	6(4)	8(7)	7(4)	4(2)

* Pseudomeningocoeles, ( ) No. of pseudomeningocoele

+ affected root, - intact root

Nineteen pseudomeningocoeles were found from total 31 avulsed roots. (61.29%)

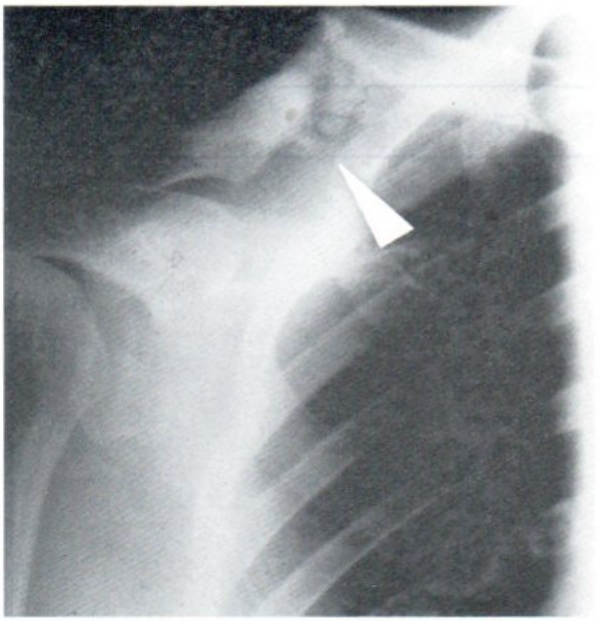

Fig. 1.1 Fracture Rt clavicle with callus in the patient who was clinically suspected. Total avulsion injury of the Rt brachial plexus. (arrowhead: callus formation of fracture site)

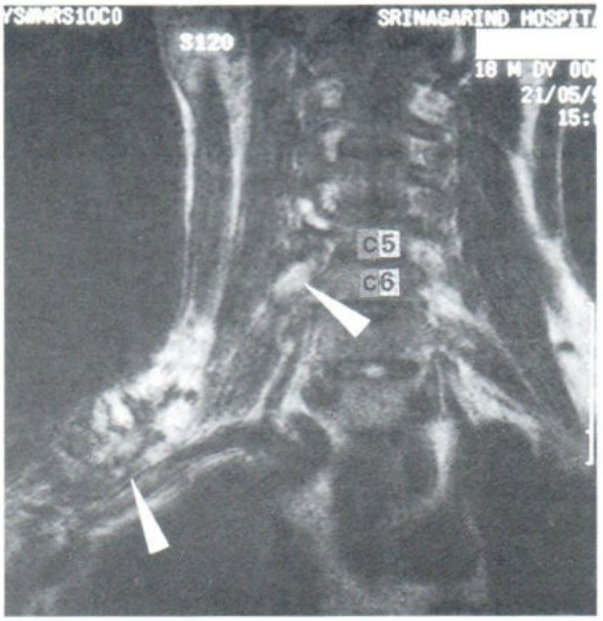

Fig. 1.2 Oedema of Rt C6 root(upper arrowhead) and entrapment of upper and middle trunks by callus(lower arrowhead). MRI of the same patient as Fig.1.1

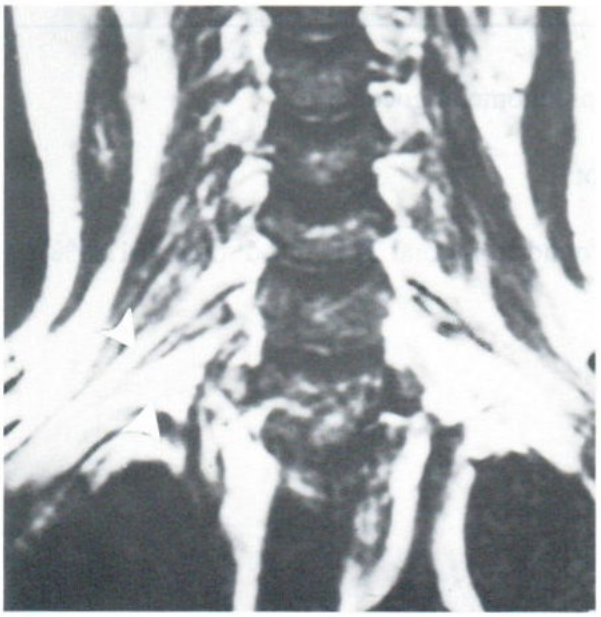

Fig. 1.3 This patient clinically presented with total loss of motor and sensory function of Rt brachial plexus and he also had Rt axillary a. injury. MRI shows normal nerves. (two arrowheads), but neurodeficit caused by extrinsic compression from the hematoma. (Hematoma not demonstrable in this figure.)

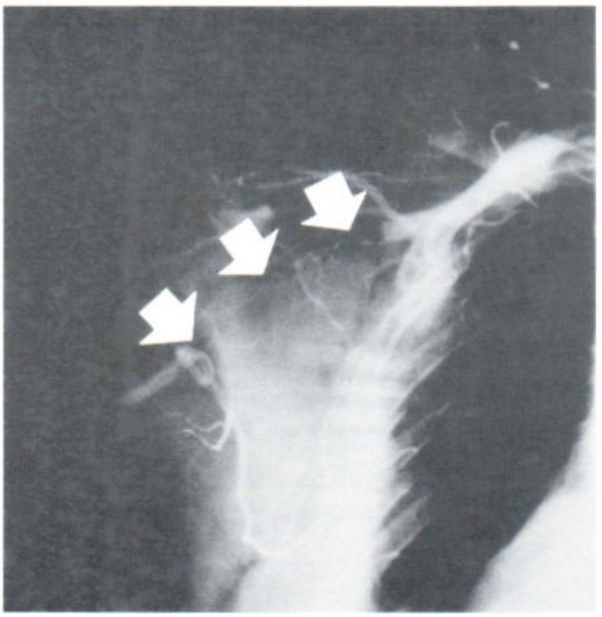

Fig. 1.4 Rt. axillary atery injury in the same patient, completely occluded segment (arrows) was identified from angiography. After thrombectomy and hematoma removal, the patient's neural function gradually improved without having nerve surgery.

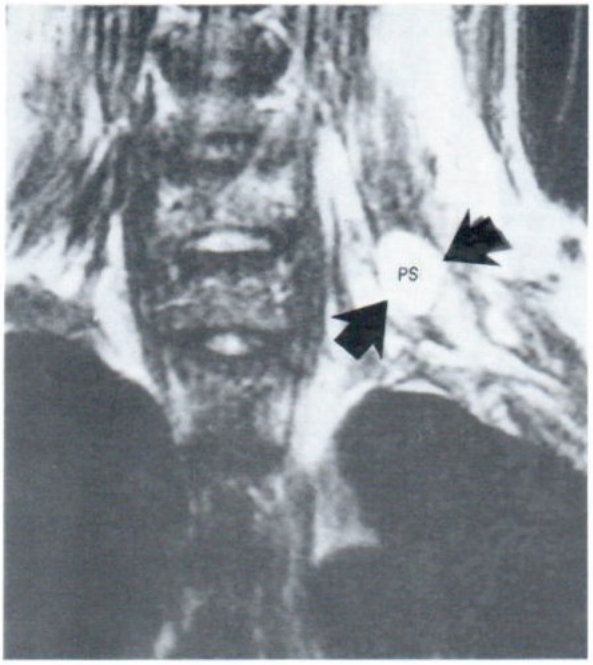

Fig. 2(1*) Coronal T2W FSE of Lt C8 pseudomeningocoele(arrows)

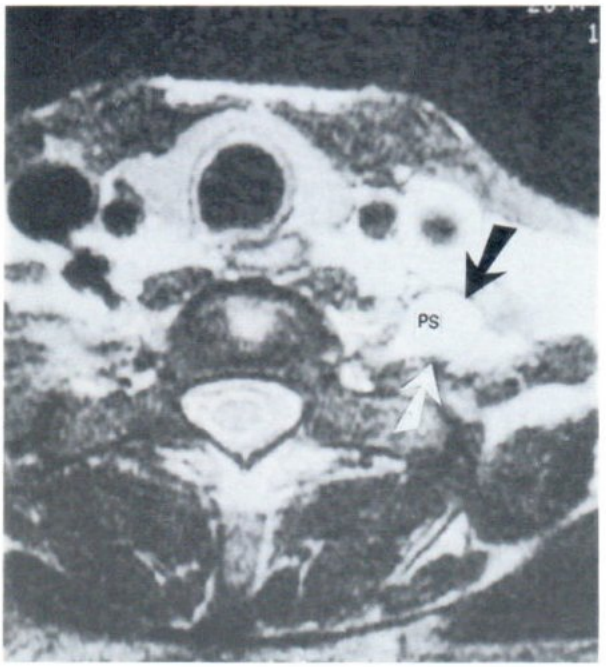

Fig. 2(2*) Axial T2W FSE of Lt C8 Pseudomeningocoele. (arrows)

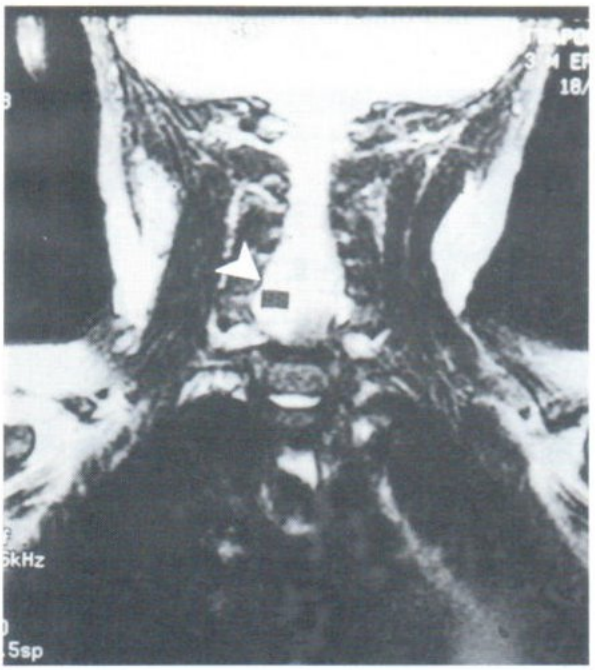

Fig. 3 Case 3 (False positive) Large pseudomeningocoele, (arrowhead) obscured the detail of nerves. Undisrupted nerves was revealed intraoperatively.

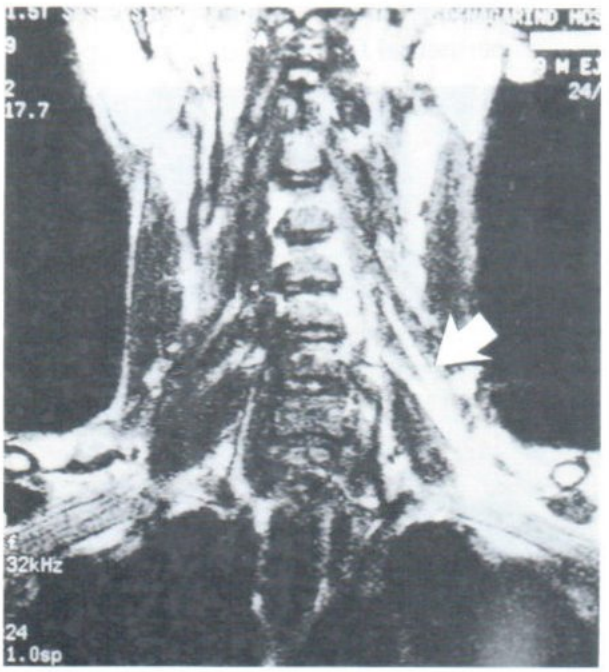

Fig. 4 Coronal FSE T2W image of neural contusion. Upstream hyperintensity of Lt brachial plexus without disruption. (arrow)

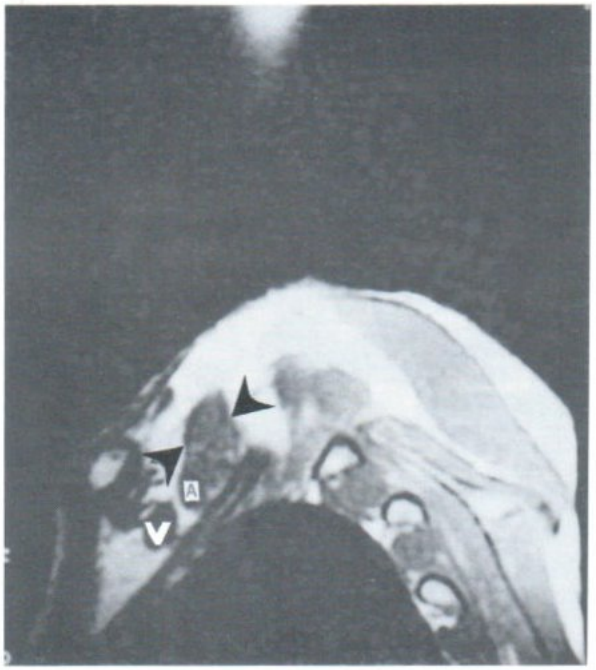

Fig. 5 Sag.T1W images show thickening of Lt brachial plexus, nerve cords (two arrowheads) above axillary atery, due to perineural fibrosis.

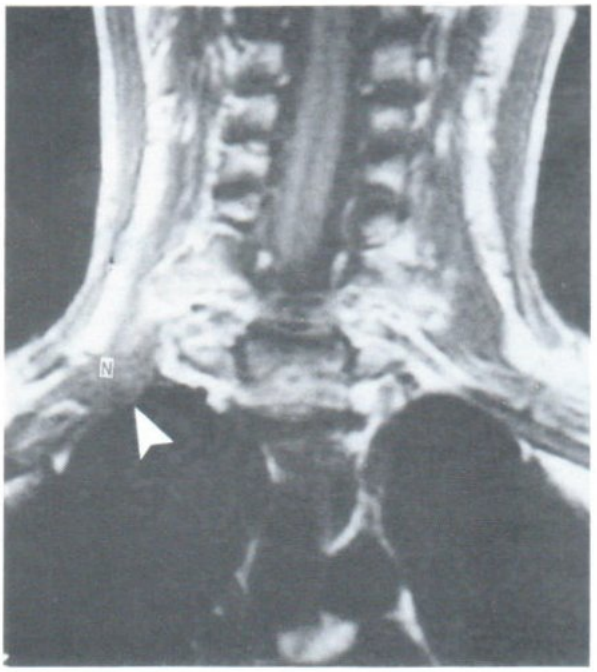

Fig. 6(1*) Coronal T1W image shows intermediate signal of Rt brachial plexus neuroma (arrowhead).

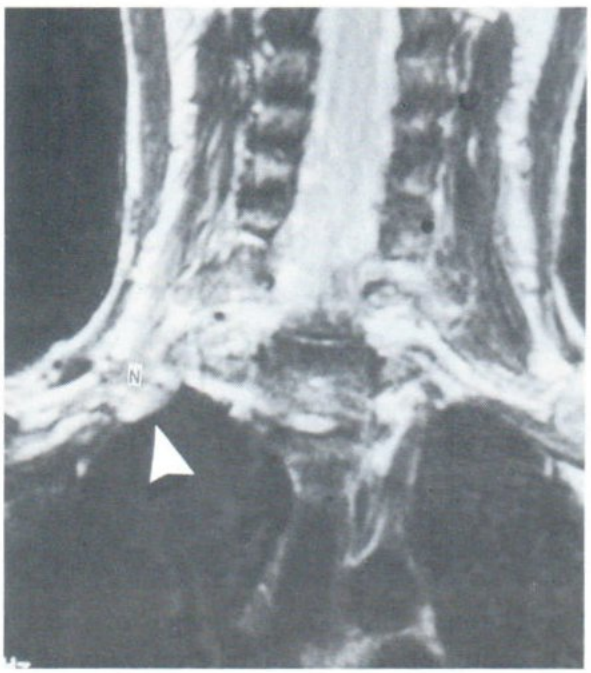

Fig. 6(2*) Coronal T2W image shows increased signal intensity of the neuroma (arrowhead).

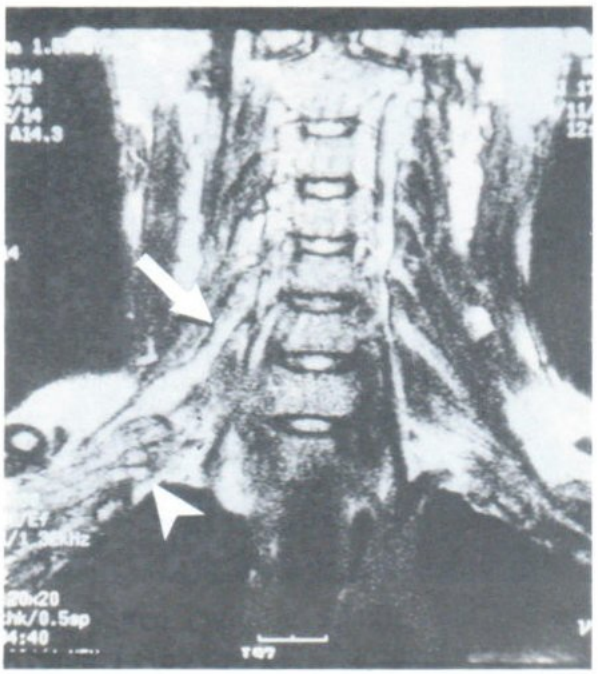

Fig. 7 Coronal T2W image shows enlargement and heterogeneous signal of Rt C5,6 roots (upper arrow) and nerve scar of distal segment. (arrowhead)

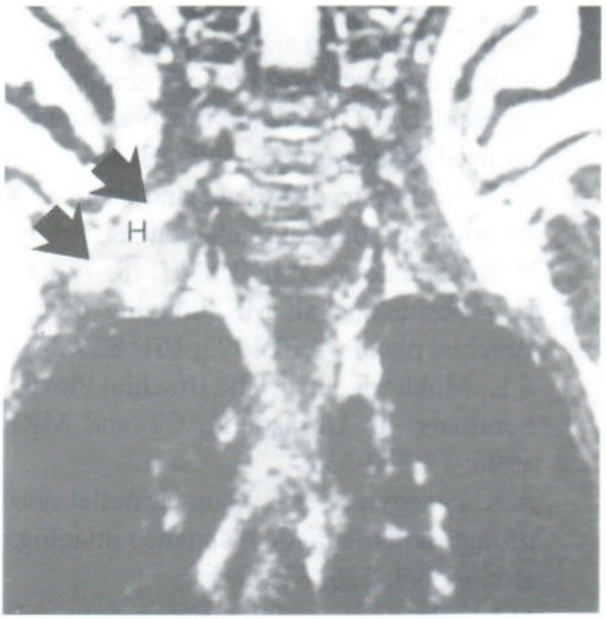

Fig. 8 Demonstration of Rt scalene hematoma (arrows)

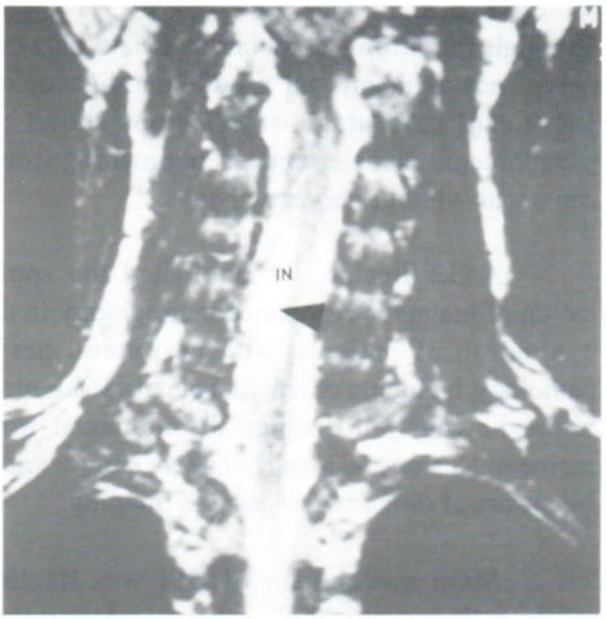

Fig. 9 Coronal T2W images shows high signal area, isointense to CSF within the cord (arrowhead) due to complication, cord infarction.

DISCUSSION

MRI findings of BPI depends on which portion of the plexus was injured and the timing of detection after injury. MRI can provide direct visualization of nerve and the surrounding soft tissue which is superior to other imaging modalities and EMG.

In this study, the majority of BPI patients had rootlet avulsion at the preganglionic level which were excellently documented from MRI, by the detection of pseudomeningocoeles (61.29%), disrupted roots and hammocking of proximal disrupted portion of roots.

The second group of neural contusion can also be clearly depicted from MRI. These patients had a favorable prognosis, associated with transient impairment of neural function, and only conservative treatment was required.

In the group of perineural fibrosis, they could be related with a longer period of time before the detection and the operation could be undertaken. Delaying in the management could be a modified factor for a good operative result.

Slower recovery than expected after neurolysis was observed in these patients, although no neural disruption documented from MRI.

G. Alexander West et al.,[2] described the use of short-tau inversion recovery (STIR) to evaluate muscle characteristics of nerve disorder (neurapraxia) in the BPI patient and other peripheral nerve injury. STIR may therefore play an important role in the predilection for clinical outcomes.

A.T. Walker et al.,[12] suggested that

although the strong association exists between nerve root avulsion and pseudomeningocoele,a significant percentage of avulsions shows no pseudomeningocoele, and pseudomeningocoele can occur without nerve avulsion.

A.G.Filler et al.,[1] published the application of magnetic resonance neurography in the evaluation of patients with peripheral nerve pathology, including of brachial plexus. In his technique, he can well distinguish intraneural from perineural lesion and localized nerve compression, by means of direct nerve fassicle imaging.

Main mechanism of BPI was traction injury, acting on preganglionic level which is well recognized from MRI. In cases of postganglionic injury, the spinal nerve is ruptured but the nerve roots are intact. The proximal stump neuroma frequently occur, not the pseudomeningocoele. (Fig6)

The sensitivity of MRI for BPI was considered good in 88.88% of cases. Particularly on T2WI, it can well demonstrate pseudomeningocoele, nerve oedema, scar (Fig 7), neuroma, hematoma (Fig 8) and complications such as localized cord infarction (Fig 9). MRI considered to be the modality of choice for evaluation of BPI patients after screening by conventional radiographs for skeletal abnormality.

REFERENCES

1. Filler., M. Kliot., et al, Application of Magnetic resonance neurography in the evaluation of patients with peripheral nerve pathology. J. of Neurosurgery 1996; 85: 299-309.
2. G. Alexander West, et al. Magnetic Resonance Imaging Signal Change in Denervated Muscles after Peripheral Nerve Injury. Neurosurgery 1994; 35: 077-1085
3. Paul C. Francel., et al. Fast spin-echo magnetic resonance imaging for radiological assessment of neonatal brachial plexus injury. J. Neurosurgery 1995; 83: 461-466.
4. G. M. Kellman., J.B. Kneeland, et al. MR Imaging of the Supraclavicular region: Normal anatomy. AJR 1987; 148: 77-82.
5. H.V. Posniak., et al. MR Imaging of the Brachial plexus. AJR 1993; 161: 823-841.
6. S.K. Mukherji., et al. The Brachial Plexus Seminars in Ultrasound, CT and MRI 1996; 17:519-538.
7. A.K. Panegyres., et al. Thoracic outlet syndromes and magnetic resonance imaging. Brain 1993; 116: 823-841.
8. H.V. Poaniak., M.C. Olson., et al. Imaging of the Brachial plexus. Postgraduate Radiology 1994; 14: 74-89.
9. Roger-B., et al. Imaging of posttraumatic brachial plexus injury. Clinical Orthopedics 1988; 237: 57-61.
10. V.S. Mehta., et al. Surgical treatment of brachial plexus injuries. British Journal of Neurosurgery 1993; 7: 491-500.
11. D. Thyagarajan., et al. Magnetic resonance imaging in brachial plexopathy of cancer. Neurology 1995; 45: 421-427.
12. A.T. Walker., et al. Detection of Nerve Rootlet Avulsion on CT Myelography in Patient with Birth palsy and Brachial Plexus Injury After Trauma. AJR 1996; 167: 1283-1287.
13. F. Gudinchet., et al. Magnetic resonance imaging of shoulder in children with brachial birth palsy. Pediatric Radiology 1995; 25: S125-S128.
14. A.A. Castagno., et al. MR Imaging in Clinically Suspected Brachial Plexus Tumor. AJR 1987; 149: 1219-1222.
15. Charles B. Higgins. Magnetic Resonance Imaging of the Body. 1997; 291-315.
16. J.H. Coert., et al. Peripheral nerve entrapment caused by motor vehicle crashes. The Journal of Trauma 1994; 37: 191-194.

RADIOLOGICAL FEATURES WITH PATHOLOGICAL CORRELATION IN MENINGIOMAS

Janjira TANVILAI [1], Jaturat KANPITTAYA [1]
Jumphol MITCHAI [2], Chaiwit TANAPAISAL [3]

ABSTRACT

A radiologic-pathological correlation of meningioma and it subtypes was studied. Forty-four patients with 50 surgically excised tumors between 1993 and 1997 were analyzed. The most common location was at the convexity (40%). The majority of meningiomas were isodense on noncontrast CT and enhanced strongly on postcontrast CT scans. Edema was often presented on CT and MRI studies. Pronounced edema was significantly correlated with lesion >3 cm in diameter. Tumor calcification was seen in 36% of CT scans.

Hyperostosis and bone erosion were found in 23% and 21% on CT scans, respectively. There was a correlation between hyperostosis and sphenoidal ridge location. On CT scans, focal non-enhancing low density areas are seen in 25% of all tumors, and correlated significantly with meningothelial subtype.

On MRI studies, the tumors were mostly isointense to the gray matter on T1-weighted images, iso and hyperintensities on PD-weighted and T2-weighted images. The lesions were strongly enhanced with gadolinium. There was no correlation between the signal intensities and histological subtype.

INTRODUCTION

Meningioma is the most common non-glial tumor consisting of approximately 15% of all operated intracranial tumors.[1] It tends to occur more often in women than in men between the age of 40-70 years. This tumor is rare in childhood, accounting for less than 2% of all intracranial tumors Meningioma arises from the meninges and the derivative, principally arachnoid cells. The variable histologic appearances of meningiomas has been categorized into four common subtypes ; meningothelial, transitional, fibroblastic and angioblastic. The other subtypes are psammomatous, microcystic, papillary and malignant. Angioblastic type tends to be more aggressive and oftenly recurs.

We aimed to described the computed tomography (CT) and magnetic resonance imaging (MRI) features of each meningioma subtype and correlate them with pathological findings.

MATERIALS AND METHODS

Forty-four patients with 50 meningiomas

[1] Department of Radiology
[2] Department of Pathology
[3] Department of Neurosurgery Faculty of Medicine, Khon Kaen University, Khon Kaen, Thailand.
Correspondence to Janjira Tanvilai Department of Radiology, Faculty of Medicine, Khon Kaen University, Khon Kaen ,Thailand.

underwent surgery between 1993-1997 at Srinagarind Hospital. Computed tomography (CT), magnetic resonance imaging (MRI) and histopathological findings of these tumors were studied retrospectively. There were 30 females and 14 males, ranging in age from 2 to 75 years, with a mean of 40. Three patients had multiple lesions.

Computed tomography scans were performed mainly on GE (General Electric Medical System. Milwaukee, WI) and Toshiba Medical System (Toshiba x-vision EX Model TSX-002A/8.). Some studies were done at private hospitals. The CT images were available for reviewed in 41 patients. Nine patients had MRI scans. All MRI studies were performed on a General Electric 1.5T Signa unit (General Electric Medical System, Milwaukee, WI). Six of them also had CT scans.

The images were analysed by one radiologist with a foreknowledge only that a meningioma had been diagnosed in each patient.

The histopathological studies of each case was reviewed by a pathologist who was blinded to the clinical and radiological findings. The predominant histological subtype of each tumor was classified according to the scheme of Russell and Rubinstein.[2]

Statistical analysis, non-parametric tests, Fisher's exact test, as appropiate, were used. A P value of 0.05 or less was accepted as significant.

RESULT

HISTOLOGICAL SUBTYPES

We found six histologic subtypes; transitional, fibroblastic , meningothelial, psammomatous, microcystic and angioblastic (Table 1). The majority were transitional (22 cases, 44%) (Figure. 1,2), fibroblastic (14 cases, 18 %) (Figure. 4) and meningothelial (10 cases, 20%) (Figure. 3).

TUMOR LOCATION

Various tumor locations were found and listed in Table 2. Convexity meningiomas were the most common (20 cases, 40 %) (Figure. 1), followed by sphenoidal ridge (6 cases, 12%) parasagittal (5 cases, 10%) and frontobasal (4 cases, 8%), respectively.

TUMOR SIZE

The frequency and percentage of tumor size were shown by Table 3. The majority of them were larger than 3 cm in diameter (38 cases, 16%).

Table 1. Histological subtypes of meningiomas (n=50)

Transitional	22 (44%)
Fibroblastic	14 (18%)
Meningothelial	10 (20%)
Psammomatous	2 (4%)
Microcystic	1 (2%)
Angioblastic	1 (2%)

Table 2. Tumor locations.

Convexity	20 (40%)
Sphenoidal ridge	6 (12%)
Parasagittal	5 (10%)
Frontobasal	4 (8%)
Cerebellopontine angle	4 (8%)
Suprasellar	3 (6%)
Olfactory groove	2 (4%)
Tentorium	2 (4%)
Intraventicular	2 (4%)
Cervicomedullary junction	1 (2%)
Petrous	1 (2%)

Table 3. Tumor size (n = 50)

0-1.5 cm	1 (2%)
1.5-3 cm	11 (22%)
over 3 cm	38 (76%)

Table 4. Comparison of tumor size and degree of edema.

	edema		
Size	mild	moderate	marked
< 1.5 cm	0	0	0
1.5-3 cm	4	2	0
> 3 cm	10	20	6

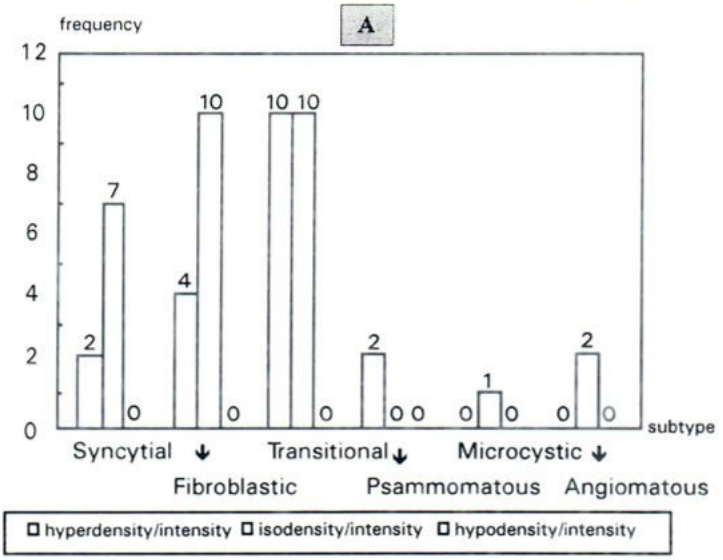

Graph 1. Plot of histological subtypes versus tumor density on CT scans revealed no correlation between two groups.

TUMOR DENSITY & SIGNAL INTENSITY

On precontrast CT scans, 32 of 47 cases (62%) of meningiomas were isodense and 18 of 47 cases (38%) of them were hyperdense relative to brain cortex. On postcontrast studies, 94% of the tumors enhanced strongly. There was no significant correlation between tumor density on CT with histological subtype (Graph. 1).

On MR images, most of the tumors were isointense to the gray matter on T1-weighted images. Eleven percent of them were hypointense. On PD-weighted and T2-weighted images, 56% were isointense and 44% were hyperintense. Marked contrast enhancement of all meningiomas with gadolinium were found (Figure 1, 2, 3). Since a small number of patient had MRI studies, an analysis of correlation between signal intensity and histological subtype was not done.

There was no correlation between the degree of contrast enhancement on CT or MRI studies and histological subtypes of the tumors.

BONE CHANGE

Eleven patients had hyperostosis. It was predominant in sphenoidal ridge meningiomas, 4 of 6 cases, when only 6 of 20 convexity tumors had such change (P=0.008) (Figure.3).

Ten cases had bone erosion (21%), the major location was convexity lesion.

BRAIN EDEMA

On CT scans, 88% of meningiomas showed surrounding white matter edema. The finding was 89% on MR images. The edema occured more frequently and significantly with larger lesion (over 3 cm in diameter) (P= 0.0164) (data shown by Table 4.).

There were no correlation between the degree of cerebral edema and histological subtype of the tumor (data not shown). Focal non -enhancing low density area, cystic change, Hemorrhage and calcification within the tumor.

On CT scans, focal non-enhancing low density area within meningiomas was found in 12 of 47 cases (25%). It was most prevalence in meningothelial (syncytial) subtype, significantly higher than other groups (P = 0.0352) (Graph 2.) (Figure 5).

Cystic change within meningiomas is not common.[2] It was found in 2 of 9 cases on MRI. No correlation between cystic change and histological subtype was noted.

Hemorrhage is rare.[3] It was observed in 4% on CT and MRI scans.

Calcification was present in 36% on precontrast CT scans. None showed any calcification on MRI.

No correlation between hemorrhage, calcification and histological feature was noted.

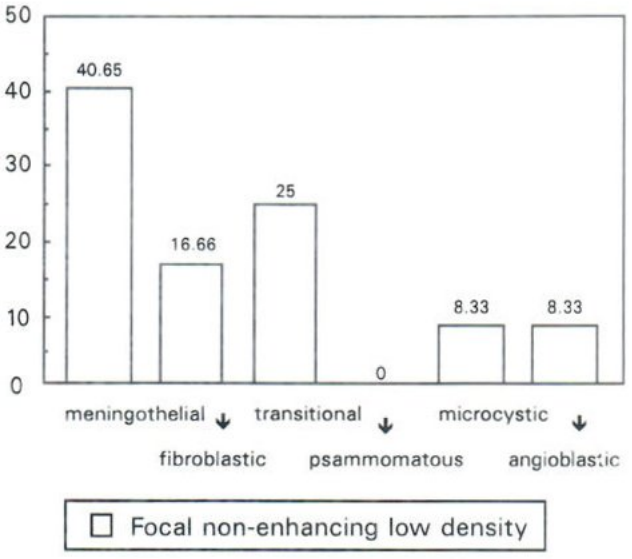

Graph 2. Presence of focal non-enhancing low density within meningiomas and histological subtype.

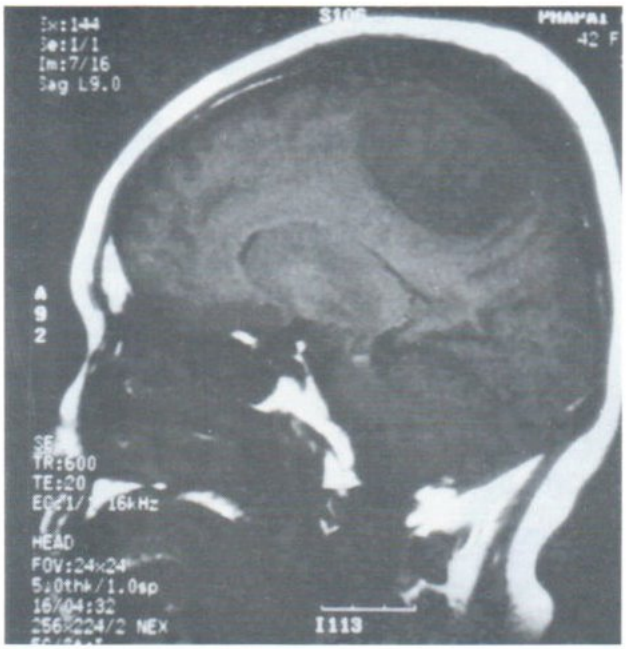

1A

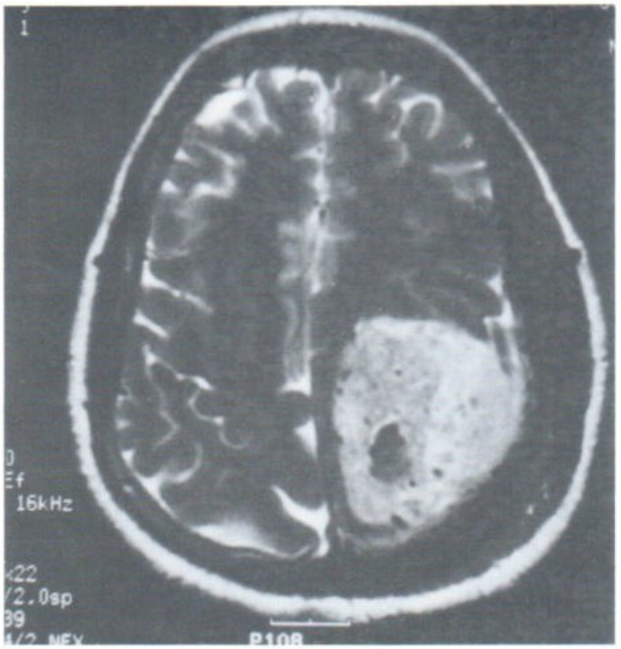

1B

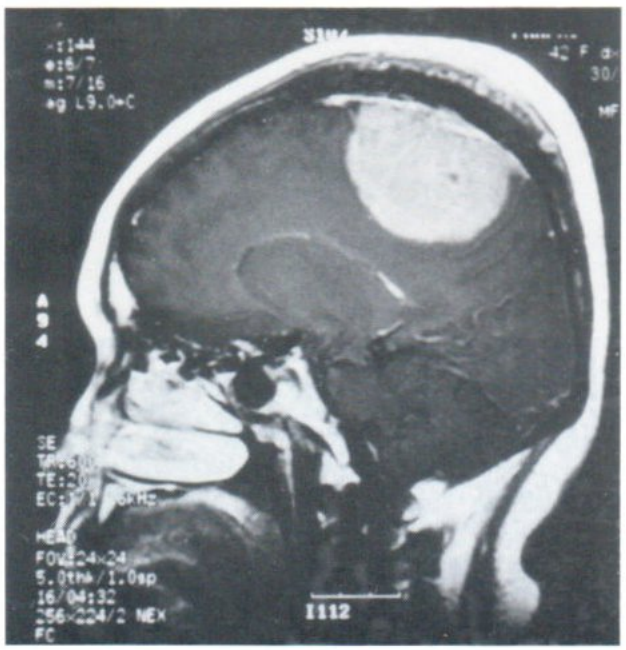

1C

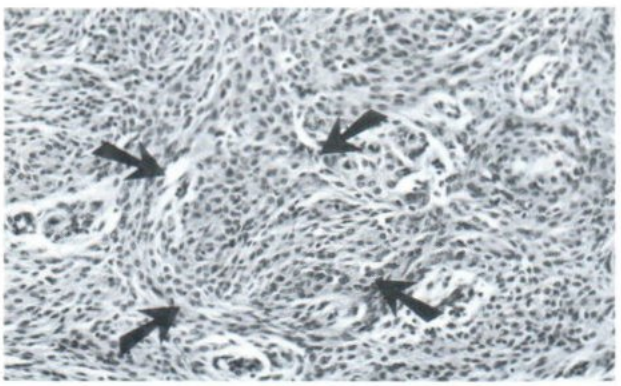

1D

Fig. 1. Parietal convexity meningioma, transitional subtype. MRI shows low signal intensity on T1-weighted (1.A) and high signal intensity on T2-weighted images relative to gray matter (1.B). Strong and homogeneous enhancement with gadolinium is noted (1.C). Hyperostosis of adjacent bone is also seen. Histologically, the tumor is characterized by whorl formations (black arrows) and seperated by spindle cells (1.D).

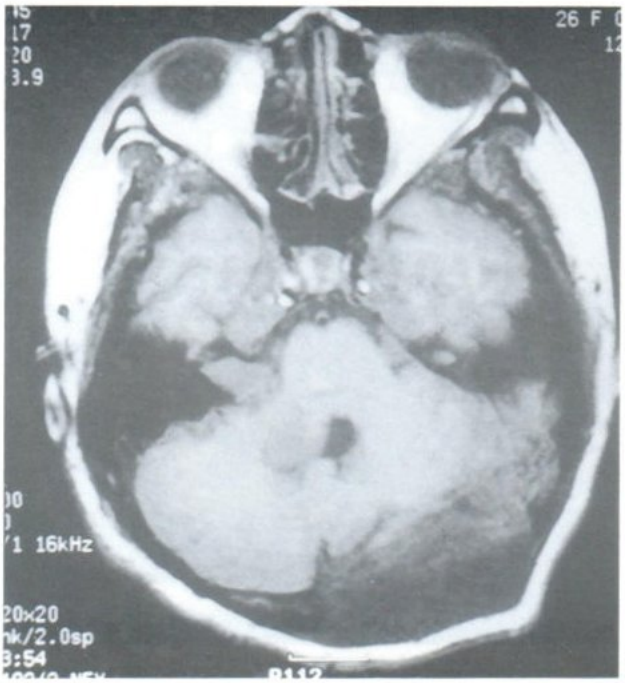

2A

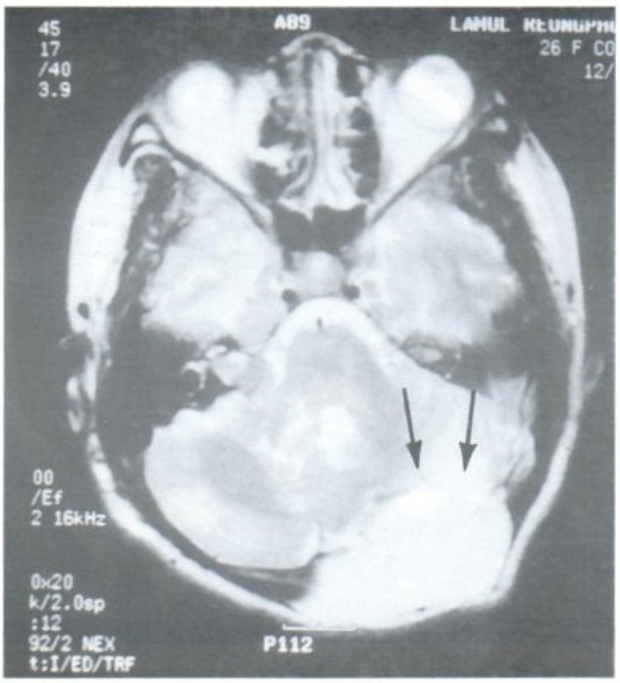

2B

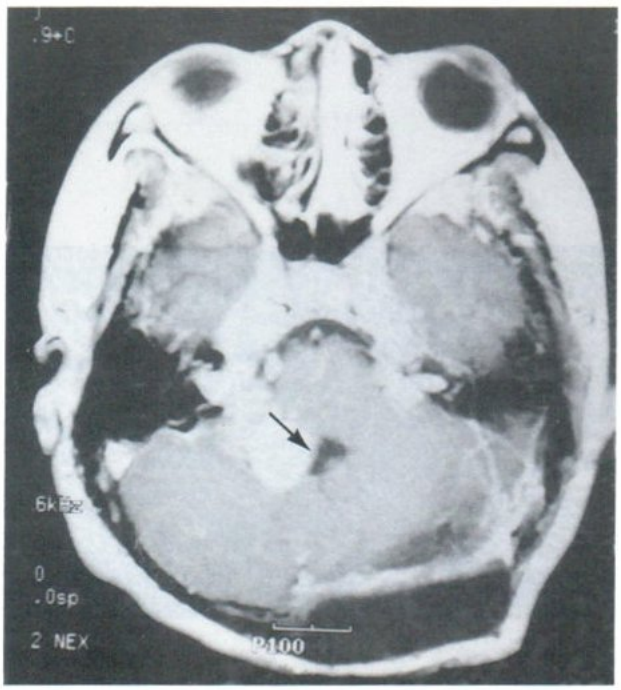

2C

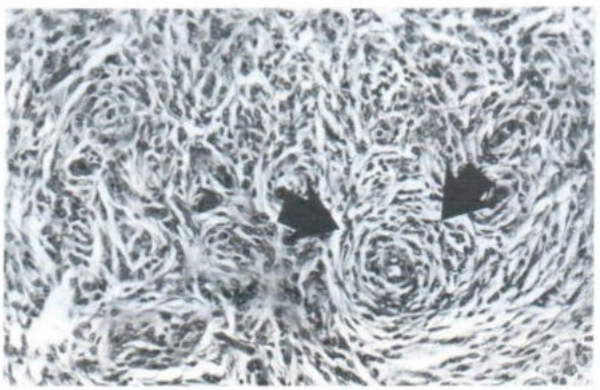

2D

Fig. 2. Recurrent, transitional subtype meningioma at both cerebellopontine angles. The tumors extend to Rt. petrous and parasellar region. The tumors is isointense to gray matter on T1 and T2 weighted images (2.A, B) and shows strong enhancement with gadolinium (2.C). Tumor compression on lateral wall of fourth ventricle is seen (short arrow). CSF collection from previous surgery is seen (long arrows). Histological finding is typical onion skin appearance (black arrows), transitional subtype (2.D).

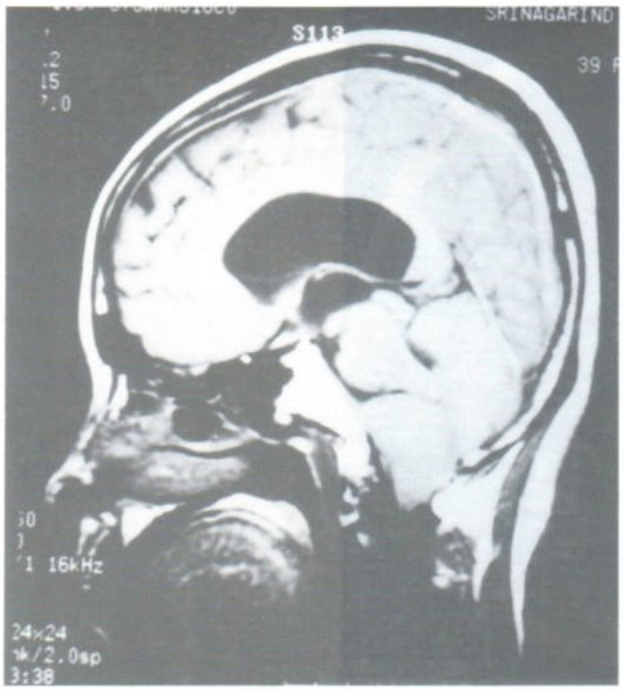

3A

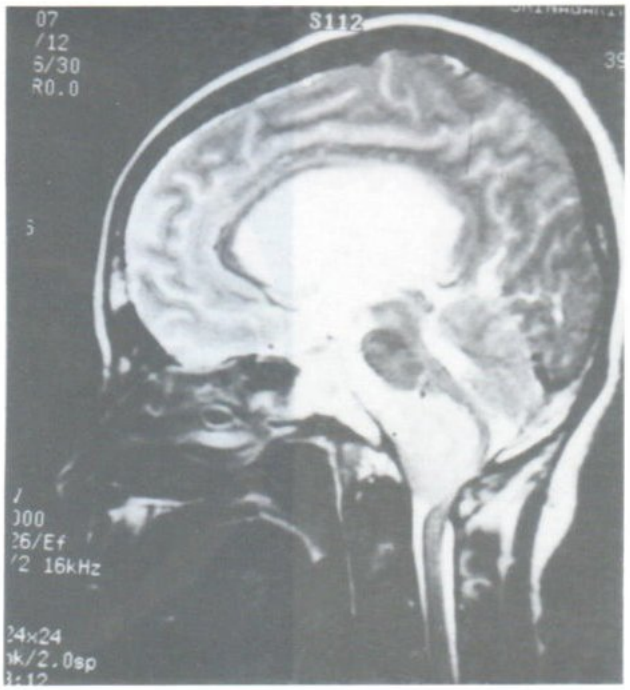

3B

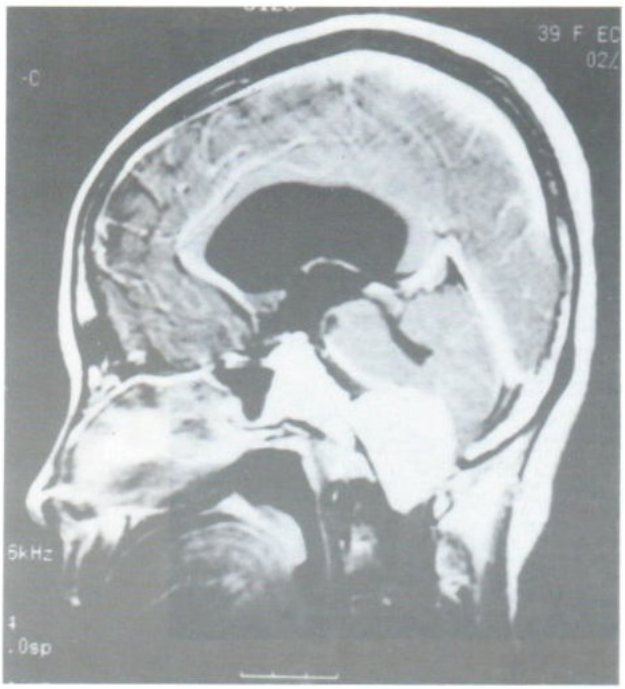

3C

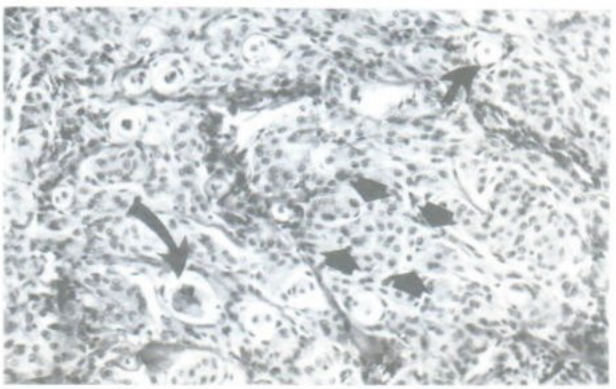

3D

Fig. 3. Cervicomedullary junction meningioma, meningothelial subtype. The tumor is isointense relative to gray matter on T1 and T2 weighted images (3.A,B), enhanced densely and homogeneously with gadolinium (3.C). The adjacent medulla is displaced posteriorly. Obstructive hydrocephalus is noted. Histologically, tumor contains syncytial cells (short arrows) that arrange in lobules. Presence of intranuclear cytoplasmic pseudoinclusions (short curve arrow) and psammomatous body (long curve arrow) are noted.

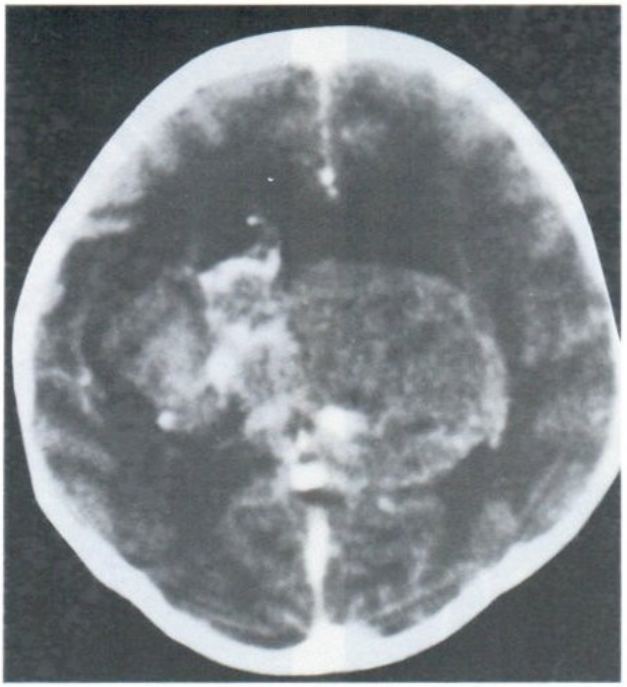

4A

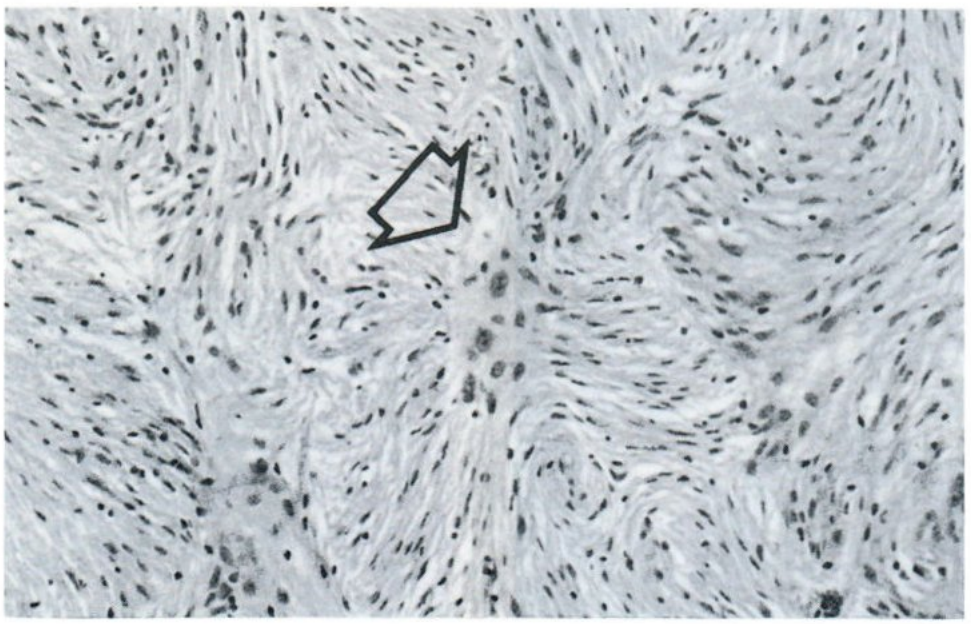

4B

Fig. 4 Atypical intraventricular meningioma with heterogeneous enhancement on post contrast CT scan (4.A). Obstructive hydrocephalus is noted. Histologically, the tumor shows storiform pattern (4.B) formed by spindle cells, characteristic of fibroblastic subtype.

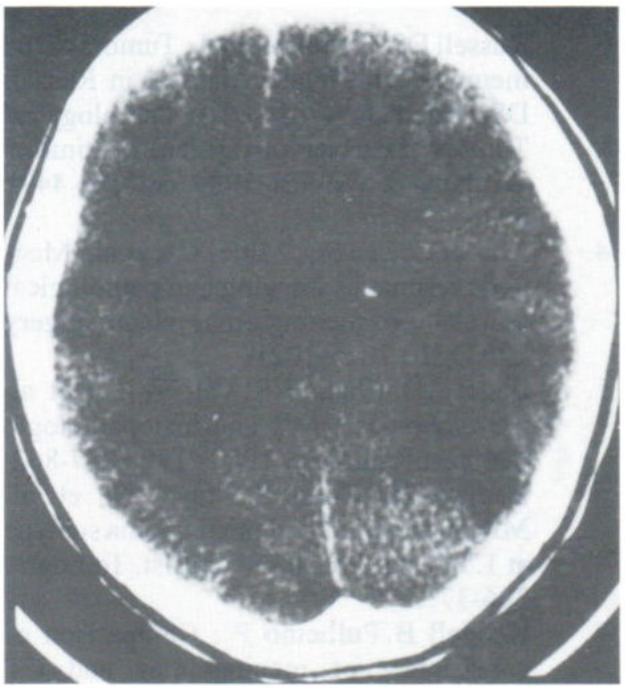

5A

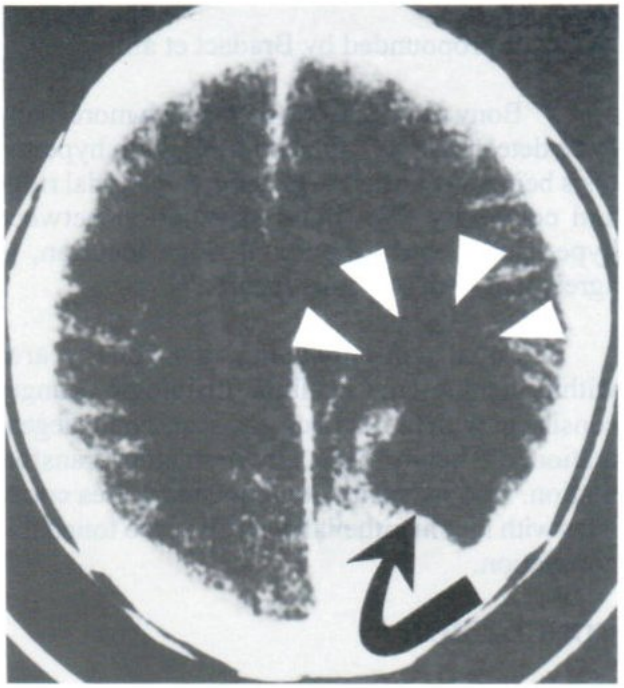

5B

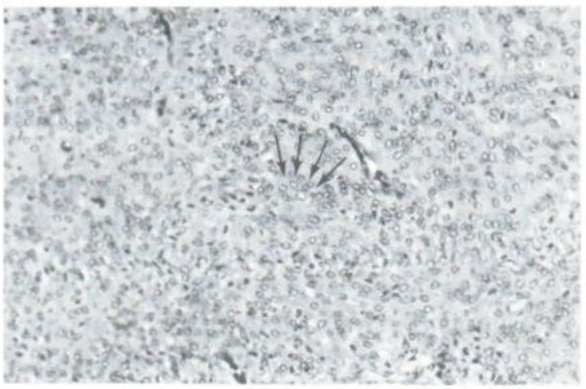

5C

Fig. 5. Lt. convexity meningioma, meningothelial subtype. The tumor is heterogeous density on noncontrast scan. Large area of focal non-enhancing low density within enhancing tumor on post contrast scan is demonstrated (black arrow). Minimal surrounding white matter edema is seen. Histologically, the tumor composes of multiple syncytial cells.

DISCUSSION

Several authors have recently reported low signal intensity on T2-weighted sequences associated with fibroblastic and transitional types, and high signal intensity on T2-weighted images correlated with meningothelial, angioblastic and malignant types.[4,5,6] Kendall and Pullicino reported no correlation between the degree of enhancement on CT scans with histological features, vascularity or consistency of the meningiomas.[7] Presence of calcium within meningiomas on CT scans usually indicated fibroblastic or transitional types.[8]

Various authors have reported increased white matter edema in angioblastic , meningothelial and in meningioma with abundant progesterone receptors.[1,5,9,10]

In this series, we found a correlation between the white matter edema and the tumor size. More pronounced edema is seen with tumor size larger than 3 cm in diameter. This finding would favour a hypothesis of edema production from mechanical effects on adjacent cerebral

tissue, as propounded by Bradact et al.[11]

Bony abnormalities were much more likely to be detected by CT than by MRI, with hyperostosis being most often seen at the spheniodal ridge and convexity. We found association between hyperostosis and sphenoidal ridge location, in agreement with previous reports.[11,12]

Focal non-enhancing low density area within meningioma exhibits histologic changes consistent with tumor necrosis, scar, cystic degeneration, old hemorrhage and lipomatous transformation.[13] Low density non-enhancing area correlates with meningothelial type.[8] We also found this correlation.

CONCLUSION

We did not found any correlation between density, signal intensity with histologic subtypes. Some points to be emphasized in our series are : firstly, significant edema occured with larger lesion (over 3 cm in diameter) ; secondly, hyperostosis was predominant in sphenoidal ridge meningioma ; and lastly, focal non-enhancing low ense area are significantly correlated with meningothelial subtype.

ACKNOWLEDGEMENTS

We would like to express our appreciation to Assistant Professor Jitjareon Chaiyakum, head of the Department of Radiology and Professor Tula Dhiensiri for their advices and comments on this paper. Thanks to Dr.Chanya Tungsriseri for her valued data analysis.

REFERENCES

1. New PFJ, Hesselink JR, O" Carroll CP, Kleinman GM : Malignant meningiomas: CT and histologic criteria, including a new CT sign. AJNR 1982 ; 3 : 267-276.
2. Chi S. Zee, Thomas Chin, Hervey D et al. Magnetic resonance imaging of meningiomas. Seminars in Ultrasound, CT and MRI 1992 ; 13 : 154-169.
3. Russell DS, Rubinstein LJ : Tumors of the meninges and related tissues, in Russell DS, Rubinstein LJ (eds) : Pathology of Tumors of the Nervous system. Baltimore, Williams & Wilkins, 1989, ed 5, pp 449-507.
4. Chen TC, Zee SC, Miller CA et al. Magnetic resonance imaging and pathological correlates of meningiomas. Neurosurgery 1992; 31 : 1015-1021.
5. Elster AD, Challa VR, Gilbert TH et al. Meningiomas : MR and histopathologic features. Radiology 1989 ; 170 : 857-862.
6. Kaplan RD, Coons S, Drayer BP et al. MR characteristics of meningioma subtype at 1.5 Tesla. J. Comput. Assist. Tomogr. : 366-371.
7. Kendall B, Pullicino P : Comparison of consistency of meningiomas and CT appearances. Neuroradiology 1979 ;18 : 173-176.
8. Vassilouthis J, Ambrose J : Computed tomography scanning apperance of intracranial meningiomas:An attempt to predict the histological features. J Neurosurg 1979;50 : 320-327.
9. Benzel EC, Gelder FB : Correlation between sex hormone binding and peritumoral edema in intracranial meningiomas. Neurosurgery 1988 ;22 : 169-174.
10. Dubois PJ. Brain tumors. In : Rosenburg RN (ed). The clinical Neurosciences, Vol.4 Churchill Livingstone Inc., New York, 1984; 311-455.
11. Bradac GB, Ferszt R, Kendall BE (eds). Cranial Meningiomas:Diagnosis, Biology, Therapy, Springer. Verlag Germany, 1990; 2, 19-41, 54-56, 124-127, 143.
12. Smith HP, Challa VR, Moody DM, Kelly DL : Biological features of meningiomas that determine the production of cerebral edema. Neurosurgery 1981 ; 8 ; 428-433.
13. Eric J Russell, Ajax E. George, Irvin I. Kricheff et al. Atypical computed tomographic features of intracranial meningioma. Radiology 1980 ; 135 : 673-682.

DIAGNOSIS OF AN ILEAL DUPLICATION BY TECHNETIUM-99M PERTECHNETATE ABDOMINAL SCINTIGRAPHY: A CASE REPORT

Molrudee EKMAHACHAI, M.D.,[1] Nuthapong UKARAPOL, M.D.,[2]
Jesda SINGHAVEJSAKUL, M.D.,[3] Sombut BOONYAPRAPA, M.D.[1]

ABSTRACT

An 8-month-old boy presenting with massive rectal bleeding was referred for Technetium-99m pertechnetate abdominal scintigraphy (Meckel's scan), due to highly suspected of a bleeding Meckel's diverticulum. The most common cause of lower gastrointestinal bleeding in infancy is peptic ulceration associated with ectopic gastric mucosa in Meckel's diverticulum. However, other congenital anomalies containing ectopic gastric mucosa such as enteric duplication, should always be included in the differential diagnosis. Meckel's scan is well accepted as the only specific diagnostic method to demonstrate the presence of ectopic gastric mucosa. The Meckel's scan revealed a large curve area of radiopertechnetate uptake in the right lower abdomen, which gradually increased in intensity with time in parallel with the gastric activity. The scintigraphic findings were typical for the presence of ectopic gastric mucosa, most likely within an ileal duplication. Surgical and histopathological findings confirmed the final diagnosis of a tubular ileal duplication containing ectopic gastric mucosa.

INTRODUCTION

Enteric duplication is a rare congenital anomaly of the gastrointestinal (GI) tract, which normally locates on the mesenteric border of the intestine in contradistinction to Meckel's diverticulum. It is a rare cause of lower GI bleeding in infant and children. It may occur anywhere in the GI tract, but most commonly locates in the ileum and ileocecal region.[1-4] It may be cystic or tubular in shape, and varying in size. But, the cystic form is more common than the tubular form.[3,4] The enteric duplication is usually solitary, but may be multiple in about 15% of the patients.[1-3] It may or may not communicate with the adjacent intestinal lumen. The communicating type is less common and found approximately 20% of all enteric duplications.[5] It has a common blood supply with the adjacent normal intestine.[2,4] The mucosal lining of the enteric duplication may be that of any part of the GI tract, and as many as 35-50% of the duplications contain ectopic gastric mucosa, which may consequently lead to peptic ulceration, hemorrhage or bowel perforation as found in Meckel's diverticulum, through the mechanism of acid-pepsin secretion from this ectopic mucosa.[1,3,4] Enteric duplication may present at any age, but 85-90% of patients present during the first 2 years of life.[2,5,6] The clinical presentations usually depend on the location, size of the duplications, the compression of adjacent structures, the type of mucosal lining, and whether it communicates with the intestinal lumen.[2,6,7] However, the most common presentations are palpable abdominal

[1] Department of Radiology,
[2] Department of Pediatrics,
[3] Department of Surgery, Faculty of Medicine, Chiang Mai University, Chiang Mai 50200, THAILAND

mass and/or symptoms of intestinal obstruction.[1-4] Other clinical presentations may include lower GI bleeding, intermittent abdominal pain, abdo-minal distention, anemia, volvulus or intussusception.[1-4,6]

Enteric duplication should always be included in the differential diagnosis of lower GI bleeding in infants and young children. Many diagnostic methods have played role for the diagnosis of enteric duplications including plain film of the abdomen.[1] contrast radiographic studies,[7,8] ultrasonography,[9,10] computed tomography [11], and Technetium-99m pertechnetate abdominal scintigraphy (Meckel's scan).[5,7,8,12-17] Among these modalities, Meckel's scan is the only specific diagnostic imaging, which can demonstrate the presence of ectopic gastric mucosa in Meckel's diverticulum, and also in other GI aberrations including enteric duplications.[18-21]

We present a rare case of a tubular enteric duplication of the terminal ileum presenting with massive rectal bleeding, which is accurately diagnosed by Meckel's scan preoperatively.

CASE REPORT

A previously healthy 8-month-old boy was presented with a history of massive bright red rectal bleeding for 3-4 times 1 day prior to admission. On physical examination, he was irritable, with moderate pale, and no jaundice. Concerning the vital signs, the temperature and the blood pressure were 38.8°C, and 110/62 mmHg. The respiratory and the pulse rate were 36/min, and 140/min respectively. The abdomen was soft without point of tenderness, and no palpable abdominal mass was found. Rectal examination revealed neither evidence of anal fissure nor palpable mass, but contained gross bloody stool. Complete blood count was normal, except for the hemoglobin, and hematocrit were 5.1 g/dl, and 16% respectively. His clinical manifestations were highly suspected of a bleeding Meckel's diverticulum. Therefore, he was then referred for a Meckel's scan. The patient was fasted for 3 hours before the study. The Meckel's scan was performed by intravenous injection of Technetium-99m (Tc-99m) pertechnetate with a dose of 1 mCi (37 MBq). The patient was placed in the supine position under a large-field-of-view gamma camera, equipped with a low-energy general purpose collimator, using the Apex SP-4 Elscint gamma camera. After a bolus injection of the radiotracer, a dynamic study of the abdomen was obtained at 2 second intervals for 60 seconds to examine blood flow, and blood pool patterns of the abdomen. Sequential anterior abdominal images were then taken at 1 minute (blood-pool image), 5, 10, 15, 30, 45, and 6 minutes after injection. Each image was acquired for 500 K counts, in 256 x 256 matrix. Additional right lateral views of the abdomen were also obtained in order to differentiate the right renal and ureteric activity from the activity in the ectopic gastric mucosa. Potassium perchlorate (5 mg/Kg of body weight) was also given orally at the termination of the study, in order to minimize the radiation dose to the patient's thyroid. The Meckel's scan revealed a large curve area of radiopertechnetate uptake in the right lower abdomen, which was first seen since blood-pool image, simultaneously with the normal uptake of the stomach. This focal area of increased uptake showed gradually increased in intensity with time, in parallel with the gastric activity (Figure.1), and it was most intense at 1 hour after injection. The right lateral views showed that the area of abnormal activity was located anteriorly, and compatible with an intraperitoneal structure. The pattern of scintigraphic findings was characteristic of the presence of ectopic gastric mucosa. However, it was much larger than the typical Meckel's diverticulum. Regarding to the size, configuration, and location of the pertechnetate uptake, a diagnosis of an ileal duplication was then reported. He underwent a laparotomy, and a 3 x 15 cm tubular duplication of the terminal ileum

was found within the mesentery approximately 10 cm from the ileocecal valve (Figure.2). The enteric duplication was anatomically separate from the terminal ileum. However, there was a small communicated tract found at the proximal end between the duplicated bowel and the adjacent ileum (Figure.3). The ileal resection with end to end anastomosis was performed. The resected specimen revealed a 0.8 cm diameter ulcer within the mucosa of the duplication, which was the cause of massive rectal bleeding in this patient. Postoperative period, the patient recovered uneventfully. The microscopic findings confirmed the final diagnosis of a tubular ileal duplication containing ectopic gastric mucosa.

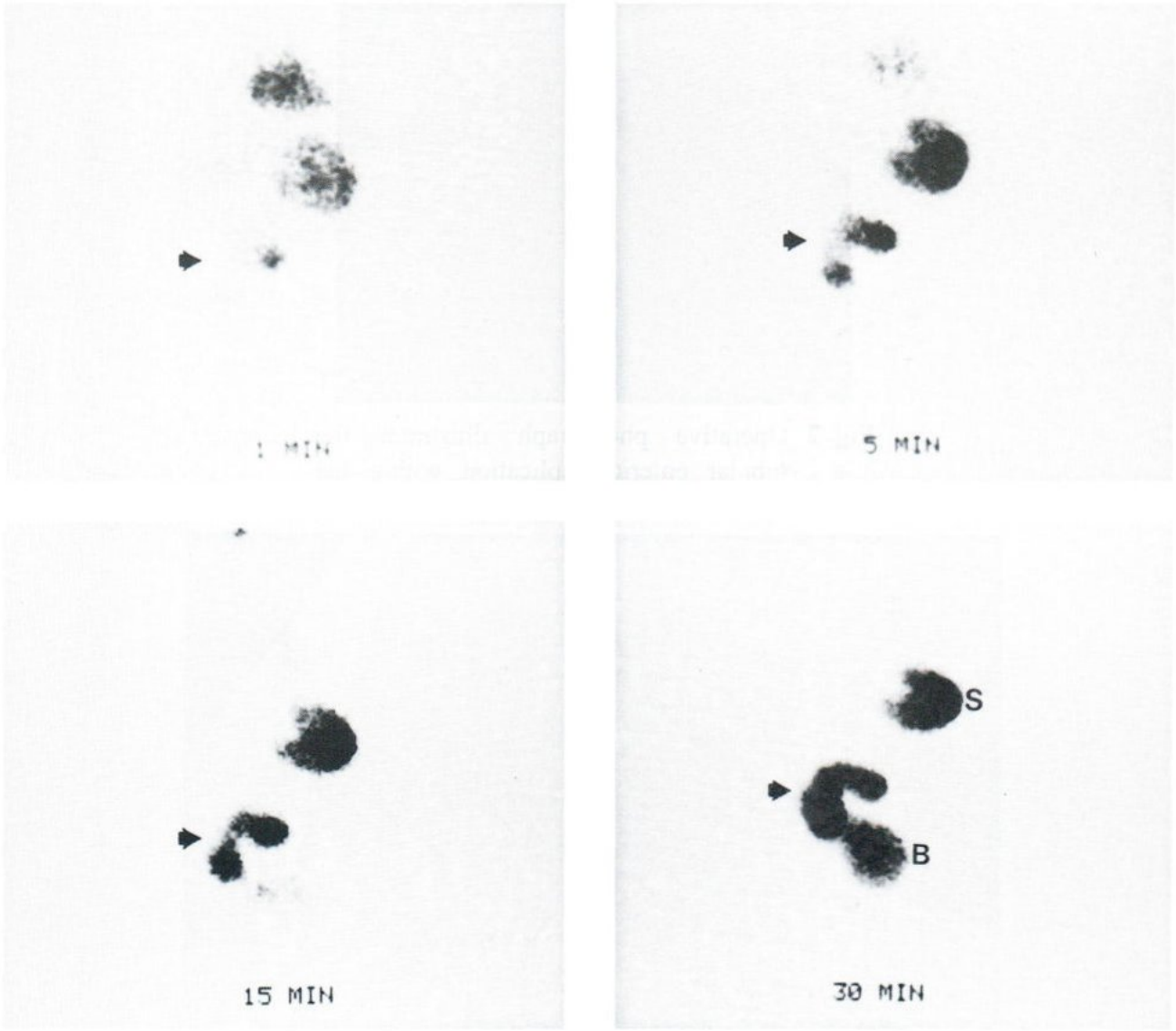

Fig. 1 Serial anterior images of the abdomen after intravenous administration of Tc-99m pertechnetate at 1 min (A), 5 min (B), 15 min (C), and 30 min (D) show a progressive accumulation of the radiopertechnetate in the right lower abdomen (arrows), which parallels with increasing gastric activity. Regarding to the size, configuration, and location of the pertechnetate uptake, an ileal duplication was diagnosed. At surgery, a 3 x 15 cm tubular ileal duplication within the mesentery was found, and resected. [S = stomach, B = urinary bladder]

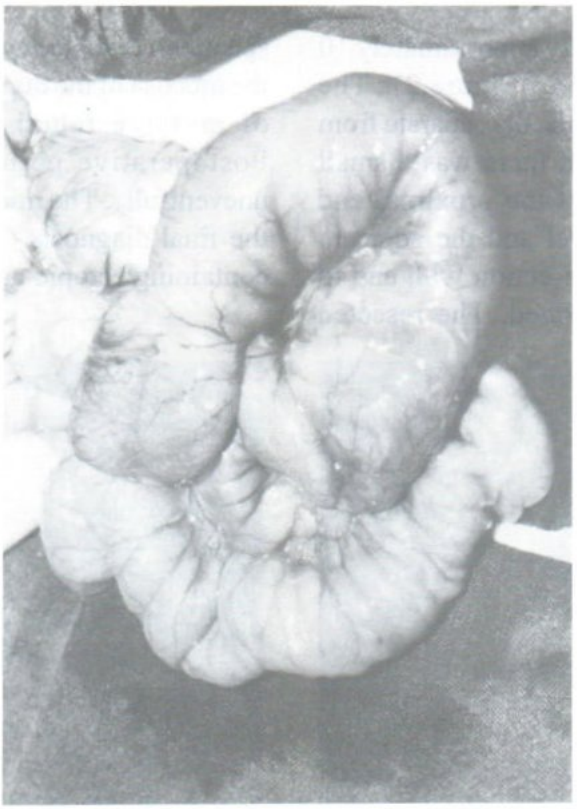

Fig. 2 Operative photograph illustrates the tubular enteric duplication within the mesentery of the terminal ileum.

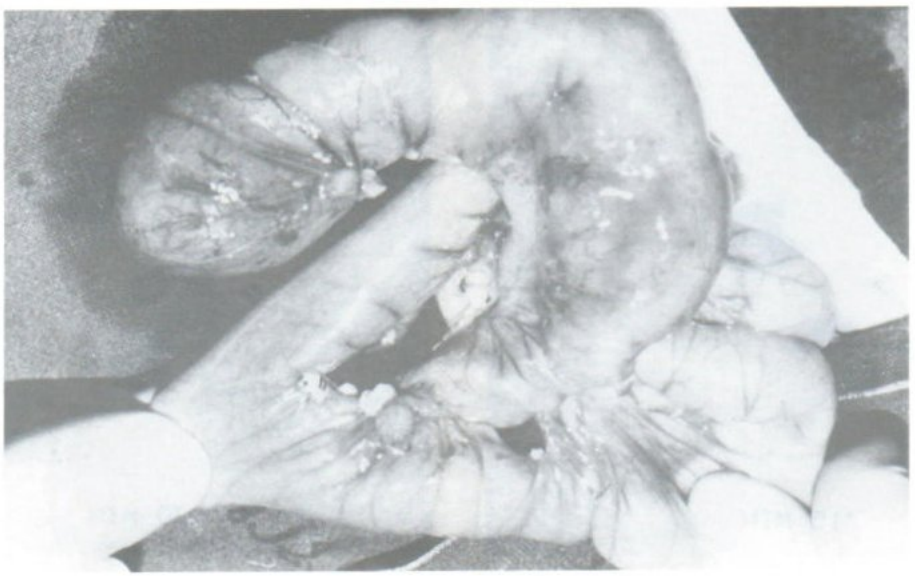

Fig. 3 Operative photograph demonstrates that the tubular enteric duplication is anatomically separate from the terminal ileum. However, there is a small communicated tract at the proximal end between the duplicated bowel and the adjacent ileum.

DISCUSSION

The most common site of ectopic gastric mucosa is in a Meckel's diverticulum, which is the most common cause of painless lower GI bleeding in previously healthy child. [18] It is worth noting, however, that other congenital anomalies containing ectopic gastric mucosa particularly enteric duplications, should always be included in the differential diagnosis. Because identical complications may occur through the mechanism of acid-peptic secretion of this ectopic mucosa.[2-4,7,8]

Meckel's scan is the investigation of choice in patients with suspected of a bleeding Meckel's diverticulum. It is well accepted as the most sensitive and specific method to demonstrate the presence of ectopic gastric mucosa in Meckel's diverticulum, as well as in other GI aberrations.[18-21] The Tc-99m pertechnetate anion will be selectively accumulated, and subsequently excreted into the intestinal lumen by the mucus-secreting cells of gastric mucosa, which is the principle of this test.[22] Ectopic gastric mucosa can be detected by scintigraphy, because it accumulates pertechnetate, and hence contrasts with the relatively low background activity of the abdomen.

The typical scintigraphic finding of Meckel's diverticulum is a small rounded area of increased pertechnetate uptake, generally in the right lower quadrant, although it may be found anywhere in the abdomen depending on the bowel motility. This activity usually appears simultaneously with the activity of the stomach, increases in intensity in parallel with the gastric activity, and persists throughout the imaging period.[18-21] Unlike in our patient, even though the radiopertechnetate uptake in the right lower abdomen was characteristic of the presence of ectopic gastric mucosa. But regarding to its large size, configuration, and location, the scintigraphic findings were compatible with an ileal duplication rather than a Meckel's diverticulum, which the final diagnosis of an ileal duplication was later confirmed by surgery.

Other sites of ectopic gastric mucosa in the abdomen will have a similar scintigraphic appearance, except that the area of pertechnetate accumulation tends to be larger, and can be found anywhere in the abdomen.[18,21] Despite the rather high incidence of ectopic gastric mucosa in the duplications, the patients present with rectal bleeding from this ectopic mucosa in only 15-20% of the cases.[1,3] The noninvasive nature of Meckel's scan makes it appropriate to be used as a screening test in pediatric patients with unexplained rectal bleeding or intermittent abdominal pain. Therefore, its value in the detection of ectopic gastric mucosa within the enteric duplications has been reported in many series.[5,7,8,12-17]

Even though, enteric duplication is relatively rare in contrast to the Meckel's diverticulum, but it should always be considered in the differential diagnosis of rectal bleeding in infants and young children. Like Meckel's diverticulum, the treatment of choice for bleeding enteric duplication is also surgical resection.[2-4,6]

In conclusion, Meckel's scan is the only simple, safe, and specific imaging to demonstrate the presence of ectopic gastric mucosa. Therefore, it is highly recommended as a routine screening investigation in the preoperative evaluation of lower GI bleeding in all infants and young children.

REFERENCES

1. Bender TM, Ledesma-Medina J, Oh KS. Radiographic manifestations of anomalies of the gastrointestinal tract. Radiol Clin North Am 1991;29:335-349.

2. Bower RJ, Sieber WK, Kiesewetter WB. Alimentary tract duplications in children. Ann Surg 1978;188:669-674.
3. Basu R, Forshall I, Rickham PP. Duplications of the alimentary tract. Br J Surg 1960;47:477-484.
4. ldstad ST, Tollerud DJ, Weiss RG, et al. Duplications of the alimentary tract. Ann Surg 1988;208:184-189.
5. Scully RE, Galdabini JJ, McNeely BU. Case records of the Massachusetts general hospital (case 16-1980): Duplication of ileum with ectopic gastric mucosa and peptic ulceration with perforation. N Engl J Med 1980;302:958-962.
6. Grosfeld JL, O'Neill Jr JA, Clatworthy HW. Enteric duplications in infancy and childhood: An 18-year review. Ann Surg 1970;172:83-90.
7. Gilchrist AM, Sloan JM, Logan CJH, et al. Case report: Gastrointestinal bleeding due to multiple ileal duplications diagnosed by scintigraphy and barium studies. Clin Radiol 1990;41:134-136.
8. Ohba S, Fukuda A, Kohno S, et al. Ileal duplication and multiple intraluminal diverticula: Scintigraphy and barium meal. Amer J Roentgenol 1981;136:992-994.
9. Lamont AC, Starinsky R, Cremin BJ. Ultrasonic diagnosis of duplication cysts in children. Br J radiol 1984;57:463-467.
10. Kangarloo H, Sample WF, Hansen G, et al. Ultrasonographic evaluation of abdominal gastrointestinal tract duplication in children. Radiology 1979;131:191-194.
11. Kelly RB, Mahoney PD, Johnson JF. CT demonstration of an unusual enteric duplication cyst. J Comput Assist Tomogr 1986;10:506-507.
12. Rose JS, Gribetz D, Krasna IH. Ileal duplication cyst: The importance of sodium pertechnetate Tc-99m scanning. Pediatr Radiol 1978:6:244-246.
13. Hitch DC, Shandling B, Gilday DL. Tubular duplication of the bowel: Use of technetium-99m pertechnetate in diagnosis. Arch Dis Child 1978;53:178-179.
14. Schwesinger WH, Croom RD, Habibian MR. Diagnostic of an enteric duplication with pertechnetate 99m-Tc scanning. Ann Surg 1975;181:428-430.
15. Wilson JP, Wenzel WW, Campbell JB. Technetium scans in the detection of gastrointestinal hemorrhage. Preoperative diagnosis of enteric duplication in an infant. JAMA 1977;237:265-266.
16. Winter PF. Sodium pertechnetate Tc-99m scanning of the abdomen. Diagnosis of an ileal duplication cyst. JAMA 1977;237: 1352-1353.
17. Garvie NW, Harrison GSM, Ackery DM. Diagnosis of an ileal duplication with sodium pertechnetate Tc-99m: Case reports. Br J Radiol 1978;51:825-826.
18. Siddiqui AR. Pediatric applications. In: Mettler FA, eds. Radionuclide imaging of the GI tract. New York: Churchill Livingstone; 1986:247-286.
19. Sfakianakis GN, Conway JJ. Detection of ectopic gastric mucosa in Meckel's diverticulum and in other aberrations by scintigraphy: I. Pathophysiology and 10-year clinical experience. J Nucl Med 1981;22: 647-654.
20. Sfakianakis GN, Conway JJ. Detection of ectopic gastric mucosa in Meckel's diverticulum and in other aberrations by scintigraphy: II.Indications and methods-A 10-year experience. J Nucl Med 1981;22: 732-738.
21. Cooney DR, Duszynski DO, Camboa E, et al. The abdominal technetium scan (a decade of experience). J Pediatr Surg 1982; 17:611-619.
22. Chaudhuri TK, Polak JJ. Autoradiographic studies of distribution in the stomach of Tc-99m-pertechnetate. Radiology 1977; 123:223-224.

QUALITY CONTROL AND DOSE REDUCTION IN GENERAL DIAGNOSTIC X-RAYS IN BANGKOK.

Jongjin PATARAMONTREE, M.Sc. (Nuclear Physics)[1]
Jajaval APAIPHONLACHAN, B.Sc. (RT), M.P.A. [2]
Parnnee CHAICHAN, B.Sc. (RT)[3] Wiwich THAMWERAWONG, B.Sc. (RT)[4]

ABSTRACT

The quality control of x-ray units has been installed in three university hospitals in Bangkok. Thermoluminescent dosemeters were used to measure the entrance surface dose of patients having general x-ray examination. New techniques are applied for dose reduction and the diagnostic quality of imaging is keeping. The effective doses were calculated by Monte Carlo techniques. Patient doses were very much lower than the permissible dose recommended by the International Commission of Radiation Protection in 1990.

Key word: Radiation protection, entrance surface dose and effective dose.

INTRODUCTION

According to the assignment of the IAEA, the experimental study of entrance surface dose in general x-ray examination was performed during Feb.1996 - Jun.1998. The grab sampling was done in teaching hospitals for technologists in Bangkok, Thailand. The outcome of new techniques for dose reduction will be put into routine practices and transfers to other hospitals. The assessment of the radiation exposure in Thailand involved in three phases: quality assurance,[1,2] dose measurement and estimation of organ dose. The minimum sample size to achieve a given level of confidence for the effective dose was assigned by the International Atomic Energy Agency (IAEA).[3,4] Therefore three hospitals collected information of ten adult patients[5] of each following seven x-ray projections: Chest PA and lateral, Lumbar Spine AP and lateral (including L5-S1), Pelvis AP, Skull PA and lateral. Each hospital estimated the frequency of examinations performed in each selected x-ray room by collecting the individual patient examination data during a period of two weeks. All selected x-ray rooms were in the outpatient department. The emergency cases were excluded. Thermoluminescent dosimeters were dosimeters of choice suitable for surface dose measurement.[6] The information of the x-ray equipment in each hospital was shown in Table 1. They were tested their quality by the physicist of Division of Radiation and Medical Devices (RMD), Ministry of Health.

OBJECTIVES

- To reduce the entrance surface dose to the patients having general x-ray examinations while the image qualities of radiographs are

[1] Department of Radiology. Chulalongkorn Hospital, Faculty of Medicine, Chulalongkorn University, Bangkok, Thailand.
[2] Department of Radiology. Ramathibodi Hospital, Faculty of Medicine, Mahidol University, Bangkok, Thailand.
[3] Department of Radiology. Siriraj Hospital, Faculty of Medicine, Mahidol University, Bangkok, Thailand.
[4] Division of Radiation and Medical Devices, Department of Medical Science, Ministry of Public Health, Nonthaburi, Thailand.

maintained.

- To assess radiation risk to the patient in term of total energy imparted to the patient or the effective dose.

METHOD AND PROCEDURE

1. Count the number of retake radiographs before and after quality control installation.

2. Study the sensitivity of film-screen combination and the variation of the optical density of radiographs according to x-ray tube potential.

3. Install the quality control on seven x-ray units in three hospitals.

3.1 QC tests for x-ray tube and generators. The test meter were Victoreen NERO 6000B.

3.2 The half value layer (HVL) measurement. The HVL experiment was setting at 80 kVp, 10 mAs, 75cm focus to chamber distance, and the beam area at chamber were 14x14 cm^2. The ionization chamber was the Victoreen Rad Check Plus.

3.3 The x-ray beam coincidence and alignment. The measurement was done using Victoreen beam alignment and collimator test tool.

3.4 The film screen speed test. Samples of cassettes were selected to test their speed by exposing to 40 kV, 80 mA, 0.04 sec, at 120 cm FFD. This nominated technique yielded density of films equal to1. The X-rite Densitometer calibrated by a standard sensi-strip produced by Kodak was used to read the optical density.

3.5 The control of view boxes. The conditions of viewing radiographs were checked by the sensitive optometer. The meter was held in contact with the viewbox. Measure the illumination level of all selected viewboxes after turned on and stabilized condition.

3.6 The control of x-ray film processor by sensitometry. Provide sensi-strips for every hospital by exposing Fuji x-ray film to Kodak sensitometer. To study the function of automatic processor, the optical density of sensi-strips were read by X-rite densitometer that was calibrated by the standard sensi-strip produced by Kodak Company.

4. Use 180 thermoluminescent dosimeters to measure the entrance surface dose of 210 adult patients of 50-75 kilogram in weight who had seven types of x-ray examination. Use grabsampling technique till quotas of ten patients were filled for one type of examination in every hospital. Three chips of LiF (TLD-100) were stuck to a patient's skin at the center of beam. Use calibrated TLD-reader, Harshaw 5500 to read the luminescence of these chips.

5. Apply the optimization technique for dose reduction to three hospitals by increasing tube potential and reducing the exposure time. Another hospital selected the method of increasing the screen-film sensitivity for optimization.

6. Measure the entrance surface dose of patients after dose optimization by thermoluminescent dosimeters. The second group of 270 adult patients weighted 50 - 75 kilogram was grabbed as a sample.

7. Radiologists or co-investigators checked all x-ray films with the record of patient dose by following the evaluation form of the Commission of the European Community.[7] They compared the image quality of radiographs taken both before and after dose optimization. The image of Victoreen R/F phantom was also a standard to check the contrast and details of imaging system.

8. Calculate the effective dose using the Monte Carlo calculation and the frequency of radiographic procedure.

9. Use t-test to find the difference between the average effective dose of pre and post optimization.

RESULTS

The quality control test was carried out. Most of x-ray units are in the limit of tolerance as shown in Table 1. The control of x-ray film processor by sensitometry in Table 2 shows the lowest speed index of film used by S. Hospital. A low speed film is one of causes that technicians had to give rather high exposure dose to patients to maintain details of diagnostic information.

In the primary study of pre-optimization, a survey of film reject analysis was carried out during two weeks in Feb.1996. The head of technician in charge checked their films before passing them to radiologists. The hospital that had film rejected rate exceeded than 10 percent should attempt to reduce it in the period of post-optimization. The success was found after the running of quality control starting in Sept 1996 and further as shown in Table 3.

The main causes of rejection are films being too dark or too light. Other causes of rejected films are mainly miss positioning, patient movement, film loss, superimpose imaging, light leakage, hair silhouette, shadow of metal, marker in wrong position, short breath, miss print, grid cut off, grid out of alignment, film stuck and paper in the cassette. The problem of positioning occurs mostly in taking lateral position of skull.

Table 1. QC test results of x-ray unit checked by the Secondary Standard Dose Laboratory, Division of Radiation and Medical Devices, Ministry of Health, Thailand (1996)

Parameters	tolerance	Hospital-Room						
		C4	C5	C6	R4	R7	S228	S235
kV_{80} accuracy	(10%)	3.1	0.3	2.8	1.2	2.6	-1.5	3.1
kV_{80} consistency	(10%)	0.2	-1.1	NM	NM	-0.5	-3.1	2.2
kV_{80} reproducible	(5%)	0.9	0.4	0.0	0.1	0.0	0	0.4
Timer accuracy	(10%)	-2.3	-2.1	NM	NM	-0.5	4.0	10
Timer reproducible	(5%)	0.1	0.0	NM	NM	0.8	-0.5	9.1
mAs linearity	(10%)	3.0	2.5	NM	NM	13.4	2.0	2.1
Output(mGy/mAs)	(10%)	8.7	1.9	0.1	0.0	0.3	0.4	3.7
Output consistency	(10%)	6.6	2.4	NM	NM	0.0	7.0	6.5
Light/radiation beam alignment	(-2%)	-0.5	0.8	0.5	0.7	0.0	-2.5	-1.0
$H.V.L_{80}$ (mm. of Al)		2.3	2.6	3.4	3.0	2.7	2.9	2.8
Total filtration (mm. of Al)		3.0*	3.4*	4.9*	3.0	2.7	2.9	2.8
Film/screen speed (pre-opt)		400	400	400	200	200	200	200
(post-opt)		400	400	400	200	200	400	400
Max. % deviation of beam alignment.		-0.5	0.8	0.5	0.7	0.0	-2.5	-1.0
Av. intensity of view boxes (candle/m^2)		1018 ± 118			966 ± 128		1104 ± 182	

Note: NM = No measurement

* = No measurement, data taken from the x-ray manufacturer

Table 2. The comparison of the base and fog, the speed index and the contrast index of film used in 3 hospitals

Hospital – processor, developer	av. temperature (°C)	av. Base + fog density	speed index (step 10)	contrast index (step13-step10)
C-Kodak, M6-Kodak	35.59	0.147	0.804	1.534
R-Kodak, M6B-M champion	35.59	0.153	0.63	1.256
R-Kodak, M8-Kodak	35	0.160	0.643	1.014
S-Kodak, M6-Fuji Hunt	35.17	0.138	0.394	1.067

Table 3. Film rejection rate of 3 hospitals in 10 days before and after optimization.

Hospital	(C)		(R)		(S)	
Observation	pre-op	post-op	pre-op	post-op	pre-op	post-op
number of x-ray room	3	3	3	3	2	1
av. film used / day	292	258	154	132	68	55
% rejected rate	8	5	3	2	13	10

Table 4. Technical characteristic of TLD system

TLD reader	Harshaw 5500
TL material	Lif-100 (ribbon)
%SD of batch	3.81
Annealing procedure	400°C/1h + 100°C/2h
Reading process	T_{max} = 300°C; time = 20 sec; N_2 flow
Reading period after exposure	1 -15 days
Calibration after each annealing procedure	yes
Source used for calibration	Co-60
Cleaning process	no

Table 5. Irradiation conditions for calibration of TLD system

KV	HVL (mm. of Al)	effective energy (keV)	nominated air kerma (mGy)	TLD reading (mGy)	energy dependence normalized to Co-60	energy response factor
50	1.513	25.7	50.1	158.197	2.59	0.317
80	2.896	33.0	49.8	154.865	2.54	0.322
120	5.613	44.5	50.0	143.519	2.35	0.348
Co-60	-	1250	49.8	61.056	1.0	0.863

Table 6. Irradiation conditions for calibration (linearity) of TLD system

kV	HVL mm. of Al	effective energy (keV)	nominated air kerma (mGy)	TLD reading (mGy)	% error of measurement
80	2.896	33.0	49.8	49.80	0.00
80	2.896	33.0	04.99	04.94	0.01
80	2.896	33.0	00.10	00.07	0.30

Table 7. The average entrance surface dose per radiograph of adults classified by type of examinations and their standard deviation corresponding to exposure techniques. (N=30)

Examination	Av. entran. surf. dose (mGy)		Av. pt. weight(kg)		kV		mAs	
	Pre-optimiz.	Post-optimiz.	Pre-op.	Post op	Pre-op.	Post op.	Pre-op.	Post op.
Chest PA	0.30 ± 0.14	0.19 ± 0.09	59.3	57.0	60-80	80-90	3-20	2-12
Chest Lat.	0.89 ± 0.48	0.50 ± 0.06	59.1	60.0	60-85	85-95	10-40	7-20
Lumbar spine AP	3.46 ± 2.09	1.39 ± 0.65	59.0	57.8	60-85	75-95	16-65	8-20
Lumbar spine Lat.	9.75 ± 5.32	4.94 ± 3.53	59.5	58.5	70-96	80-100	36-150	24-50
Pelvis AP	1.84 ± 1.08	1.08 ± 0.47	56.2	59.3	60-85	75-90	6-48	5-22
Skull PA	1.64 ± 0.8	0.80 ± 0.26	56.0	56.8	60-75	75-90	16-50	6-30
Skull Lat.	1.32 ± 0.65	0.55 ± 0.17	56.8	56.5	58-73	70-90	8-40	6-20

Table 8. Mean effective doses for radiographic projections classified by hospital. (n = 10)

Hosp.	Mean effective dose (mSv)								
	C			R			S		
Examination	Pre-op	Post-op	% reduct.	Pre-op	Post-op	% reduct.	Pre-op	Post-op	% reduct
Chest PA	0.02	0.03	+	0.04	0.03	25	0.03	0.02	33
Lat	0.01	0.03	+	0.10	0.07	30	0.06	0.02	67
L.Spine AP	0.2	0.09	55	0.60	0.03	50	0.49	0.16	67
Lat	0.12	0.07	42	0.24	0.21	12	0.26	0.06	77
Pelvis AP	0.10	0.11	++	0.42	0.19	55	0.35	0.22	37
Skull PA	0.007	0.005	29	0.012	0.007	42	0.02	0.01	50
Lat	0.01	0.003	70	0.01	0.006	40	0.02	0.009	55

\+ Mean effective dose is increased due to limitation of kV increasing.

++ Mean effective dose is increased due to the average body weight of patients in pre and post optimization were different.

Table 9. Typical organ doses classified by examination type in ...x10^{-3} mGy.

Exaination	Chest		Lumbar Spine			Pelvis		Skull	
Projection	PA	L. lat	AP	L. lat	R. lat	AP	AP	PA	L.Lat
kV	80	85	85	85	85	80	75	75	73
H.V.L	3.0	3.0	3.0	3.0	3.0	3.0	3.0	3.0	3.0
E.S.D (mGy)	0.26	0.97	2.81	7.97	7.97	1.59	1.37	1.37	1.09
Projection freq.	1.16	1.25	1.24	1.29	1.29	1.11	1.17	1.17	1.64
Organ	Mean organ doses (.....x10^{-3} mGy)								
Brain	0.5	1.6	0	0	0	0	230	240	354
Eye lens	0.3	4.1	0	0	0	0	1500	13.6	728
Thyroid	11.1	59.4	0.8	0.7	0.8	0	107	31.9	37
Thymus	19.0	103	11.5	7.7	6.3	0.3	1.2	0.7	0.9
Heart	41.9	122	116	32.3	44.7	1.5	0.3	0.2	0.1
Lungs	124	265	71.4	49.2	44.0	1.1	1.5	1.5	1.1
Breast	22.8	307	20.7	6.8	6.4	1.4	0.6	0.1	0.3
Esophagus	56.7	95.1	135	28.5	64.7	1.4	4.8	6.8	3.9
Stomach	27.8	17.4	1410	55.0	529	54.0	0	0	0
Spleen	117	11.3	312	41.9	2930	15.6	0	0	0
Adrenal	138	87.7	222	372	374	5.8	0	0	0
Kidney	92.6	62.2	233	968	968	31.1	0	0	0
Liver	55.8	302	824	1490	49.9	33.5	0	0	0
G bladder	19.9	67.8	1270	497	146	87.2	0	0	0
Pancreas	54.6	47.1	646	196	940	16.4	0	0	0
ULI	3.1	7.8	1160	641	288	528	0	0	0
Small int	2.3	4.9	970	470	496	457	0	0	0
LLI	0.5	0.5	532	43.1	562	438	0	0	0
Ovaries	0.3	0.9	707	489	474	387	0	0	0
U bladder	0.1	0.3	616	65.1	67.0	872	0	0	0
Uterus	0.4	1.0	924	234	239	514	0	0	0
Tot. bone	78.7	140	117	258	259	102	166	121	184
RBM	36.5	64.8	117	221	223	57.2	27.2	22.6	30.7
Skin	28.1	114	178	349	251	147	53.5	54.5	58.8
Eff. dose (μSv)	35.3	85.4	422	192	307	291	17.3	13.0	17.6
E.S.D (mGy)	0.26	0.97	2.81	7.97	7.97	1.59	1.37	1.37	1.09

kV, mAs and film density relationship

mAs	0	5	10	15	20	25	30	35	40	45	50	55
60 kV	0.19	0.2	0.3	0.44	0.6	0.78	0.94	1.14	1.28	1.44	1.52	1.68
70 kV	0.19	0.34	0.68	1.14	1.52	1.82	2.05	2.26	2.48	2.58	2.67	2.72
80 kV	0.19	0.66	1.34	2.02	2.5	2.7	2.8	2.9	2.92	2.96	3.02	3.07
90 kV	0.19	1.22	2.13	2.64	2.82	2.95	2.98	3.02	3.04	3.06	3.07	3.08

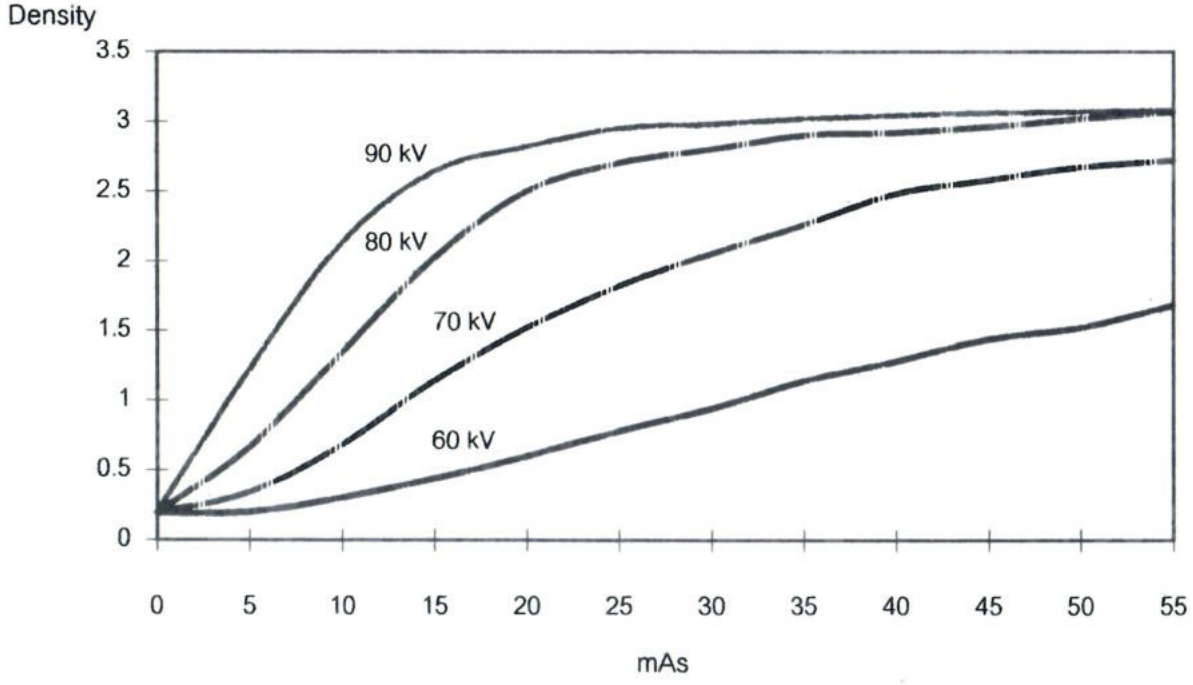

Fig 1. The relation of kV, mAs and optical film density shows that keeping the optical density constant the mAs will decrease while the tube potential increases.

The objective of the primary study was patient dose measurement of seven examinations, using TLD dosemeters that their responses varied less than 10% over the range of diagnostic x-ray qualities. Dr. John Heron, a senior scientific advisor of the primary standard laboratory, National Radiation Laboratory, Christ Church, New Zealand did the calibration of TLD reader.

Table 4 showed the technical characteristic of TLD system while Table 5 and Table 6 showed the irradiation conditions of calibration due to the energy dependence and the linearity of reading. From Table 5 the energy response of dosemeters varied by less than 5% over the range of diagnostic x-ray qualities, so factor of 0.322 was applied as the quality factor for the particular reading process.

The investigation of the film sensitivity corresponding to tube potential shows increasing of 10 kV and reducing mAs [8] to the half yielding the similar optical film density. The relation of kV, mAs and density is plotted on the figure 1. This technique is carried out in C. Hospital, and R. Hospital for the secondary study or the post optimization for dose reduction, while S. Hospital uses the rare earth cassette for optimization. The difference of two averages of entrance surface dose (pre- and post-optimization) in Table 7 was tested by t-test. They are highly difference at 99.9 % confident level (Siegel and Casellan 1988). The method of optimization reduces patient surface dose to the half. This fulfill the 'as low as reasonably achievable' (ALARA) principle. The two columns at the right hand side of the Table 7 showed the range of tube potential and exposure (mAs) using in each projection during the pre and post optimization. Radiation dosages of Thai patients are less than that of CEC recommendation.[7] Thai are thin enough to expose to low kV technique of wide latitude exposure. Table 7 also shows the average entrance surface dose per radiograph classified by hospital.

The surveys of both image quality and patient dose in efforts to reduce patient doses to such an extent that the diagnostic quality of the images is not degraded, are performed. The image quality can be affected by low doses in three distinct ways, which should be kept in mind.

- Too low a dose can simply result in images that are too faint and that can not be clearly discerned.
- Quantum mottle is a source of image degradation.
- Using the high-speed screen can lower doses and resulted in poorer spatial resolution.

Radiologists or co-investigators were continuously assessing clinical image quality. The diagnostic value of the images was realized through the radiologist's skill often carried out subconsciously. The interpretation of anatomical features according to recommendation of CEC[1] study group would be subjective interpretation. It was a simple means of checking performance against a recognized standard. So a level of uniformity can be established. To reduce bias, two radiologists in the team of research consultants did the image evaluation. Most of the films are fully acceptable. The surveys show less correlation between dose and image quality. Whereas nearly all images are declared to be diagnostically acceptable, the patient doses vary enormously as shown in Table 7.

The tertiary study was the calculation of effective dose of various organs.[9] The gonad doses and bone marrow doses were mainly important. In x-ray diagnosis, organs inside useful beams were given a higher dose at high dose rate while organs outside main beams received a relatively small dose at lower dose rate. Dr. J. Heron, National Radiation Laboratory, New Zealand, wrote the program named XDOSE to calculate the effective dose for x-ray diagnosis. By using Monte Carlo calculations that performed at the National Radiological Protection Board, XDOSE was a part

of a software report NRPB-SR262. The dosimetry performed in XDOSE was for an average 70 kg. patient. Therefore there would be some error of effective dose in Table 8 because the average of body weight of patients in this study was 58 kg. To calculate the effective dose the mean number of radiographs per projection were obtained by rejected film analysis. The value was close to unity for most examinations, the major exceptions being the lateral lumbar spine and lateral skull that the collection factors were 1.2 -1.6. The result shows the limitation of dose reduction by tube potential for mass chest x-ray unit. The x-ray beam is hard enough to give a proper contrast image in pre-optimization. It is not useful to increase more penetrating power through the patients. Technologists selected 95 kV as the maximum tube potential in taking radiographs. In case of pelvis examination, at C. Hospital, the mean patient weight in the secondary study is increased from 56 kg to 60 kg, the effective dose increasing correspondingly. However the average of effective dose after post optimization is reduced nearly to the half at 99.9% confidence level. Compare Table 7 to Table 8 in details, the relationship between average entrance surface doses and the effective dose is not in the same order because of the tissue weighted factor. The mean organ doses per examination in Table 9 show that the direction of beam projection influences the amount of effective dose. The left lateral lumbar spine and the posterio-anterior skull projection give lower dose than the opposite projections.

DISCUSSION AND CONCLUSION

Methods for dose reductions in diagnostic radiology aim to reduce the organ dose exposed from x-ray procedures. S. Hospital increases the speed of the film screen combination by using Kodak TMS/RA and Lanex. Other hospitals increase the tube potential by 10 kV. The average reduction factor is about 0.5. The penetration and scattering radiation inside the patients are modified so that reductions of the average entrance surface doses do not imply reduction in the effective dose by the same factor.[10] There is the limitation of dose reduction because of increasing of the effective dose. The average entrance surface dose per radiograph is quite lower than that recommended by the CEC. The lowest entrance surface doses are seen in applying high kVp (low mAs) technique incorporating with the using of the high speed film-screen combination: fast film and rare earth screen combination. Methods for dose reductions carry on at all teaching hospital of school of technologist. Therefore these new techniques will be accepted in all hospitals in Thailand in the next three years. The average entrance surface dose in table 7 may represent the exposure dose of adult patients going to have their radiographs at university hospitals in Bangkok. The intervention of dose reduction by increasing 10 kV and using the rare earth screen would reduce exposure as low as reasonably achievable.

ACKNOWLEDGEMENT

The authors would like to thank the Faculty of Medicine, Chulalongkorn University and the International Atomic Energy Agency (IAEA) for the financial support of this project. Particular thanks to Dr. Somjai Wangsupachart and the advisory group who encourage and give support during this work. The co-operation of many patients and staff of all contributing hospitals is also acknowledged. Sincere gratitude also goes to Professor Dr. Kunying Nitaya Suwanwela, the head of Department of Radiology, Faculty of Medicine, Chulalongkorn Hospital who points out the importance of the quality control in diagnostic x-rays for the benefit of the population.

REFERENCES

1. NRPB/RCR. National Radiological Projection Board / Royal College o f Radiographers. Patient Dose Reduction in Diagnostic Radiology. Document of the NRPB. London : HMSo 1990; 1 (3).
2. Russel J.G.B. Assessment of priorities when introducing some radiation protection methods in radiodiagnosis. Br.J.Radiol. 1986; 59: 153-156.
3. Heron J.H. Estimation of effective dose to the patient during medical x-ray examinations from measurements of the dose -area product. Phys. Med. Biol. 1992; 37: 2117-2126.
4. IPSM/NRPB/RCR Institute of Physical Sciences in Medicine/National Radiological Protection Board / Royal College of Radiographers. National Protocol for Patient Dose Measurement in Diagnostic Radiology. Document of the NRPB. London. 1990.
5. IAEA-CRP RC 573 Radiation Protection in Diagnostic Radiology in Asia and the Far East. Document of the International Atomic Energy Agency. Vienna, Austria 1995.
6. Warren-Forward H.M., Millar J.S. Optimization of radiographic for chest radiography. Br. J. Radiol. 1995; 68: 1221-1229.
7. The Commission of the European Communities (CEC) Study Group. Quality Criteria for Diagnostic Images. Brussels, CEC Working Document 2nd edition - June 1990.
8. Martin C.J., Darragh C.L., McKenzie G.A., et al. Implementation of a programme for reduction of radiographic doses and results achieved through increases in tube potential. Br. J. Radiol. 1993; 55: 228-233.
9. ICRP Publication 60, Radiation Protection, 1990 (Pergamon Press, Oxford)
10. Padovani R., Contento G., Fabretto M., Malisan V., Barbina V., and Gozzi G. Patient doses and risks from diagnostic radiology in North-east Italy. Br. J. Radiol. 1987; 60: 155-165

COMPARISON OF RADIOGRAPHIC METHODS AND COMPUTED TOMOGRAPHY SCANOGRAMS FOR MEASURING LEG LENGTH DISCREPANCIES

Wanna TRIVITAYARATANA, M.D.[1], Pichit TRIVITAYARATANA, M.Sc.[1], Chavalit VONGSABARN, B.Sc.[2], Songthip NUKROO, B.Sc.[3]

ABSTRACT

Four radiographic methods for measuring leg length discrepancies were compared to computed tomography (CT) scanograms by exposing a polyvinyl chloride (PVC) phantom. Central ray of X-ray machine was checked. At 180 cm focal film distance (FFD), the elongation error at hip, knee and ankle joints of teleroentgenography(except knee joint), teleroentgenography mixed with orthoroentgenography, orthoroentgenography, spot orthoroentgenography and CT scanograms were 20, 5, 0, 0 and 0 mm, respectively. Although the elongation error was found in the first two methods, the whole leg length could be visualized in single exposure radiograph. No elongation error occured in orthoroentgenography, spot orthoroentgenography because of the central ray centered directly over the three joints of lower limb, but they had several disadvantages. Three separate roentgenograms were needed and entired leg pathology could not be seen on one radiograph. CT scanograms was the most accurate and was the standard method for leg length measurement. However, this technique was more expensive and needed more time to complete an examination than the radiographic methods.

INTRODUCTION

Leg length inequality affects the personality especially occured on childhood and necessary to have an early treatment.[1-3] The most common causes of leg length inequality were congenital anomalies, trauma, tumor, infection and neuromuscular disease.[1,4-8] Before the pattern of growth of unequal limbs is plotted and before starting the treatment,[9,10] accurate radiographic measurement must be made.[1] Various radiographic methods were more accurate than clinical method.[5,8,11-15] Each of the radiographic methods had a different limitation, advantages and disadvantages. To determine the most accurate roentgenographic technique for the measurement of limb length discrepancies, comparing the magnitude of elongation error of four radiagraphic methods and CT scanograms were measured. The advantage, disadvantage, cost and time of examination were also determined. A PVC phantom of long leg was designed and used to avoid the abnormalities of extremities, such as flexion contractures of the hip or knee which cause increased magnification and distortion of the image.[8,12,16-19]

[1] Dept. of Radiological Technology, Faculty of Medical Technology, Mahidol University.,
[2] Dept. of Radiology, Faculty of Medicine, Ramathibodi Hospital, Mahidol University.,
[3] Kumkunkaew Hospital, Ministry of Public Health.

MATERIALS AND METHODS

A phantom was made of 4 PVC tubes diameter 4 cm, 1 mm thickness, 35 cm length to represent the leg length. For identifying the level of cross-surface of PVC tubes, Pins was fixed at the upper edges, lower edges and at the middle point of cross-surface of PVC tubes as shown in fig.1.

The center ray of Hitachi X-ray machine (Model DR 155 HN) was checked by beam alignment test tool before using for radiography. A PVC phantom and orthopaedics ruler were placed on a 30x90 or 35x42 cm cassette, as shown in fig 2. Four radiographic methods: teleroentgenography, teleroentgenography mixed with orthoroentgenography, orthoroentgenography, spot orthoroentgenography were compared to CT scanograms by exposing the PVC phantom and orthopeadics ruler 4 times in each method using the same exposure technique (50 kVp, 100mA, 0.1 s) and FFD (100, 180 cm). Diagrams of 5 methods were shown in fig. 3.

RESULTS

From beam alignment test tool, the deviation of center ray was less than 2% at 100 cm FFD or less then 3 degrees from central axis of X-ray beam. This deviation is the acceptable range.[20]

Radiographic images of a PVC phantom and orthopaedics ruler were analysed. The results showed that elongation error of teleroentgenography at hip and ankle joint were 20 mm, but no elongation error occured at knee joint. No elongation error occured at any joints in orthoroentgenography, spot orthoroentgenergraphy and CT scanograms. The elongation error at all joints in teleroentgenography mixed with orthoroentgenography were 15 mm at 100 cm FFD and 5 mm at 180 cm FFD as shown in table 1. No scale error occurred in all methods. CT scanograms was needed more time to complete an examination and more expenditure per case than radiographic methods as shown in table 2. From fig. 4A, edge of a PVC phantom was at the scale 10 cm, while the radiographic image appeared at 10.2 cm. So elongation error of teleroentgenography was 20 mm. The 3 pins was overlapped on a radiographic image of orthoroentgenography and CT scanograms. It means that no elongation error was seen in fig. 4B and 4C.

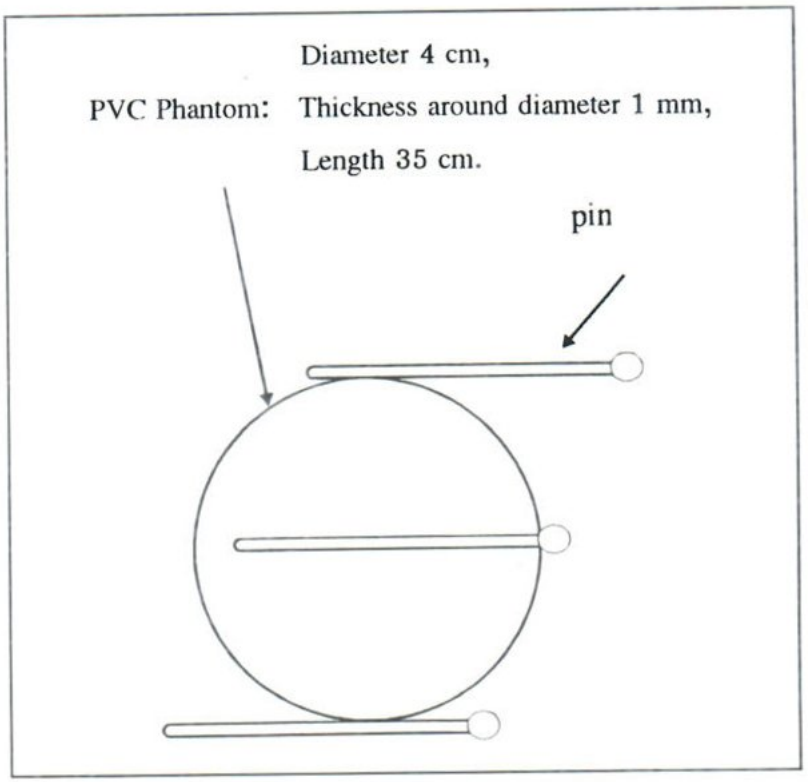

Fig. 1 Identifying the level of cross surface of a PVC phantom by the tip of 3 pins

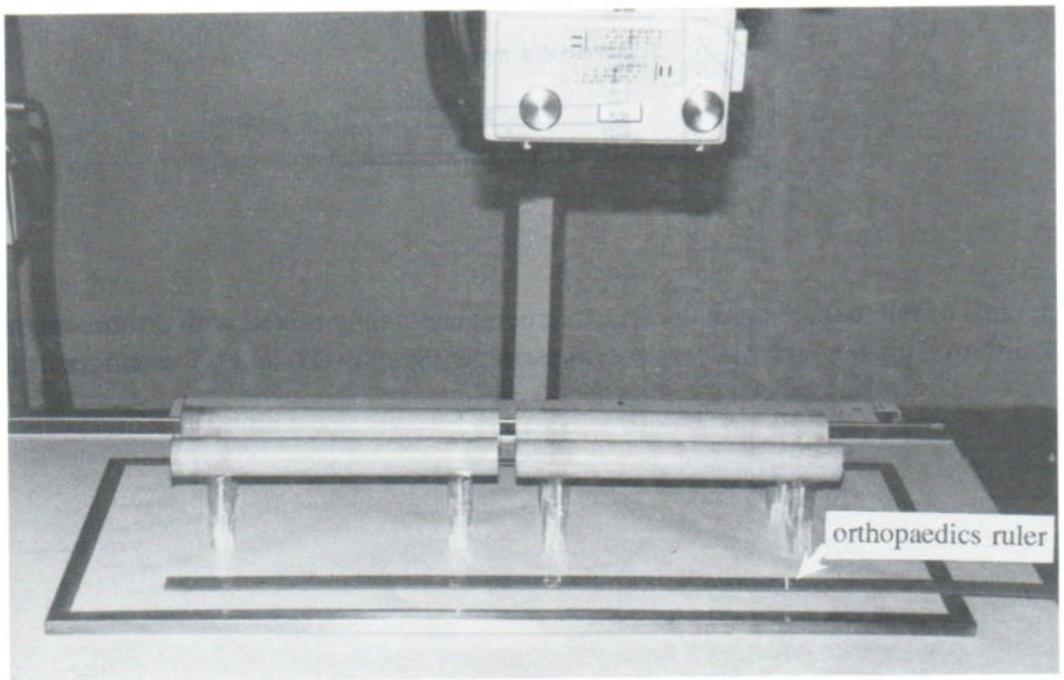

Fig. 2 Showing the arrangement of the 4 PVC tubes arranging to be the representative of two legs and one orthopaedics ruler arranging on a 30x90 cm cassette.

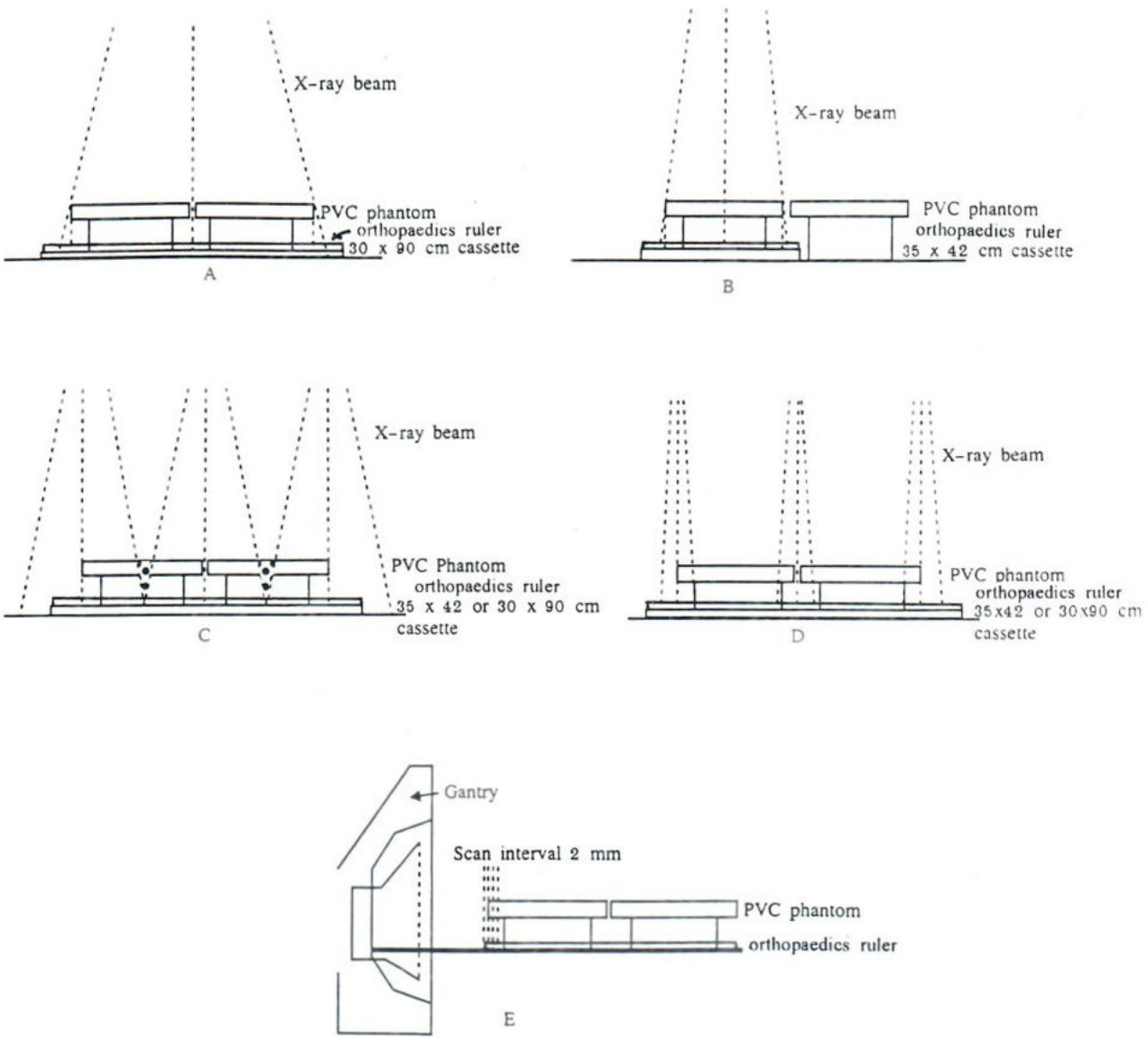

Fig. 3 Diagrams of teleroentgenography (A), teleroentgenography mixed with orthoroentgenography (B), orthoroentgenography (C), spot orthoroentgenography (D) and CT scanograms (E)

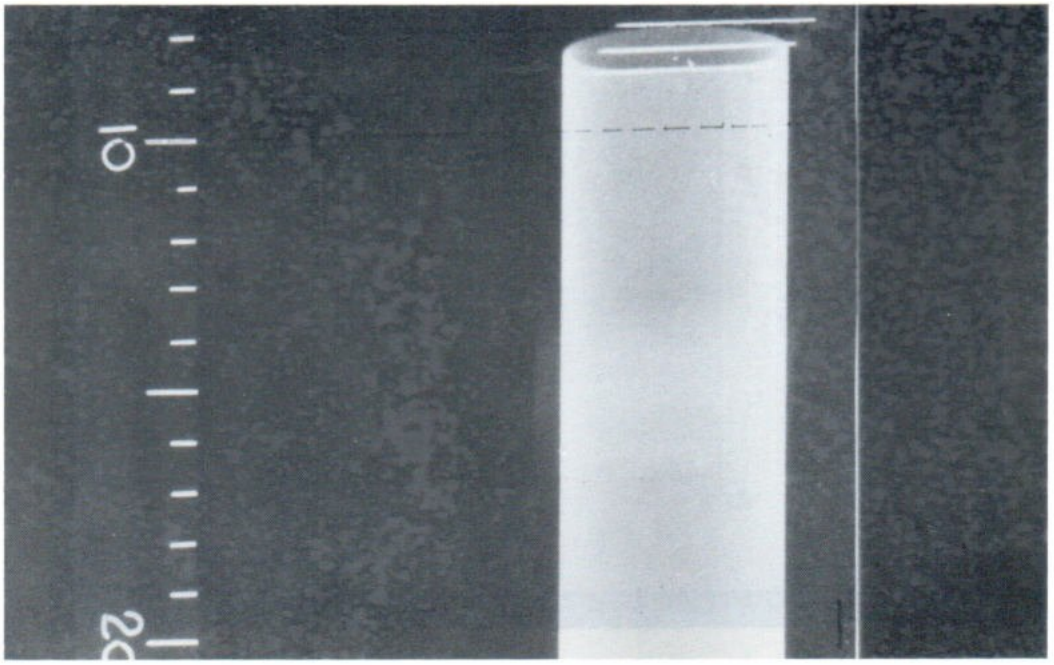

4A.

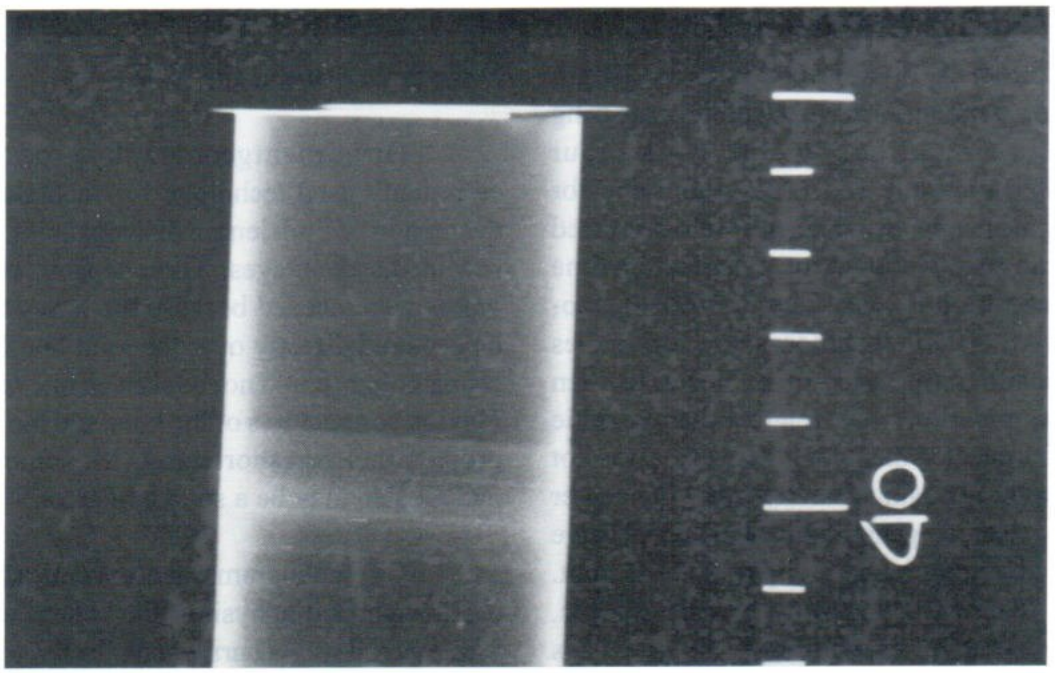

4B.

Fig. 4 Radiographic appearance of teleroentgenography (A): the accuracy of the length is not acceptable, orthoroentgenography (B): The accuracy of the length is acceptable, and CT scanograms (C): most accurate.

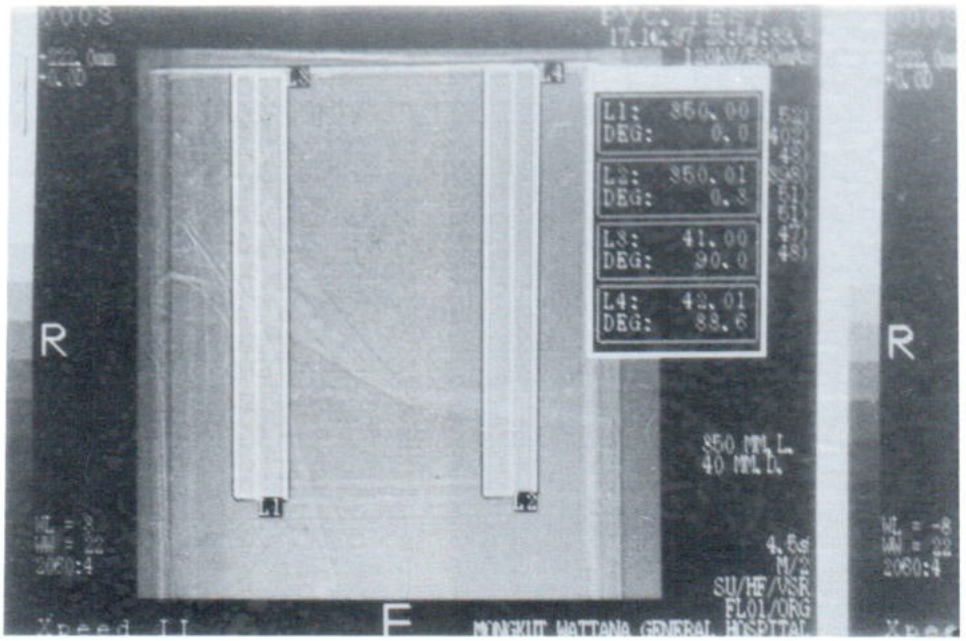

4C.

DISCUSSION

In order to obtain an exact leg length equalization, reliable and reproducible measuring methods are required. In this work, four radiographic methods and CT scanograms for measuring leg length discrepancies were discussed by comparing elongation error, examination time and expenditure per case. The orthoroentgenographic, spot orthoroentgenographic techniques and CT scanograms were more accurate than clinical examination[11] and teleroentgenographic method. It indicated that elongation error was not occured when exposing directly over the center of joint. So teleroentgenography obtained the large effects of diverging beam at hip and ankle joint. However, teleroentgenography was the simple, convenience and low expenditure technique. This procedure took about 15 minutes to perform. The entired length of both lower limbs was visualized on a single radiograph. The radiation dosage is noting more than x-raying a hip, a knee, and an ankle separately.[21] I predict that elongation error may be eliminated by placing orthopaedics ruler at the same plane as the bone.

Orthoroentgenography was the most commonly used technique for roentgenographic evaluation of limb length discrepancies, but it had several disadvantages. Three separate roentgenograms were needed because the X-ray tube must be centered directly over the joint but the entired leg pathology could not be seen on one radiograph. Flexion contractures of the knee and hip can cause projectional foreshortening. Movement by the patient also may be a source of error.[8]

CT scanograms had several advantages. e.g. the whole diaphysis of the bone is visualized. This method was accurate and effective,[22] but more expensive and needed more time to complete an examination than radiographic methods. The radiation dose was reduced to fivefold[8] or twelvefold[22] when comparing with orthoroentgenography and conventional techniques.

Table 1 Elongation error and scale error of radiographic methods CT scanograms

Method	FFD (cm)	Part exam	Elongation error (mm)	scale error (mm)	elongation-scale error difference(mm)
Teleroentgenography*	180	hip	20	0	20
		knee	0	0	0
		ankle	20	0	20
Teleroentgenography mixed with orthoroentgenography	100	hip	15	0	15
		knee	15	0	15
		ankle	15	0	15
	180	hip	5	0	5
		knee	5	0	5
		ankle	5	0	5
Orthoroentgenography	100, 180	hip	0	0	0
		knee	0	0	0
		ankle	0	0	0
Spot orthoroentgenography	100, 180	hip	0	0	0
		knee	0	0	0
		ankle	0	0	0
CT scanograms		hip	0	0	0
		knee	0	0	0
		ankle	0	0	0

* Radiograph can not be taken at FFD 100 cm due to the field size is too small to cover the entired leg length.

Table 2 Examination time and expenditure per case of radiographic methods and CT scanograms

Method	Examination time(min)	Expenditure per case(Bahts)
Teleroentgenography	5	240
Teleroentgenography mixed with orthoroentgenography	10	360
Orthoroentgenography	10	360
Spot orthoroentgenography	10	360
CT scanograms	15	4,000

REFERENCES

1. Siffert RS. Current concepts review lower limb length discrepancy. J Bone Joint Surg 1987;69-A:1100-1106.

2. Margaret A, Green WT, Messner MB. Growth and predictions of growth in the lower extremities. J Bone Joint Surg 1963; 45A:1-14.

3. Vade A, Eissenstat R. Radiographic features of bone lengthening procedures. Radiology 1990; 174: 531-537.
4. Chapurlat RD, Duboeuf FP, Liens D, Meunier PJ. Dual energy X-ray absorptionmetry in patients with lower limb reflex sympathetic dystrophy syndrome. J Rheumatol 1996;23:1557-1559.
5. Hernefalk L, Granstrom P, Messner K. Sequential scintigraphy and orthoradiographic measurement of femoral shortening after femoral neck fracture. Arch Orthop Trauma Surg 1997;116:198-203.
6. Bal BS. A technique for comparison of leg lengths during total hip replacement. Am J Orthop 1996;25:61-62.
7. Mattassi R. Differential diagnosis in congenital vascular-bow syndromes. Semin Vasc Surg 1993; 6: 233-44.
8. Aaron A, Weinstein D, Thickman D, Eilert R. Comparison of orthoroentgenography and computed tomography in the measurement of limb length discrepancy. J Bone Joint Surg 1992;74-A:897-902.
9. Walker CW, Aronson J, Kaplan PA, Molpus WM, et al. Radiologic evaluation of limb-lengthening procedures. AJR 1991;156:353-358.
10. Paley D. Current techniques of limb lengthening. J Pediatr Orthop 1988;8:73-92.
11. Lampe HI, Swierstra BA, Diepstraten AF. Measurement of limb length inequality : comparison of clinical methods with orthoradiography in 190 children. Acta Orthop Scand 1996;67:242-244.
12. Tjernstrom B, Jakobsson O, Pech P, Rehnberg L. Reliability of radiological measurements of the distraction gap during leg lengthening. Acta Radiol 1996; 37:162-165.
13. Pfeifer T, Mahlo R, Franzreb M, Heiss U, et al. Computed tomography in the determination of leg geometry. In vivo 1995;9:257-261.
14. Minty I, Maffulli N, Hughes TH, Shaw DG, et al. Radiographic features of limb lengthening in children. Acta Radiol 1994; 35:555-559.
15. Atiken GF, Flodmark O, Newman DE, Kilcoyne RF, et al. Leg length determination by CT digital radiography. AJR 1985: 144:613-615.
16. Rhodes DW, Mansfield ER, Bishop PA, Smith JF. Comparison of leg length inequality measurement methods as estimators of the femur head height difference on standing X-ray. J Manipulative Physiol Ther 1995;18:448-452.
17. Rhodes DW, Mansfield ER, Bishop PA, Smith JF. The validity of the prone leg check as an estimate of standing leg length inequality measured by X-ray. J Manipulative Physiol Ther 1995;18:343-346.
18. Stricker SJ, Faustgen JP. Radiographic measurement of bowleg deformity: variability due to method and limb rotation. J Pediatr Orthop 1994;14:147-151.
19. Cleveland R, Kushner D, Ogden M, Herman T, et al. Determination of leg length discrepancy: a comparison of weight-bearing and supine imaging. Invest Radiol 1988;23:301.
20. National Council on Radiation Protection and Measurement (NCRP). Quality control in diagnostic imaging. NCRP report no. 99. Maryland: NCRP, 1988.
21. Soon TN. Radiographic methods of measuring leg length discrepancies. Medical Radiographer 1985;4:49-55.
22. Helms CA, McCarthy S. CT scanograms for measuring leg length discrepancy. Radiology 1984; 151: 802.

CORRECTION OF ELONGATION ERROR BY PRODUCING EQUILIBRIUM ERROR

Wanna TRIVITAYARATANA[1], Pichit TRIVITAYARATANA[1], Chavalit VONGSABARN[2], Songthip NUKROO[3]

ABSTRACT

The equilibrium error was produced by raising adjustable orthopaedics ruler to the same plane of a PVC phantom of leg to be possible to use teleroentgenographic method. The results showed that by this method the scale error occurred in the same amount as the elongation error. The measured limb length on radiograph was closely approximate to the actual length. It indicated that elongation error was eliminated by producing equilibrium error. The effect of centering the X-ray tube at various levels for measuring the anterior surface of the bone to the film (ASBF) was identified. The center ray of X-ray beam at the upper, middle and lower border of a cross-surface phantom were performed by lateral cross table radiography. The results showed that there is no statistically significant difference between the ranks* of the values of the three measured ASBF ($P>0.05$). It indicated that X-ray beam centered at skin from ventral to dorsal of leg did not affect the measured ASBF. It is convenience for routine work in clinical practice.

N.B. : ranks* is the special term in statistics and is used in cases when the values analyzed are not enough to find the mean. ASBF = Anterior Surface of the Bone to the Film.

INTRODUCTION

The difference in the length of the lower limbs usually is relatively small (1.0 to 2.5 cm) and rarely symptomatic and may be cosmetically acceptable with or without shoe-lifts. Most orthopaedic surgeons do not consider that the operative procedure is indicated for a discrepancy of less than approximately 2.5 cm.[1] The actual causes of limb-length discrepancy must be known before limb lengthening. Sometimes their causes are indirectly affected from pelvic obliquity, scoliosis, contracture of hip, knee or ankle.[2,3] Radiographic method for limb length inequality was used to determine the pattern and the amount of lengthening. Orthoroentgenography with orthopaedics ruler was more accurate than other radiographic methods. Computed tomography (CT) scanograms was significantly more accurate than orthoroentgenography in the measurements of length of the tibia and the total length of the limb when the knee was flexed to 30 degrees or more. No statistically significant difference in the measurements of the length of the femur was found between the two methods at neutral or at 15, 30 or 45 degrees of flexion of the knee.[4] Moreover, the radiation dosage from CT scanograms was lower than radiographic methods.[4-8]

Direct measurements on radiographs such

[1]Dept of Radiological Technology, Faculty of Medical Technology, Mahidol University,
[2]Dept of Radiology, Faculty of Medicine, Ramathibodi Hospital, Mahidol University,
[3]Kumkunkaew Hospital, Ministry of Public Health.

as teleroentgenography, teleroentgenography mixed with orthoroentgenography are subjected to a various degrees of magnification because an orthopaedics ruler was placed in the different planes of the bone. So the magnification or elongation error occured. The soft tissues surrounding the long leg prevent the bones to be closely contact to the cassette. Moreover, the effect of diverging beam especially in teleroentgenography is added to produce a larger magnification. Orthopaedics ruler could be placed closely to the cassette so that the scale error did not occur. The correction of differences of the elongation error and the scale error was made in order to get the actual length of lower limbs by placing another orthopaedics ruler in the same plane as the bone. The scale error was produced in the same amount of elongation error, and it is called equilibrium error. The aim of this study was to prove that the differences between the elongation error and the scale error was eliminated by an equilibrium error. ASBF was determined before placing the orthopaedics ruler parallel to the bones of the legs. If the center of the X-ray beam was not placed directly to middle part of the bone, the measured ASBF would be affected. To solve this problem, the lateral cross table radiography of a soft tissue phantom was done by centering at the upper, middle and lower border of the phantom.

ASBF = Anterior surface of the bone to the film

MATERIALS AND METHODS

1. The center ray of Hitachi X-ray machine (Model DR 155 HN) was checked by beam alignment test tool.

2. A PVC phantom of leg and an adjustable height orthopaedics ruler was placed in the same plane and parallel to each other on the 30x90 cm cassette. The exposed factors of 50 kVp, 100 mA, 0.1 s and 180 cm focal film distance was used by teleroentgenography as shown in fig 1. The elongation error and scale error were measured on a radiograph and the differences between elongation error and scale error was calculated in table 1.

3. ASBF was measured from the lateral cross table radiography of a cross-surface phantom by centering at the upper, middle and lower border of the phantom performing 3 times as shown in Fig.2 and 3. In table 2, the mean of the three measured ASBF was compared to the 10.9 cm actual ASBF. Kruskal-Wallis test was used to analyze the ranks* of the values of the three ASBF with $\alpha = 0.05$.

RESULTS

From beam alignment test tool, the deviation of the center ray was less than 2% at 100 cm FFD or less than 3 degrees from the central axis of X-ray beam, and it was in the acceptable range[10].

The scale error occured in the same amount of elongation error when raising the orthopaedics ruler to the same plane of a PVC phantom as shown in table 1. The value of limb length on radiographs was approximately equal to the actual length as shown in fig 4.

Lateral cross table radiography of a cross surface phantom by centering at the upper, middle and lower border of the phantom were done to determine the effect of different centering in measuring the ASBF. The results showed that the means ASBF at the upper, middle and lower border were 11.03, 10.87 and 10.93 cm, respectively. The differences of the 3 measured ASBF from radiographs and the 10.9 cm actual ASBF was shown in table 2. From Kruskal-Wallis test, the ranks* of the values of ASBF at the three centering points were not significantly different. ($P>0.05$)

Table 1 The difference between elongation error(A) and scale error(B) from teleroentgenography

part examination	elongation error (mm)	scale error (mm)	A-B difference (mm)
hip joint	20	20	0
knee joint	0	0	0
ankle joint	20	20	0

Table 2 The mean of measured ASBF at various center points of X-ray beam and the differences of measured ASBF and actual ASBF

center point of X-ray beam	mean of measured ASBF (cm)	difference of measured ASBF and actual ASBF(mm)
upper border	11.03	+0.13
middle	10.87	- 0.03
lower border	10.93	+0.03

ASBF = Anterior surface of the bone to the film

* see N.B.

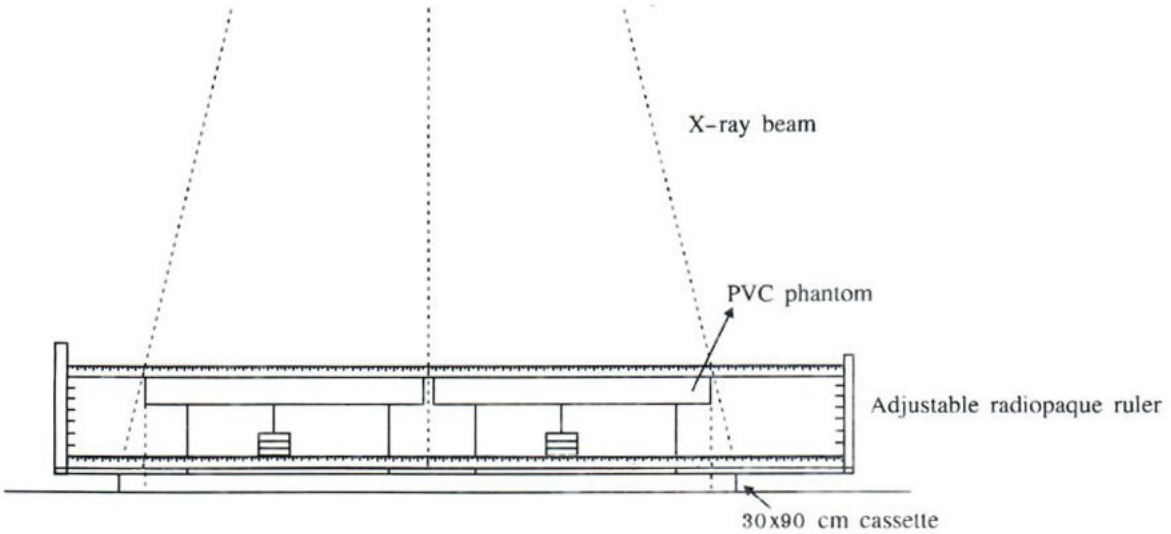

Fig.1 A PVC phantom and an adjustable height orthopaedics ruler were placed on 30x90 cm cassette. The orthopaedics ruler was not at the same plane as the phantom (A). The orthopaedics ruler was raised to the same plane as the phantom (B).

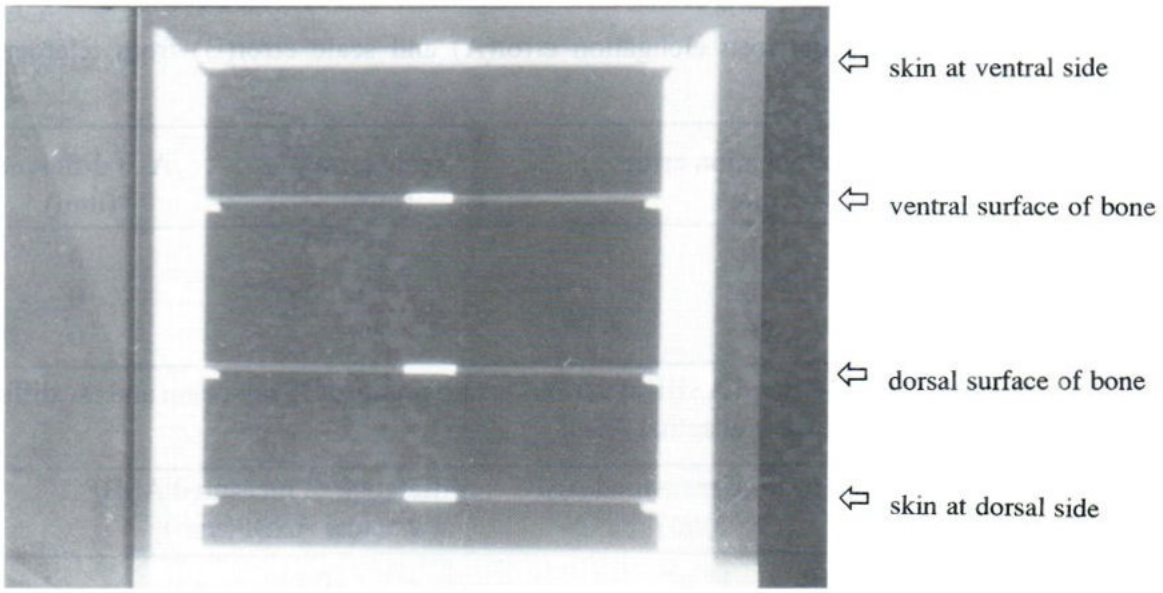

Fig. 2 Cross table radiograph of a cross surface phantom of leg

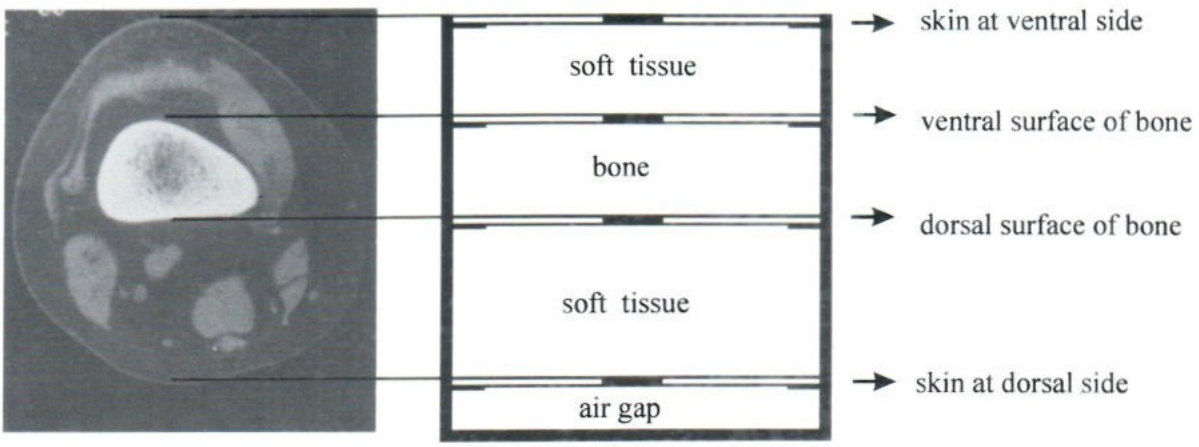

Fig. 3 Cross surface phantom represent the soft tissues of leg on CT radiograph

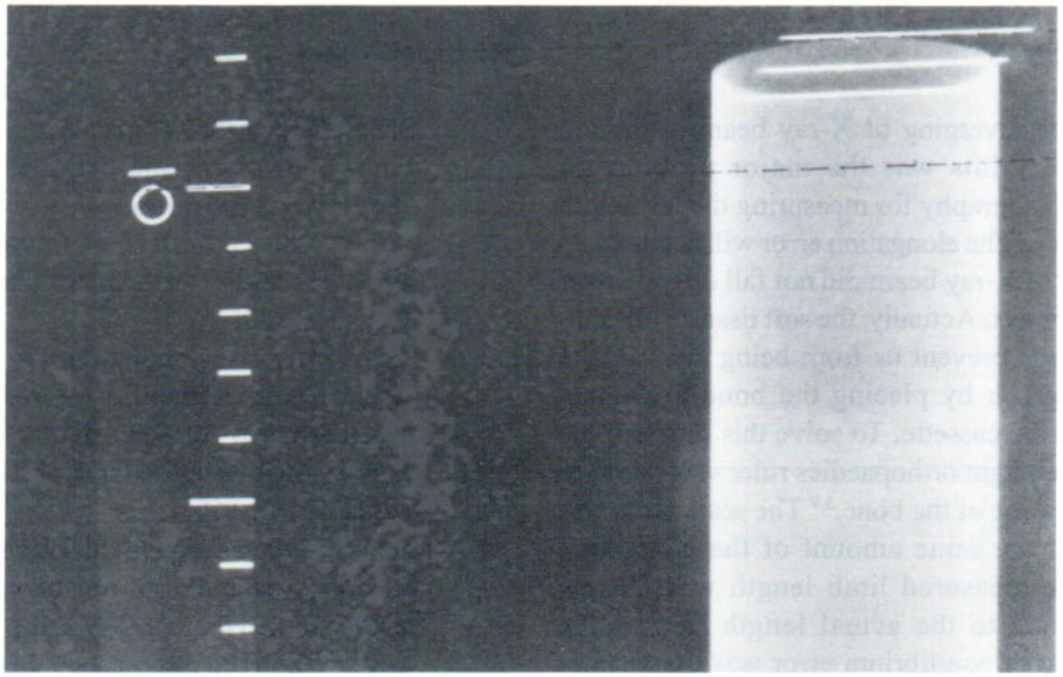

4A.

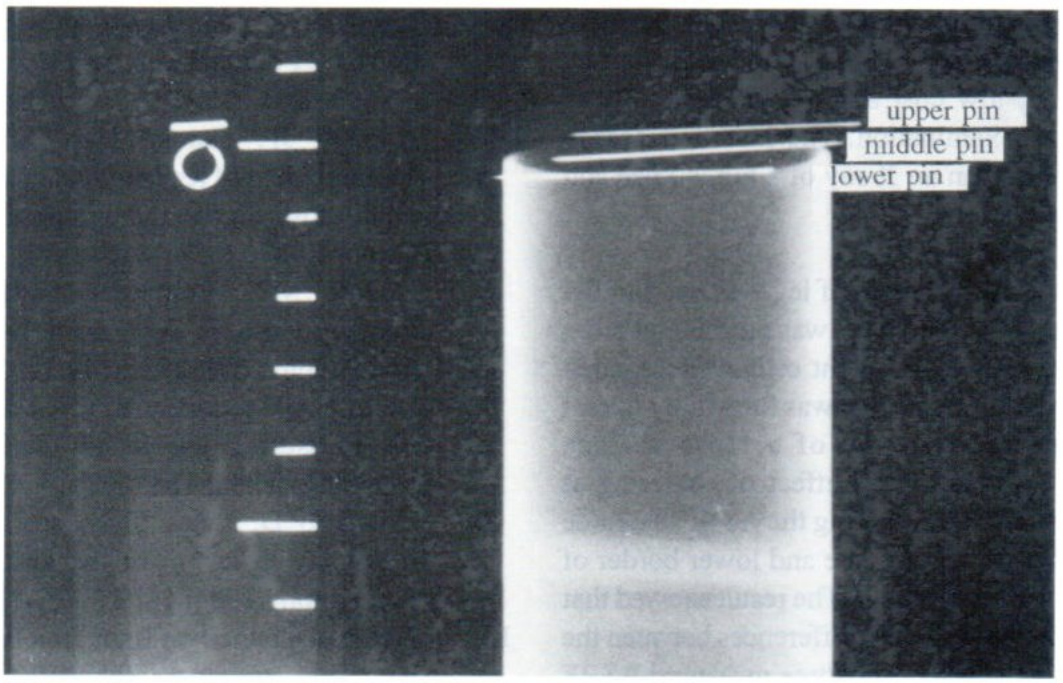

4B.

Fig. 4 With reference to fig.1, if the position of the PVC phantom and the orthopaedics ruler is difference (A), an elongation of the phantom is about 20 mm. No elongation occur when the orthopaedics ruler was raised to the same plane as the phantom as in fig.1(B)

* see N.B.

DISCUSSION

The diverging of X-ray beam to the hip and ankle joints was the major problem of teleroentgenography for measuring the leg length discrepancy. The elongation error will occur when the center of X-ray beam did not fall directly over the thick object. Actually, the soft tissue surrounding the bone prevent us from being able to take the radiograph by placing the bone to contact closely to the cassette. To solve this problem the adjustable height orthopaedics ruler was raised to the same plane of the bone.[3,9] The scale error was created at the same amount of the elongation error. The measured limb length was closely approximate to the actual length (Fig. 4 B). Production of equilibrium error was the attempt to use of the teleroentgenographic method for measuring the actual length of the limbs. The whole leg length could be visualized in a single exposure radiograph. This method was simple, widely used, low cost and needed less time to complete an examination. The radiation dosage was not more than an X-ray of a hip, a knee and an ankle separately.[11]

The entired length of leg was not parallel to the cassette, so the ASBF was measured before placing the adjustable height orthopaedics ruler. The object to film distance was known by lateral cross table radiography of a cross surface phantom. To identify the effect of centering at different levels for measuring the ASBF, the three center points (upper, middle and lower border of the bone), were performed. The result showed that no statistically significant differences between the ranks* of the values of the three measured ASBF ($P>0.05$). It indicated that X-ray beam centered at skin from ventral to dorsal of leg did not affect the measured ASBF. It is convenience for routine work in clinical practice.

ASBF = Anterior surface of the bone to the film

* see N.B.

REFERENCES

1. Siffert RS. Current concepts review lower limb-length discrepancy. J Bone Joint Surg 1987;69-A:1100-1106.
2. Siffert RS. The effect of trauma to the epiphysis and growth plate. Skel Radiol 1977;2:21-30.
3. Tjernstrom B, Jakobsson O, Pech P, Rehnberg L. Reliability of radiological measurements of the distraction gap during leg lengthening. Acta Radiol 1996;37:162-165.
4. Aaron A, Weinstein D, Thickman D, Eilert R. Comparison of orthoroentgenography and computed tomography in the measurement of limb-leg discrepancy. J Bone Joint Surg 1992;74-A:897-902.
5. Aitken AGF, Flodmark O, Newman DE, Rilcoyne RF, et al. Leg length determination by CT digital radiography. AJR 1985; 44:613-615.
6. Altongy JF, Harcke HT, Bowen JR. Measurement of leg length inequalities by micro-dose digital radiographs. J Pediat Orthop 1987; 7: 311-316.
7. Kogutt MS. Computed radiographic imaging ; use in low dose leg length radiography. AJR 1987;148:1205-1206.
8. Helm CA, McCarthy S. CT scanograms for measuring leg length discrepancy. Radiology 1984; 154: 802.
9. Horsfield D, Jones SN. Assessment of inequality in length of the lower limb. J radiography 1986; 52: 223-227.
10. National Council on Radiation Protection and Measurement (NCRP). Quality control in diagnostic imaging. NCRP report no.99. Maryland: NCRP, 1988.
11. Soon TN. Radiographic methods of measuring leg length discrepancies. Med Radiographer 1985; 4: 49-55.

Message from

Professor Dr. Kawee Tungsubutra

Editor-in-Chief, The Asean Journal of Radiology.

At last we come to the fifth year of the Asean Journal of Radiology. In this journal we have a variety of topics in all branches of Radiology including Medical Physics.

We published not only papers from Asean Association but also interesting papers from other parts of the world.

Our first paper in this issue is about the training in Neuroradiology by the President of the European Society of Neuroradiology.

The other papers are in Diagnostic Radiology including all the sub-subspecialties, i.e., CT, MRI, Ultrasonography, Interventional Radiology, etc. Nuclear Medicine also appears in this Number of the V Volume. Three papers on researches in Medical Physics are also included in this Volume.

If we can keep the standard of our publications at this level, I am sure that our Journal will be included in the Index Medicus next year.

Please continue to support us by sending papers to be published in this Journal.

Wishing you a prosperous new year.

Kawee Tungsubutra.

Kawee Tungsubutra

January-April 1999.

1. The AAR Journal of Radiology publishes the papers on Radiological Sciences, such as research work, review articles, case reports, innovations in Medical Sciences related to all branches of Radiology, and letters to the editor. The aforementioned materials can be written in English only.

2. The authors have to submit 2 copies of the manuscript and a diskette: **to Prof. Dr. Kawee Tungsubutra,** 318 Kaweevej Hospital, Tarksin Road, Dhonburi, Bangkok 10600, Thailand. **or to the Associate Editors** at the Radiological Society of Malaysia, Indonesia, Philippines, Singapore and Brunei. The names and adresses of the Associate Editors in each country were published in the front page of this Journal.

3. The original copy to be submitted must be typed in a double space on one side of the page of 8.1/2"x 11.1/2" paper.

4. The format of the article must include :

a. Title page and address of the author (s)
b. Abstract
c. Introduction (Background)
d. Material and Method
e. Results and discussion (Tables and Illustrations)
f. Acknowledgement (if any)
g. References (Follow the Vancouver style developed by ICMJE)

5. We will provide 20 copies of reprints for the author (s) who submit (s) an article for publication in the AAR Journal.

6. The illustrations and tables must be clearly prepared with legends in English as they are the art works to be reproduced.

7. The authors are responsible for the contents of the article as to its facts and findings.

8. Ethics.

Paper reporting studies which might be interpreted as human experimentation (e.g. controlled trials) should conform to the standards of the Declaration of Helsinki (see British Medical Journal 1964:2:177) and should indicate that, approval that such studies may proceed, has been granted by the local or hospital Ethics Committee.

When reporting experiments on animals indicate whether the institution's or the National Research Council's guide for, or any national law on, the care and use of laboratory animals was followed.

บริษัท กรุงสิทธิวรรณ จำกัด
SONGSITTIVAN CO.,LTD.
Tel. 910-1999 Fax : 910-1888

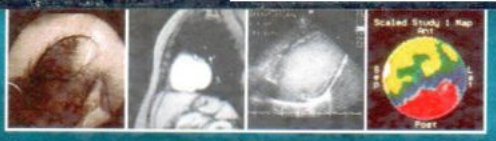

Keeping an eye on imaging

X-ray

MRI

US

NM

Magnetic Resonance Imaging

Ultrasound

Nuclear Medicine

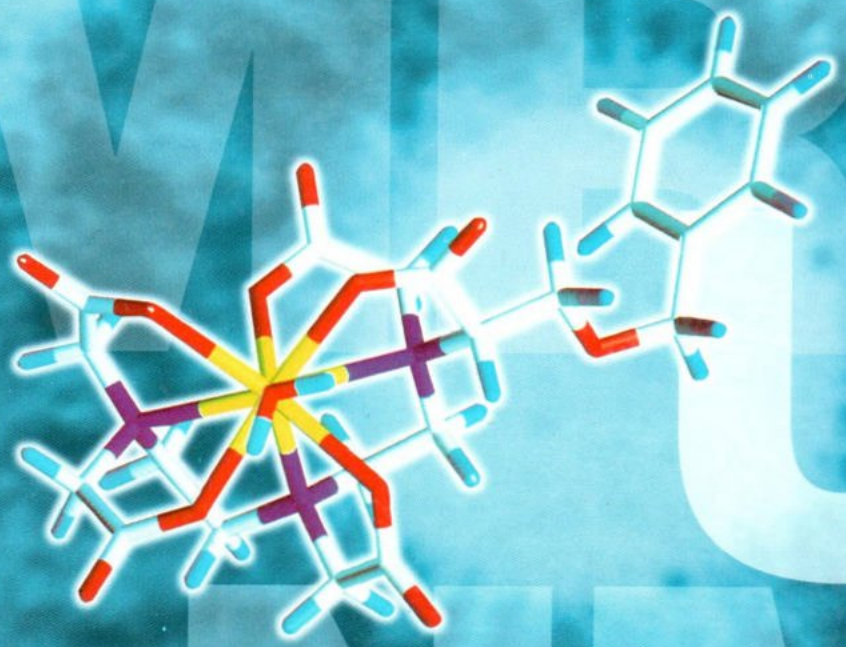

BRACCO IMAGING

Harmony in contrast